UNIVERSITY OF OKLAHOMA

GRADUATE COLLEGE

DESIGN GUIDANCE FOR INSTALLING VIBRATION SENSITIVE EQUIPMENT IN INDUSTRIAL FACILITIES

A THESIS

SUBMITTED TO THE GRADUATE FACULTY

in partial fulfillment of the requirements for the

Degree of

MASTER OF SCIENCE

By

KEVIN D. WISE
Norman, Oklahoma
2016

DESIGN GUIDANCE FOR INSTALLING VIBRATION SENSITIVE EQUIPMENT IN INDUSTRIAL FACILITIES

A THESIS APPROVED FOR THE
SCHOOL OF CIVIL ENGINEERING AND ENVIRONMENTAL SCIENCE

BY

_____
Dr. P. Scott Harvey Jr., Chair

_____
Dr. J. David Baldwin

_____
Dr. Royce W. Floyd

To my wife, Jennifer.

Acknowledgements

I want to begin by thanking my advisor, Dr. Scott Harvey, for providing me the opportunity to continue my education. Dr. Harvey was always available to answer any of my questions and his pleasant, cheerful attitude made every interaction a welcome experience. Most importantly, he asked me well thought-out, leading questions that directly improved my understanding of the concepts at hand as well as keep me on track to complete my education in a reasonable time. I could not have asked for a better mentor.

Additionally, I want to thank the rest of my committee, Dr. Royce Floyd and Dr. David Baldwin. They took time out of their summer schedules to provide support for this work and received nothing in return, but this small thank you. I greatly appreciate their help.

I want thank the Engineering Directorate, specifically Jeff Catron, Thad Lewis, and Belinda Wilson, at Tinker Air Force Base for maintaining an environment that encourages and backs that encouragement up with the resources necessary for continuing education. It is not an overstatement that I would never have been able to pursue this degree without their help. I want to explicitly thank my supervisor, Marc Owen, for agreeing to fill in for me for an entire year. Not only did Marc afford me this opportunity, but he has provided me consistent mentorship over the last 14 years from his engineering and general life experiences. Anytime my confidence was faltering, he has enabled me to succeed. Additionally, I want to thank the management team at Tinker AFB that approved my study path, Bruno Morf, Robert Roman, David Goss, Joseph Cecrle and Dr. Kristian Olivero.

As with most things, the man you see is really the summation of those closest to him. In that light, I must thank my family for the unseen support that they continually provide. Thank you to my wife for picking up the slack I left on days where I bit off a little more than I could chew, like mowing the out of control grass at times. Thank you to my kids Eleanor and Joseph for reminding me of the important things in life and that I need to take breaks and do something fun from time to time. Also to my son, David, who showed up half way through this endeavor, thank you for not being a too demanding baby and for smiling every time I see you.

There were many more people who helped me as well, which I could go on forever listing, even some that I am assuredly unaware of their efforts, but I am forced to end this and simply say “thank you.”

Table of Contents

List of Tables

List of Figures

Abstract

The need to understand floor vibrations in an industrial facility has increased in recent years as the drive for tighter manufacturing tolerances has increased. This drive has led to an increase in manufacturing equipment that is sensitive to floor vibrations. The main contribution of this thesis is the experimental verification of a method to predict the effects of nearby vibrating equipment on vibration sensitive equipment. By using this method, a designer may be able to avoid the installation of special isolation foundations for vibration sensitive equipment by either demonstrating the lack of need for the special foundation or locating the other vibration sources far enough away to allow for sufficient attenuation. To achieve this, vibration levels were measured at four sites from multiple vibration sources at each site. These measurements were used to create a model for how vibrations attenuate from a single source with distance. Measurements were also taken while multiple vibration sources were operating to quantify how vibration waves combine. The results of the measurements allowed for the creation of a vibration attenuation model that conservatively estimates ground vibrations, as well as a method for accounting for multiple vibration sources on a floor space. The culmination of this was shown to provide conservative predictions of the floor vibrations near sensitive equipment from multiple nearby vibration sources. Additionally, by closely analyzing the experimental results, the vibration waves at the frequencies under consideration, less than 100 Hz, created from equipment installed on concrete slabs on grade primarily traveled through the underlying soil and behaved accordingly.

1. Introduction

Engineers working in modern industrial manufacturing facilities are often confronted with problem of mitigating the effect of floor vibrations on sensitive equipment. At first, this seems like a trivial problem with a trivial solution simply install all of the industrial vibrating equipment and sensitive equipment on separate vibration isolation foundations, reducing the equipment vibrations transmitted to the facility concrete slab and the soil beneath it and eliminating the transmission of ground vibration to the sensitive equipment. In addition to isolation foundations, ensure that there is significant distance between the vibration sources and vibration sensitive equipment to attenuate the vibrations before reaching the sensitive equipment. Figure 1-1 shows a coordinate-measuring machine (CMM) which is a common piece of moderately vibration sensitive equipment and an instrument grade vacuum pump which is an example of a vibration source that could be installed near the CMM.

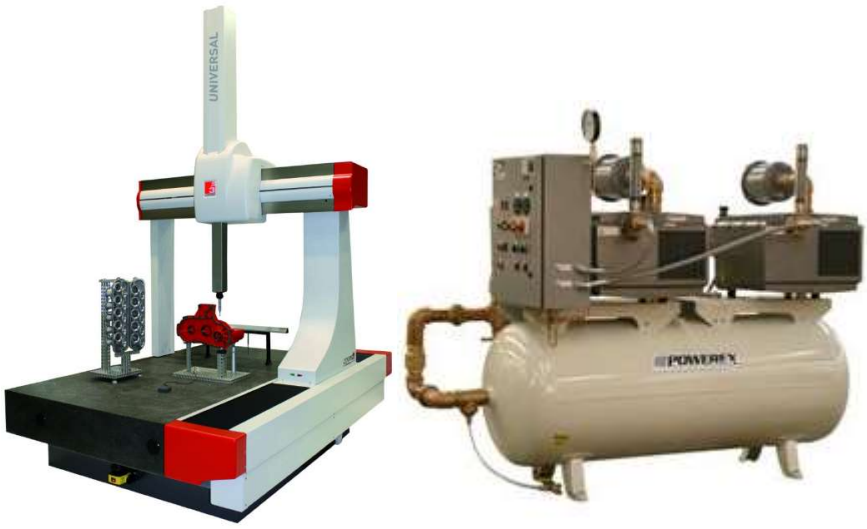

Figure 1-1: Sensitive Equipment, CMM (Left) and Vibration Source, Vacuum Pump (Right)

The design of industrial foundations that limit the transfer of vibrations both from vibrating equipment and to sensitive equipment is well understood and well documented in Krishna Bhatia's book Foundations for Industrial Machines: Handbook for Practicing Engineers (2007). However, the techniques and designs for isolation foundations are not the subject of this thesis. Conversely, the main objective in this thesis is to known more precisely when advanced vibration isolation foundations can be completely avoided without adverse effect to vibration sensitive equipment.

The problem can be stated simply as follows: How far apart do vibration sources need to be from vibration sensitive equipment to be installed (a) in the same facility and (b) on the same continuous concrete slab? Yet, in a real facility, there are a multitude of vibration sources, so to answer this question it is more realistic to examine the combined effect of multiple vibration sources on a location under consideration for sensitive operation.

This thesis will provide, in the frame of reference of design guidance, a method for estimating the maximum floor vibrations that can be expected at a given location from nearby vibration sources. To achieve this, the background theory and previous studies will be described in Chapter 2. Chapter 3 will describe the required tools used in this research to take vibration measurements on the level necessary for moderately sensitive equipment. Chapter 4 will show the measured vibrations at several locations from several different types of vibrating equipment. The chapter will highlight some of the challenges with taking and interpreting accurate measurements as well as some of the complex behavior associated with vibration decay over a distance. Based on these measurements, recommendations will be provided for creating attenuation models at

any facility. Chapter 5 will present the results of measured vibrations from multiple equipment at specific locations. This chapter will integrate all of the measurements and observations into a model to estimate floor vibrations over an entire floor space from multiple equipment. The last part of Chapter 5 will demonstrate the method with a real world example. Finally, Chapter 6 will summarize and conclude this thesis.

Not only is it important to know what this thesis will cover, it is just as important to realize what it does not cover. First, this work has no intention of covering extremely vibration sensitive equipment associated with nanotechnology. The intended limit of the lower bound of vibration magnitude is items at or above the sensitivity level VC-C (defined in Chapter 2). Second, this work covers only floor spaces consisting of a concrete slab on a grade, and not a suspended floor system. And finally, the method described is not intended to find the precise floor vibration at a given time, but rather a maximum, reasonably expected floor vibration considering the nearby vibration sources.

The question may arise as to "if the ways to mitigate ground vibrations are already known, why would engineers need this method?" The answer to this question is obvious to anyone associated with a manufacturing facility, and that is "cost". Everything has a cost. Installing isolation foundations has an upfront cost in both time and dollars. A foundation is a relatively permanent item that confines equipment to an immovable location, and modern production requires a facility to be as flexible as possible to layout changes. Even separating the vibration sources from sensitive equipment can have costs in increased production item travel time and run counter with

the current manufacturing trend to cellularize production shops (place all of the necessary tools and equipment to produce an item at a single location in a "cell").

An informed person may consider the follow-on question, "why not just set a vibration sensor (accelerometer or similar) for some amount of time at the location of the vibration sensitive equipment?" This seems like a good design decision, especially when considered alongside the other industry method of "guess and hope", and it is in fact the current primary method of practice (e.g., Dematto 2015). However, a modern facility poses some significant challenges to this. First, not only do operations move in new vibration sensitive equipment as implied in this question, but they even more frequently move in new vibration sources or merely move existing sources around. Moving vibration sources around only to check their impact on a sensitive piece of equipment after the fact can be very risky. The other problem with this method is not as straight forward. It can be difficult to run all vibration sources near a sensitive location at the same time such that they produce the most critical vibrations. To complicate matters, a measurement at one specific point will be different than another point because there will be multiple attenuation paths (one piece of equipment is further from the point than another piece of equipment) and possible constructive and nonconstructive interference between vibration waveforms (see Chapter 5). These complications show the need for a predictive model as opposed to simply taking a measurement.

The next chapter will expound on previously researched areas related to the material presented in this thesis as well as some of the theoretical background to how vibrations travel through an industrial facility slab on grade system.

2. Background and Literature Review

To begin, it is necessary to examine previously completed research related to this topic. This chapter will review the criteria for sensitive equipment, the foundations of wave motion and attenuation, and discuss previous experiments that were similar in nature to the work in this thesis.

2.1 Vibration Criteria for Equipment

One of the most common methods for classifying ground vibrations with regards to vibration sensitive equipment is known was the vibration criterion (VC) curves. These vibration spectra were originally created by Colin Gordon in the early 1980's in response to the need for facility designers to have a baseline criteria for designing vibration sensitive facilities before the actual equipment going into these facilities were specifically known. These curves were published by SPIE in 1991 and IEST 1993 for general use and have been accepted worldwide (Gordon 1991 and 1987). Table 2-1 contains a description of the vibration levels of each curve. Gordon's criterion were based on three principles. First, maximum sensitivity to vibrations for both people and equipment tends to lie on a curve of constant velocity across a spectrum. For this reason, the curves are typically defined in terms of constant RMS (root mean square) velocity. Second, since vibrations consist of both tonal and broadband elements, a proportional bandwidth in terms of third octave bands is used to conservatively account for both elements. Octave bands are frequency ranges where the end (higher) frequency is double the beginning (lower) frequency, using 1,000 Hz as an arbitrary reference. For example, 500, 1,000, and 2,000 Hz are center frequencies of octave bands. The edge frequencies are the center frequency multiplied by the square root of ½ and the

square root of 2, respectively. Third octave bands follow the same pattern except they are one third the size (Shin and Hammond 2008). Finally, since most equipment has a lowest natural frequency above 8 Hz, vibrations below 8 Hz can be larger without an adverse effect on sensitive equipment.

Originally, there were five VC curves labeled A through E with decreasing vibration limits as the letter increased (see Table 2-1). Since that time, increasingly sensitive equipment has necessitated the addition of curves F and G (Cai et al. 2013).

Table 2-1: Vibration Criteria Curve Description[1, 2]

Criterion Curve	Max Level (1) micrometers/ sec,rms	Detail Size (2) microns	Description of Use
Workshop (ISO)	800	N/A	Distinctly feelable vibration. Appropriate to workshops and nonsensitive areas.
Office (ISO)	400	N/A	Feelable vibration. Appropriate to offices and nonsensitive areas.
Residential Day (ISO)	200	75	Barely feelable vibration. Appropriate to sleep areas in most instances. Probably adequate for computer equipment, probe test equipment and low-power (to 20X) microscopes.
Op. Theatre (ISO)	100	25	Vibration not feelable. Suitable for sensitive sleep areas. Suitable in most instances for microscopes to 100X and for other equipment of low sensitivity.
VC-A	50	8	Adequate in most instances for optical microscopes to 400X, microbalances, optical balances, proximity and projection aligners, etc.
VC-B	25	3	An appropriate standard for optical microscopes to 1000X, inspection and lithography equipment (including steppers) to 3 micron line widths.
VC-C	12.5	1	A good standard for most lithography and inspection equipment to 1 micron detail size.
VC-D	6	0.3	Suitable in most instances for the most demanding equipment including electron microscopes (TEMs and SEMs) and E-Beam systems, operating to the limits of their capability.
VC-E	3	0.1	A difficult criterion to achieve in most instances. Assumed to be adequate for the most demanding of sensitive systems including long path, laser-based, small target systems and other systems requiring extraordinary dynamic stability.

[1] "As measured in one-third octave bands of frequency over the frequency range 8 to 100 Hz" (Gordon 1999).

[2] "The detail size refers to the line widths for microelectronics fabrication, the particle (cell) size for medical and pharmaceutical research, etc. The values given take into account the observation that the vibration requirements of many items depend upon the detail size of the process" (Gordon 1999).

Additional research was performed by Salyards and Firman (2009) comparing the generic VC curves to actual sensitive equipment specifications. They found that there is some variation between the methods used by manufactures to describe specific equipment vibration limits and the limits of allowable vibrations described by the VC curves. Their recommendation was to use specific manufacture specifications when available. Still, they found the VC curves to provide reasonable approximations compared to manufacturing specifications, and comparisons to field conditions are more straight forward with VC curves than with some manufacture's specifications.

2.2 Wave Motion

This section describes the existing knowledge on general wave motion on an elastic half space and is broken into two parts: (i) body waves in the form compression and (ii) shear waves and surface waves in the form of Rayleigh waves. Richard Woods (1967) created Figure 2-1 to show the relative distribution between these types of waves.

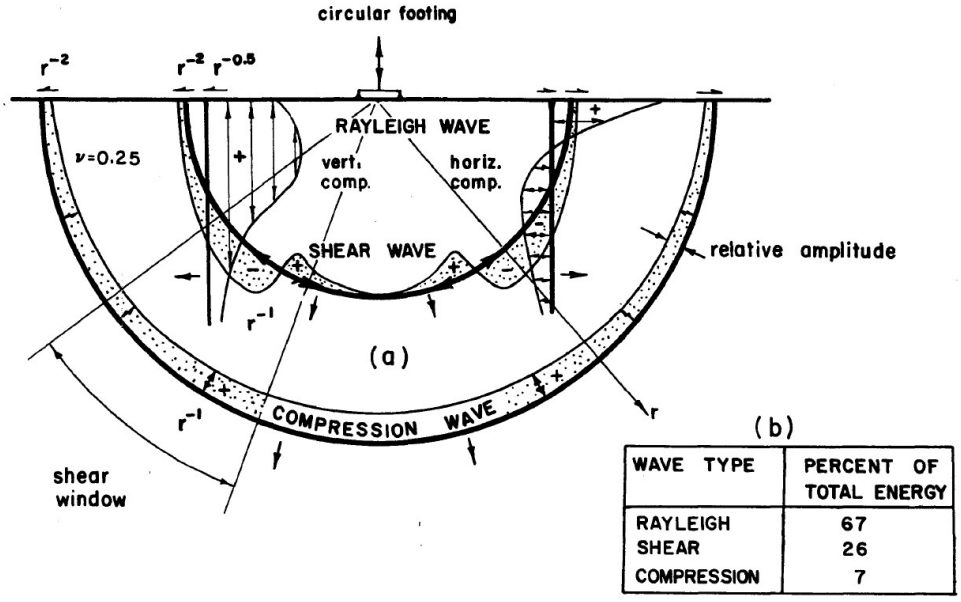

Figure 2-1: Distribution of Waves on an Elastic Half Space (Woods 1967)

2.2.1 General Seismic Wave Motion

The general motion of a wave traveling through an elastic half space has been well understood for some time and documented in many sources (Kramer 1996, Das 1993, Tedesco 1999). The basic derivation involves taking the three-dimensional equilibrium equations with respect to time and applying Hooke's law, which gives the equation of motion in terms of displacements. Equation (2-1) shows one direction of the above described equation of motion. Note that λ here is the material property "Lame's first parameter" and not wavelength; also, μ is the modulus of rigidity and the same as shear modulus (G).

$$\rho \frac{\partial^2 u}{\partial t^2} = (\lambda + \mu) \frac{\partial \overline{\varepsilon}}{\partial x} + \mu \nabla^2 u \qquad \textbf{(2-1)}$$

By looking at only at the change in volumetric strain, a wave can be derived that has no rotation and only dilatation. This wave is termed the compression wave or primary wave (p-wave). Solving Equation (2-1) for the velocity of the p-wave, v_p, gives:

$$v_p = \sqrt{\frac{G(2-2\nu)}{\rho(1-2\nu)}} \qquad \textbf{(2-2)}$$

As Poisson's ratio, ν, increases toward 0.5, the velocity increases rapidly.

Another form of wave motion can be derived from the same set of equations of motion, by looking at only distortion without dilation. The solution is not as obvious, by can be obtained but differentiating the equations of motion in the x and y directions with respect to x and y, respectively, and subtracting one expression from the other.

This allows for a wave known as a shear wave (s-wave) to be seen. The velocity for this wave is given by:

$$v_s = \sqrt{\frac{G}{\rho}} \tag{2-3}$$

Comparing equations (2-2) and (2-3), it can be seen that the p-wave velocity always exceeds the s-wave velocity. Of perhaps more importance for this work, is the notion that the velocities between the concrete directly supporting equipment and the subgrade supporting the concrete are not likely to be the same. The implications of this will be discussed later in this thesis (Section 4.6.1).

2.2.2 General Surface Wave Motion

The previous section discussed wave motion as the wave travels in a space that is infinite (and homogeneous) in all directions. Of greater concern here is what happens at the boundary of the vibrating space. Generally, wave motion is termed to be happening in an elastic half space meaning that there is a clear boundary beyond which the waves do not propagate. In other words, the earth's surface is the boundary of the half space. Although there are multiple types of waves other than from p-waves and s-waves, most discussion centers around what is termed a Rayleigh wave. This type of wave has also been studied for over a century and is well documented (Kramer 1996, Das 1993, Tedesco 1999).

Rayleigh waves are a combination of s-waves and p-waves occurring at the surface of a half space. In other words, Rayleigh waves dilate and distort. The solution to the equations of motion describing Rayleigh surface waves are complex and will not

be presented here.[3] However, a few important aspects of Rayleigh waves will be mentioned. First, they travel slightly slower than shear waves for typical values of Poisson's ratio. For example, for a Poisson's ratio of 0.3, the Rayleigh wave velocity is about 93% as fast as the shear wave velocity. Second, for practical intents, the vertical component of the Rayleigh wave (a) does not extend past a depth of two times its wavelength, and (b) has an amplitude of motion of only 20% of the surface amplitude at a depth of one wavelength. Third, the horizontal amplitude of the wave reduces more quickly with depth than the vertical amplitude and becomes 90 degrees out of phase by a depth of 0.2 wavelengths. This motion corresponds to retrograde elliptical particle motion. As evident, the depth that a Rayleigh wave penetrates into a homogeneous half space is dependent on the wavelength of the motion. This is illustrated in Figure 2-2.

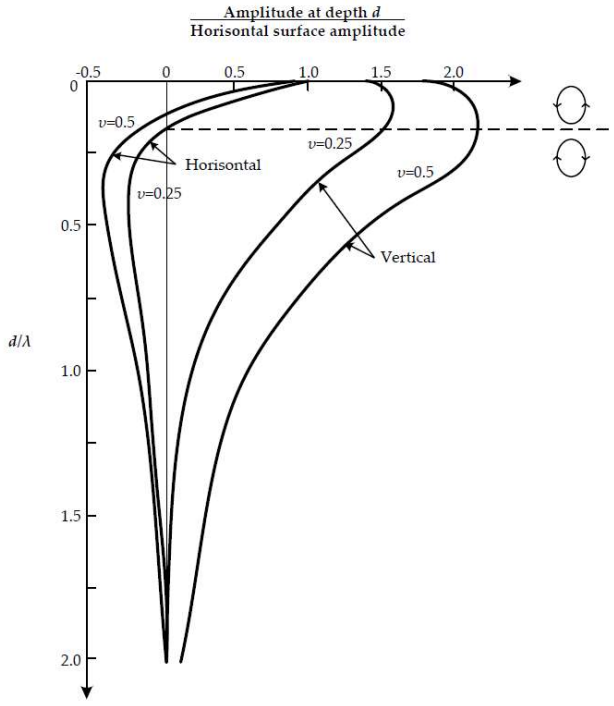

Figure 2-2: Horizontal and Vertical Vibration Amplitudes of Rayleigh Waves (Richart et al. 1970)

[3] See Kramer (1996) or Das (1993) for a derivation and detailed description.

2.3 Dissipation of Wave Energy

This section describes the basic theory behind vibration wave attenuation. It is broken into three sections. The first section discusses geometric damping (i.e., reduction in vibrations from the wave spreading out). The second section describes a current theoretical model for determining material damping (i.e., the conversion of motion into heat). The third section describes various experiments to measure the total attenuation of a vibration wave.

2.3.1 Geometric Damping

Geometric damping, also referred to as radiation damping, is well understood and documented (Kramer 1996, Das 1993). The basic concept of this type of damping is based on energy spreading. As a wave moves from a point source, the energy that was introduced from this covers remains constant, but with each increase in the distance from the source that same energy must be transferred to more mass. This is termed a reduction in the specific energy of the wave and results in a decrease in the amplitude of the motion. For p-waves and s-waves, the wave is assumed to propagate in a spherical fashion which results in an amplitude reducing of $1/r$. For surface waves, the wave is assumed to propagate in a cylindrical fashion which results in a reduction of $1/\sqrt{r}$. This shows that surface waves attenuate geometrically slower than p-waves and s-waves.

An important item to consider here is that when the excitation is located on the surface along a line as opposed to a point, such as a train, road or pedestrian aisle, there is no damping of the surface wave since it should be assume that the wave propagates as

a surface line and not a cylinder (Amick 1999). Table 2-2 shows theoretical values for geometric damping coefficients.

Table 2-2: Theoretical Geometric Attenuation Coefficients (Amick 1999)

Source	Wave Type	Location	Power	dB/Doubling
Point of Surface	Rayleigh	Surface	0.5	3
Line on Surface	Rayleigh	Surface	0	0
Point at Depth	Body	Surface	1	6
Point at Depth	Body	Depth	1	6

2.3.2 Material Absorption (Theoretical)

Kramer (1996) uses a Kelvin-Voigt solid model with viscous damping to derive the effects of material damping. The full derivation can be reviewed in the Kramer text, but a few critical points will be highlighted here as they directly relate to the damping assumptions used in this research. By looking primarily at the shear-waves traveling in either the horizontal direction or vertical direction, the Kelvin-Voigt model creates an elliptical path where the energy dissipation is assumed to be the area of this path. The energy dissipation of ΔW is given by

$$\Delta W = \int_{t_0}^{t_0+2\pi/\omega} \tau \frac{\partial \gamma}{\partial t} dt = \pi \eta \omega \gamma_0^2 \qquad \textbf{(2-4)}$$

where η is the viscosity, ω is the angular frequency of loading and γ_0 is the magnitude of the harmonic shear strain.

Equation (2-4) highlights a physical problem with this assumption of a Kelvin-Voigt solid. Whereas Equation (2-4) says that the amount of dissipation per cycle is directly proportion to the angular frequency of loading, and at least the soil component

is known to actually dissipate energy hysteretically by grain slippage, which is independent of frequency. However, it is still mathematically convenient to use the Kelvin-Voigt solid, and the frequency dependence can be indirectly eliminated by solving the system in terms of damping ratio.

Using the notion that the damping ratio, ξ, is related to the area contained by the force-displacement or stress-strain loop, the relationship between the dissipation energy calculated from Kelvin-Voigt viscous damping, ΔW, and the peak energy of a cycle.

$$\xi = \frac{1}{4\pi}\frac{\Delta W}{W} \tag{2-5}$$

Now, substituting the results for Kelvin-Voigt dissipation and peak energy from basic mechanics into Equation (2-5), the expression for the viscosity is given by

$$\eta = \frac{2G}{\omega}\xi \tag{2-6}$$

which is conveniently in terms of the shear modulus and damping ratio. Note that the viscosity is inversely proportional to the angular frequency, which allows for the cancellation of the angular frequency later.

Substituting the Kelvin-Voigt model back into the wave equilibrium equation discussed earlier and simplifying for a single direction of a shear wave, a wave motion equation including material damping is determined as follows:

$$u(r,t) = Ae^{k_2 r}e^{i(\omega t - k_1 r)} \tag{2-7}$$

where the constant exponents k_1 and k_2 are given by

$$k_1^2 = \frac{\rho\omega^2}{2G(1+4\xi^2)}\left(\sqrt{1+4\xi^2}+1\right) \tag{2-8}$$

$$k_2^2 = \frac{\rho\omega^2}{2G(1+4\xi^2)}\left(\sqrt{1+4\xi^2}-1\right) \tag{2-9}$$

Since this is a real wave, k_1 must be the positive root and k_2 must be the negative root. When there is no damping ($\xi = 0$), k_2 becomes zero and k_1 becomes the stiffness. This solution has k_2 as a constant that represents the amount of dissipation for a given damping ratio. The dissipation is an exponentially decaying function.

At this point it is important to list some experimental values for the damping ratio, ξ, and shear modulus, G, since they are fundamental to the theoretical models. Figure 2-3 and Figure 2-4 are from research performed by Vucetic and Dobry (1991) analyzing the effects of soil plasticity on cyclic response. Figure 2-3 shows the damping ratio for clays at different plasticity indices (PI). For applications such as the small vibrations studied here, it is possible to see that the damping ratio does not vary considerably for small strains (~0.001%) for a given plasticity index and appears to have limits between 1 and 5 percent. Figure 2-4 shows that, as the level of strains increase, the shear modulus decreases and with a rate that depends on the plasticity index. However, once again for small strains, the plasticity index has no significant effect and the shear modulus does not decrease.

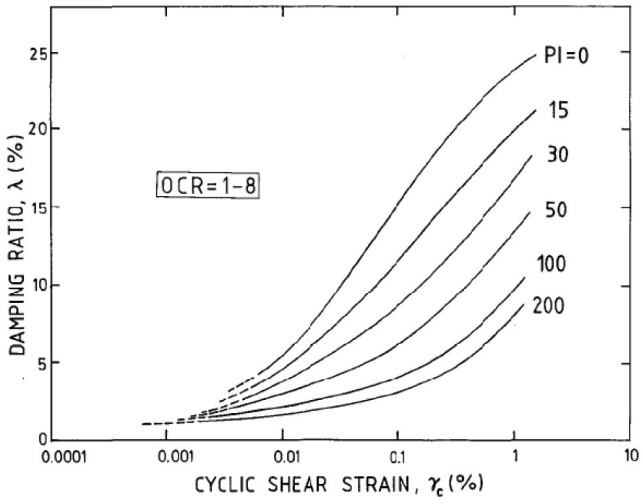

Figure 2-3: Damping Ratio Percent vs. Cyclic Shear Strain Percent for Clay

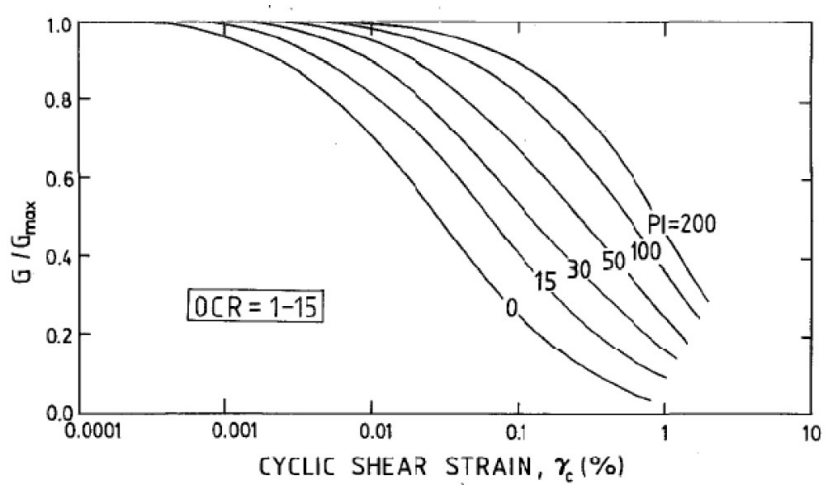

Figure 2-4: Ratio of Shear Modulus vs. Cyclic Shear Strain Percent for Clay

2.3.3 Real World Examples of Dissipation

Now, when it comes to applying the aforementioned standard theory to actual field measurements, there have been several studies and several modifications to these theoretical equations.

Most field measurements are taken at the surface, and a surface wave propagation, typically Rayleigh wave, model is assumed. This leads to the first obvious challenge in that both geometric and material attenuation are simultaneously occurring. To facilitate this, Bornitz (1931) proposed an equation for surface wave attenuation commonly referred to as the Bornitz formula:

$$\overline{w_n} = \overline{w_1}\sqrt{\frac{r_1}{r_n}}exp[-\beta(r_n - r_1)] \qquad \textbf{(2-10)}$$

where $\overline{w_n}$ and $\overline{w_1}$ are vertical amplitudes at distances r_n and r_1, respectively, and β is termed the absorption coefficient. It should be noted that (a) this formula coincides with the mathematical prediction of the constant geometrical damping, (b) the surface wave diminishes at a rate proportional to the square root of distance traveled, and (c) the

wave further diminishes exponentially by a material constant β independent of angular frequency.

Unfortunately, the predicted attenuation of the Bornitz formula and its derivatives have not perfectly played out in all research, particularly when the distances are on the order of meters and not kilometers. Several adjustments have been proposed and incorporated, typically to the absorption coefficient, in an effort to merge experimental field measurements with theoretical calculations. For reference, using Equation (2-9) for concrete, with an upper limit damping ratio of 5%, a frequency of 50 Hz (angular frequency of 314 rad/s), concrete shear modulus of 1.4 million psi, and density of 145 pounds per cubic foot the attenuation coefficient, k_2, comes to 0.0023 per foot.

Amick (1999) published a paper listing several attenuation coefficients compiled from other sources. Table 2-3 shows some of these values. He lists a value for the attenuation coefficient he calls α (same as β) as 0.006 per foot for a four to six inch concrete slab resting on compact granular fill. This is about 150% larger than predicted by the theoretical equation.

Table 2-3: Various Attenuation Coefficients Compiled by Amick (1999)

Investigator	Soil Type	β (ft^{-1})
Forssblad (1965)	Silty gravelly sand	0.04
Richart (1962)	4-6 in concrete slab over compact granular fill	0.006
Barkin (1962)	Saturated fine grain sand	0.03
Barkin (1962)	Saturated clay with sand and silt	0.012-0.036
Barkin (1962)	Clayey sand, clay with some sand	0.012
Dalmatov et al. (1968)	Sands and Silts	0.008-0.11
Peng (1972)	Soft Bangkok clay	0.079-0.134

In addition to just listing some historical values, Amick derived an approach to account for frequency effects on attenuation. The premise of his theory, based on

studies by Barkan (1962) and Dowding (1996), is that soil attenuates on a per wavelength basis. Note that this is an extension of Bornitz type formulas (Equation (2-10)) and not (Equation (2-7)). To use this theory, Amick defines a material constant ρ as shown here:

$$\rho = \frac{2\xi}{c} \tag{2-11}$$

where ξ is the damping ratio and c is the speed of the wave. He replaces the α term (β in Bornitz) with

$$\alpha = \rho \pi f \tag{2-12}$$

where f is circular frequency.

Using a vibration source with a narrow band of frequency content, Amick determined a value of ρ, and applied this value to field measurements of the vibration attenuation from different earth-moving large equipment. It was not well documented how well this method predicted vibration attenuation levels. He included the maximum RMS velocity values measured as a function of distance for five different types of earth-moving equipment. What is clear from his results is that the attenuation coefficient cannot be constant.

Kim and Lee (1999) used a similar formula as Amick for applying frequency to the absorption coefficient of the Bornitz formula. They stated that the results for material damping matched well; however, they made an interesting statement about how, if they used the expected geometric attenuation characteristics, the soil damping was too high to be realistic, and thus they adjusted the geometric constants and left the damping alone to fit the data.

An interesting study that is worth mentioning as it highlights some unexpected results about seismic wave decay was performed by Günther et al. (2004) at Stanford University, titled "Seismic waves from elephant vocalizations: A possible communication mode?" The idea of the study was centered on the notion that, since air waves attenuate faster than a theoretical Rayleigh waves on a very hard surface, elephants may be able to communicate further with other elephants using ground waves instead of air sound waves. The absorption coefficient used by Günter is given by

$$\alpha = \frac{\pi f}{Qv} \tag{2-13}$$

where f is the circular frequency, v is the shear-wave velocity, and Q is a material property called the quality factor. The quality factor is another way to look at the damping coefficient.

The conclusion of the study was that real-world measurements tended to not propagate as far as predicted by low-noise, low-attenuation theoretical models, and thus elephants probably do not use this method of communication.

Although not perfectly aligned for equipment vibrations, Albert et al. (2013) produced a detailed study on the propagation of air and seismic waves with regards to the prediction of property damage from munitions detonations. In opposition to the standard theory, Albert stated that that no clear sign of exponential decay in the ground seismic waves was observed and proposed the following expression for the decay of amplitude A with radius r:

$$A(r) = A_0\left(r^{-\beta}\right) \tag{2-14}$$

where A_0 is the amplitude of the source and β is a constant including all forms of geometric, material and boundary effects. Albert reported values of β between 1.1 and

1.6. Still, this might not be the best model for sensitive equipment since, as Albert and his colleagues pointed out, the seismic waves not associated with acoustic coupling were negligible compared with the waves that were, and thus were left out of their calculations. This does indicate some of the difficulty in predicting ground motions and the differences in opinion between interpreting results.

In a U.S. Geological Survey (USGS) research project, King et al. (1991) fit a form of Equation (2-14) to data from multiple types of sources such as “pick-up trucks”, “Bobcats”, “railroad trains”, “freeways”, “helicopters”, and “aircraft”. King and colleagues used a constant β for each source to predict vibration levels over a distance even though the plotted spectrum over distances clearly showed frequency dependence. The values for each β were not documented as the purpose of the study was to determine if vibrations would cause damage to archeological sites.

Gutowski and Dym (1976) reviewed research related to the propagation of ground vibrations. Other than improvements in equipment for measuring vibrations, it appears not much has changed in the past forty years. They cited references that proposed mathematical models for wave dissipation similar to those mentioned previously, including how a blast wave seems to follow Equation (2-14), how some believe dissipation is frequency independent while others do not, and just how much variability in the measured vibration attenuations there seems to be. Gutowski and Dym did challenge how representative the existing experimental data is and stated that some of the listed absorption coefficients from these experiments seem too high.

Up to this point in this section, it has been implicit that all damping or dissipation is coming from a signal type of waveform. In reality, the surface motion,

particularly for a steady-state type of excitation, is at least a partial combination of surface and body waves for example Rayleigh, p-waves and s-waves (refer to Figure 2-1). Yang (1981) added a term he called ξ_0, not to be confused with damping ratio, to account for the attenuation characteristics of body waves, assuming that the previously mentioned attenuation equations were solely based on surface waves. He provided the ξ_0 factors in a table based on the distance from the source and applied them as follows:

$$a_r = a_0\sqrt{\frac{r_0}{r} - \xi_0\left(1 - \frac{r_0}{r}\right)}\, exp[-f_0\alpha_0(r - r_0)] \qquad \textbf{(2-15)}$$

where a_r is the acceleration amplitude at distance r, a_0 is the acceleration amplitude at distance r_0, ξ_0 is a correction factor for body waves, f_0 is the frequency of the waveform, and α_0 is the frequency dependent attenuation coefficient.

2.4 Dynamic Effects

It is well known and understood (Kramer 1996, Das 1993, Tedesco 1999, Moretti 2000) that vibrations, whether mechanical or of a waveform, can be amplified or de-amplified depending on the forcing frequency and the system's natural frequency. This can be visualized by considering a pendulum being excited at its support. If the support oscillates from side to side at low frequencies (less than the system's natural frequency), the pendulum will closely follow the support (in phase), which represents motion below the resonant frequency. However, if the support oscillates at high frequencies (greater than the system's natural frequency), the pendulum will experience lower (total) accelerations than the support, which represents motion above the resonant frequency. Finally, if the support oscillates at a frequency close to the system's natural frequency, the pendulum's response will be larger than the support motion, which represents a motion near the resonant frequency. This example represents a simple

single-degree-of-freedom (SDOF) mechanical resonance, but the basic concept holds for multiple-degrees-of-freedom systems and waveform motion albeit in a more complicated form.

2.4.1 Resonance Effects of Seismic Waves

The concept of resonance or the need of a transfer function for seismic waves traveling through different layers or types of media is well documented (Kramer 1996). For a vertically propagating shear wave, when half the wavelength of a seismic wave in a layer is the same as the thickness of the layer, a type of resonance occurs, and this frequency is termed the natural (or fundamental frequency) of the soil deposit. For each successive higher frequency that is a whole number multiple of the natural fundamental frequency (termed wave number), another resonance occurs, but at a lesser magnitude for real damped soil systems. For a single layer of soil setting on an elastic rock, the following transfer function was derived by Kramer:

$$F(\omega) = \frac{1}{\cos(\omega H/v_{ss}^*) + i \cdot \alpha_z^* \sin(\omega H/v_{ss}^*)} \quad \textbf{(2-16)}$$

where ω is angular frequency, H is the thickness of the soil layer, i is the imaginary number for complex notation, α_z^* is the complex impedance ratio between the soil layer and the layer the waveform previously came from, and v_{ss}^* is the complex shear wave velocity given by:

$$v_{ss}^* = \sqrt{\frac{G}{\rho}}(1 + i\xi) = v_s(1 + i\xi) \quad \textbf{(2-17)}$$

This equation can be applied in the frequency domain to determine how individual amplitude components of individual frequencies either amplify or de-amplify. Although the de-amplification of higher frequencies in the transfer function and

material attenuation appear similar and both include the damping ratio, they are not the same as the transfer function shows energy not transferred into the layer and material attenuation is energy turned into heat in the layer. Figure 2-5 shows amplitude ratio F versus circular frequency (in Hz) for a 15 foot thick soil layer on relatively stiff rock. The figure shows multiple resonant peaks that occur at multiples of $f_r \cdot (n\pi - n + 1)$ where f_r is the first resonant frequency and n is an integer, and the magnitude of the peaks decrease with increasing frequency.

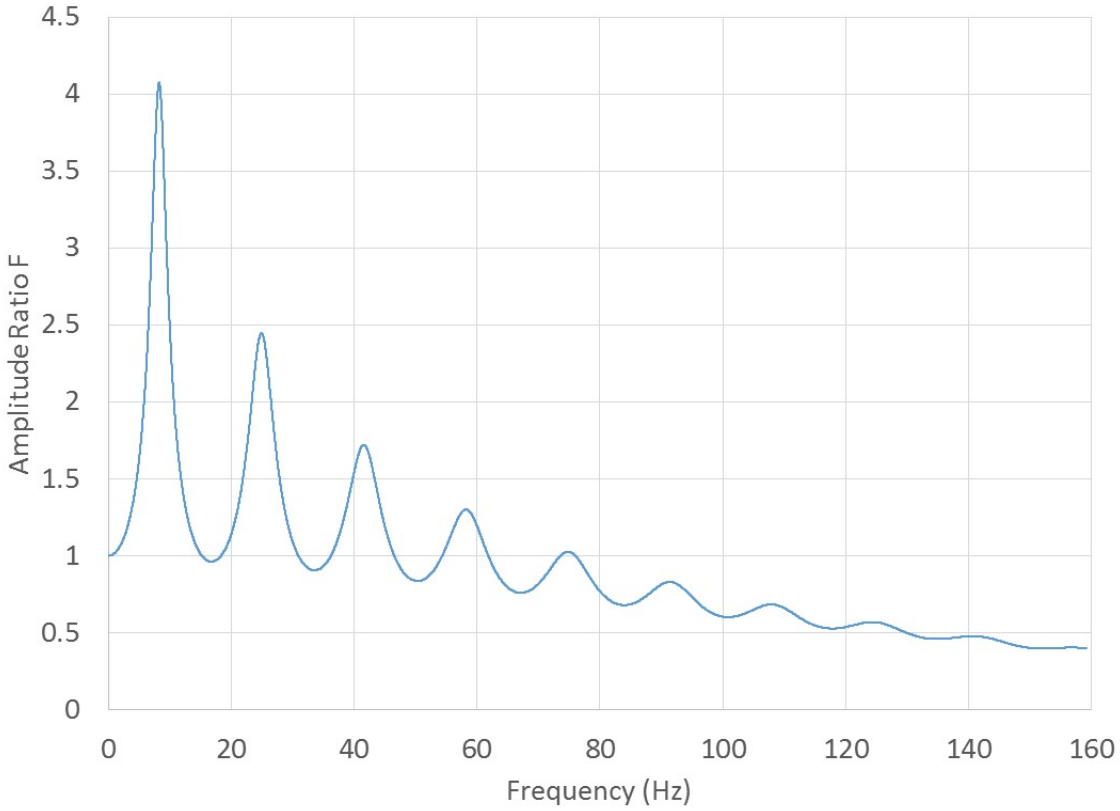

Figure 2-5: Example Soil Transfer Function, Response Ratio vs. Frequency

2.4.2 Energy Transfer from the Source to the Ground

Similar to seismic waves, another transfer function is derived for the mechanical energy transfer, which for the purposes of this thesis, deal with the transfer of the vibrating source energy into the concrete slab and soil system. Although only indirectly

applicable to this thesis, the same theory applies to the concrete slab and soil system transferring the vibration energy into the vibration sensitive equipment.

The theory behind the transfer of dynamic motion is described in detail by Kramer (1996), Das (1993), Tedesco (1999), and Moretti (2000) among others. The response *x(t)* of a for a SODF mechanical system, subjected to a harmonic excitation is given by:

$$x(t) = Xe^{-\xi\omega_n t}[sin(\omega_d t + \phi)] + \frac{X_0}{\sqrt{(1-r^2)^2 + (2\xi r)^2}} sin(\Omega t - \psi) \quad \textbf{(2-18)}$$

where the first half of the expression represents the transient response that exponentially decays with time, where X and ϕ are determined on initial conditions, ω_n is the natural frequency of the system, ξ is the damping ratio, and ω_d is the damped natural frequency. The second half of the expression represents the steady-state motion where X_0 is the static amplitude, Ω is the excitation frequency with phase angle ψ, and r is the ratio of the excitation frequency Ω over the natural frequency ω_n. The transfer function is taken from the steady-state portion of the expression and is given by:

$$F(r) = \frac{1}{\sqrt{(1-r^2)^2 + (2\xi r)^2}} \quad \textbf{(2-19)}$$

The transfer function shows that as frequency ratio r goes to one, the response blows up in the absence of damping ($\xi = 0$) or reaches a maximum for $\xi \neq 0$.

2.5 Related Previous Research and Experiments

Nugent and Zapfe (2012) performed three case studies of vibration levels near rail lines. The first scenario involved a location where a facility that would house a MRI machine would be constructed very close to a freight rail line; in fact, the rail line ended up passing through a tunnel made by the facility. Over twelve days, vibrations

levels where taken at three places on the surface, 13, 52, and 115 feet from the tracks, and from the bottom of bore holes below each surface location at depths of 21, 23, and 118 feet, respectively.

Before construction, the general trend was for lower frequency vibrations to not attenuate very much and higher frequencies to attenuate quickly. With regards to depth, the vibration levels attenuated rapidly at lower frequencies, but the difference in attenuation between the surface and the 118 feet deep location decreased with increasing frequency to near similar values at 200 Hz. However, the shallower depth of 23 feet showed increasing attenuation with increased frequency. The facility foundation ended up being a mat-type foundation supported on piers to bedrock, the 118 feet depth. The foundation system had a modest reduction on the vibration levels, and a specialized MRI machine foundation was not installed.

Case two involved the construction of a vibration sensitive facility roughly 600 feet from a rail line. Although the foundation did not have as large of an effect at suppressing the train vibrations as needed, it did provide a noticeable reduction in vibration levels.

Case three is of particular interest. This case involved the installation of an 80 kip inertial block setting on air springs with half inch air gaps separating the block from the surrounding slab. This foundation performed exactly as expected in that there was vibration amplification at the natural frequency of 1.5 Hz, including ambient levels, followed by no amplification at 2 Hz, and reduction in vibrations above 2 Hz. It is important to note that, with this sophisticated isolation foundation, the only path for energy to travel was through the air springs, which simplified the vibration behavior.

Amick (1999) performed an experiment at a single location to compare the performance of a large solid concrete slab, a small island slab and a small island slab supported on piles. He used instrumented hammer blows a few centimeters from an accelerometer measuring the responses. He found several notable results. First, in the vertical direction, which he notes to typical be the dominate concern, the island on piles clearly had the best performance except for near-field excitations between 50 and 100 Hz where the solid slab performed the best. Second, for nearfield excitation between 1 and 50 Hz, there was no appreciable difference between the island and the solid slab. Finally, horizontal vibrations were even less conclusive as each system outperformed the others at certain frequencies.

Amick (2004) performed a similar test on a single 6 inch slab where he compared an isolated slab to a solid slab. Amick pointed out that simply cutting a slot around the perimeter of a concrete slab in an attempt to attenuate vibrations was not the best solution. First, below 50 Hz there was almost no attenuation between a solid slab and an isolated slab. Second, there was up to an order of magnitude increase in the horizontal vibrations in the isolated slab which can add new problems. Third, above 50 Hz the vertical vibrations did have some level of reduction.

Several recent studies have focused on predicting on how vibrations from railways are generated and travel from the source (Koroma et al. 2014, Domínguez 2007, Hussein and Hunt 2006). These studies primarily focused on modeling how railway vibrations are created and travel very near the source. There is one study of particular interest relating to how inhomogeneity of soil profiles in the path of vibration generated by a railway have a frequency dependent effect on the surface vibrations

(Jones and Hunt 2012). The methods used to determine this effect were completely theoretical, but a large number of cases were computationally simulated, which led the authors to the conclusion that, for an accurate model, the effects of layering must to be considered.

2.6 Summary

The specific case under investigation in this thesis has not been thoroughly documented in the literature. The one mention of determining how far vibrations would travel from equipment located inside a building (Amick 1999) said that the absorption values from that site could not be applied to other sites, and that the behavior is complicated. There is also no mention of how vibrations from multiple sources near a piece of sensitive equipment would affect vibration levels. This thesis seeks to fill existing gaps in our understanding of multiple-source vibrations and attenuation through experiments and model fitting. The results of this research will benefit practicing engineers who need more information as to the nature of vibrations traveling from sources nearby moderately vibration sensitive equipment to make informed design decisions.

3. Experimental Procedure

Chapter 3 describes the general experimental procedure used for all of the data collection experiments referred to in this paper. This chapter also describes the data processing used up to the point where measured acceleration, velocity, and displacement spectrum were created. The data processing and interpretation using the created spectrum is discussed in later chapters.

3.1 Data Acquisition Hardware

For the purposes here, data acquisition hardware refers to all of the physical components used for taking acceleration measurements, namely, accelerometers, cabling, signal conditioners, analog to digital converters, and a computer.

3.1.1 Sensors

Accelerometers are the single most critical and unique piece of equipment for these experiments. Figure 3-1 shows the required sensitivity in micro-g RMS against frequency in Hz to measure to a vibration criteria of "C," which was the lowest level considered in this thesis. As shown in the figure, the required sensitivity to accelerations increases as frequency decreases down to 8 Hz, below which the maximum sensitivity is constant at 63 micro-g.

The sensors used for these tests were miniature, seismic, ceramic flexure integrated-circuit piezoelectric (ICP) accelerometers manufactured by PCB-Piezotronics (PCB, Depew, NY, USA), model number 393B04. These sensors are capable of measuring accelerations of 3 micro-g RMS over a spectrum of 0.04 to 450 Hz with an accuracy of ± 5%. They have a nominal signal conversion rate of 1 Volt per g, with a maximum output of 5 Volts (5 g's). These specifications show that these sensors are

capable of measuring at the level necessary for this project, as well as allowing their use for other types of dynamic measurements of the higher maximum acceleration of 5 g.

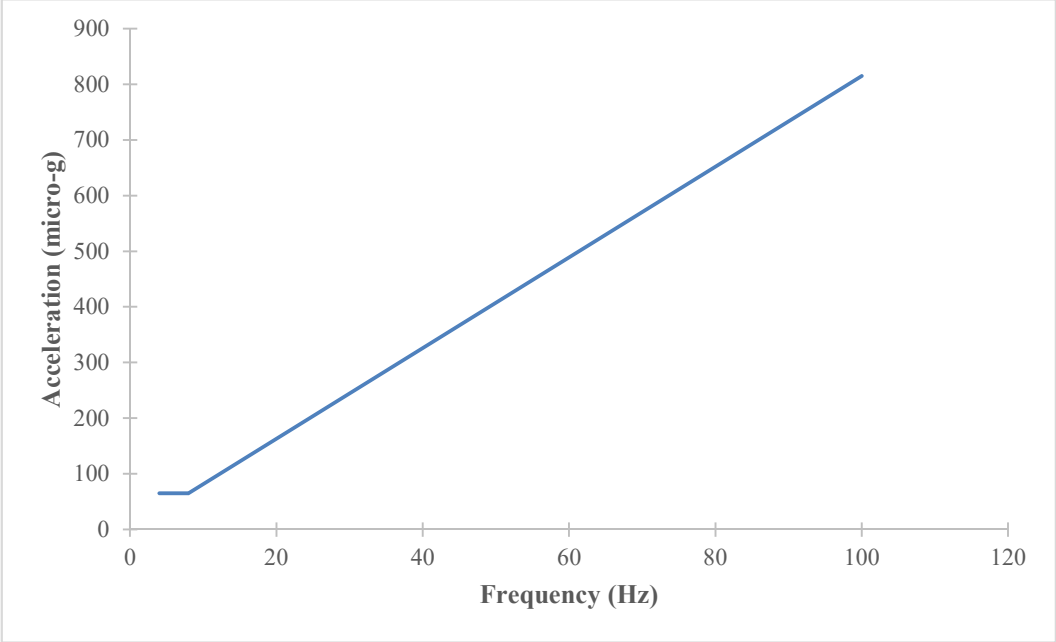

Figure 3-1: Required Sensitivity to Measure Vibration Criteria Level C[4]

However, there are some drawbacks to these sensors. In order to measure at the maximum sensitivity of 3 micro-g, a voltage reading of 3 micro-Volts musts be taken accurately. This has some inherent signal to noise risks. Also, these sensors have a settling time up to 100 seconds and a discharge constant between 5 and 15 seconds. These two factors combine to create risks of taking measurements before the sensor has "settled" and making small measurements at very low frequencies more difficult.

3.1.2 Signal Processing Equipment

ICP sensors have the convenience of using only a single pair of wires, in this case a coaxial type of cable, but the inconvenience of needing to condition the signal by adding a direct current (DC) power signal in the form of a constant current to the

[4] Plot created by taking the derivative in frequency domain of the velocity data in (Gordon 1991)

sensor. This brings the necessity of the next piece of hardware, a signal conditioner. The PCB model 482C05 signal conditioner was used for these tests. This conditioner works with the PCB sensors to effectively power and separate the acceleration signal off of the power signal. The conditioner itself is powered by standard 120 Volt AC electricity, and it can power up to four sensors. The conditioner has a unity gain for simplicity and can handle a sensor acceleration voltage up to ±10 Volts. One drawback to the conditioner is that it has up to a 0.02 VDC offset, and this offset slowly varies causing spurious signal that must be further filtered via software.

The cables between the sensors and the signal conditioner were PCB Model 003C20, low-noise coaxial cable, blue TFE jacket, 20 feet long, with 10-32 coaxial plug on the sensor end and BNC (Bayonet Neill-Concelman) plug on the conditioner end. These cables are significantly thinner than a classic coaxial cable and specially made for accelerometer cabling. The overall cable diameter is 2 mm and the internal individual wires are 29 AWG (0.279 mm).

National Instruments (NI) equipment was used for analog to digital conversion and sending the captured digital information to a laptop via USB. A NI 9239 four channel analog input module with BNC connectors (National Instruments, Austin, TX, USA) was to covert the analog voltage signal from the signal conditioner. The converter used a ±10 V scale on 24 bits with a maximum sampling rate of 50 kS/s (a minimum sampling rate of 1.613 kS/s is required). This makes for about 1 bit per micro-Volt (or micro-g since the conversion used is 1 Volt per g), and allows for almost 3 bits per smallest sensor resolution of 3 micro-g), in other words the converter is more sensitive than the sensors. The noise rating of this module is 70 micro-Volts; however,

most of the input noise was at frequencies outside of the spectrum considered for this project.

The same kind of cable was used between the signal conditioner and the NI 9239 except that both ends are BNC plugs and the cable is only ten feet long.

The analog to digital NI module ran in an eight slot NI CompactDAQ chassis model cDAQ-9178 with 2.0 USB cable output.

The final piece of hardware was a standard windows laptop with a USB port. The laptop ran NI LabVIEW 2015 and saved the data to an external Western Digital hard drive.

Figure 3-2 shows the generic hardware setup with one sensor. Up to four sensors, each with their own isolated cable, can be connected to a single signal conditioner. For each sensor, there is also a separate BNC to BNC cable between the signal conditioner and the NI CompactDAQ. There is only one USB cable.

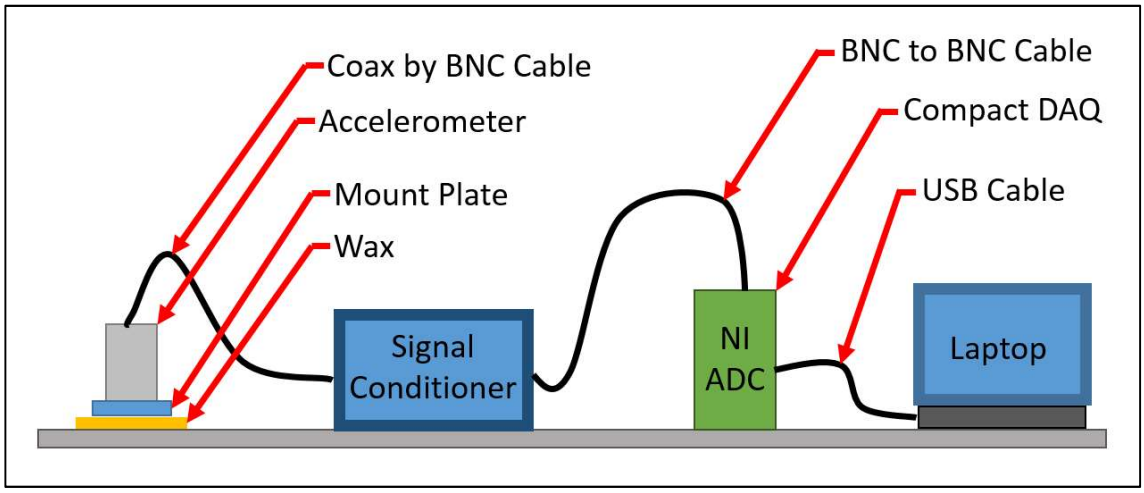

Figure 3-2: Diagram of Hardware Setup

3.1.3 Recommendations on Hardware Improvements for any Future Tests

There are a few changes that could be made to this set up to possibly make more accurate measurements and definitely make processing more reliable with less effort. First, it is worth the signal to noise ratio to use sensors that are 10 Volts per g, instead of 1 Volt per g. This will reduce the impact of the signal condition not being able to perfectly remove the DC from the power part of the signal in the ICP sensors. Second, PCB now makes a better signal conditioner that is more applicable to this type of work, the model 482C24. This signal conditioner can directly deal with sensor settling and compensate for it. The conditioner can apply a specified gain to the output to eliminate the noise concerns of the analog to digital converter. Granted, the signal conditioner costs three times as much as the one used for this work, these two changes would reduce some headaches.

3.2 Data Acquisition Software and Programming

There are a multitude of things that cannot necessarily be seen or physically felt while taking measurements on this level of detail; therefore, it is necessary to create a way to monitor the vibrations in real-time to better ensure the fidelity of the measurements. To do this, a National Instruments virtual instrument (VI) was created that filtered the incoming signals and then plotted the incoming signal and spectra for each channel.

Figure 3-3 details the program flow. First, a sampling frequency and buffer length in seconds is set on the user interface and applied to the input signal in the DAQ controls. For measurements of steady state vibrations, the sampling frequency was set to 2 kS/s and the buffer was set to 5 seconds. The buffer is the length of the data set

that is run through the program at a single time. For these tests, it applies to the filter and fast Fourier transform (FFT) windows as well as the individual frequency widths in the output spectrums. Using the scale feature in the DAQ, a scale of 100,000 was applied to each incoming signal to reduce the decimal lengths of the values so that the standard auto scaling features in the NI charts would function smoothly. If this program was remade, 1,000,000 would be a better choice of scaling factors so that micro-g could be read directly off of the spectrums.

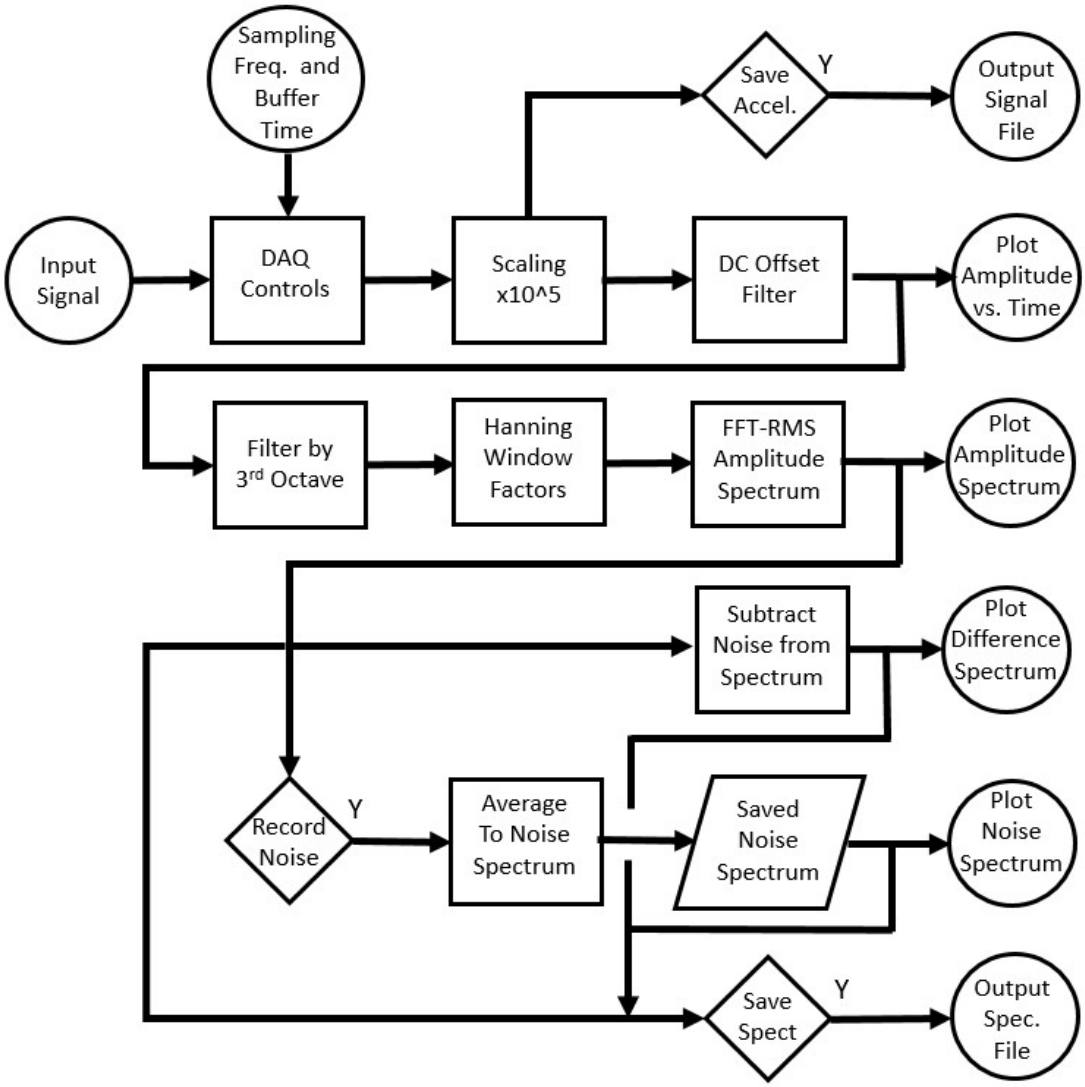

Figure 3-3: NI VI Program Flow Chart

From this point, a user input in the form of a button on the user interface decides if the acceleration data is to be saved to a NI TDMS file. The typical length of data stored for each test was 40 seconds or 80 kS. In addition to the raw, scaled acceleration data, the TDMS file stores the sampling rate, buffer length, total length and absolute times of the data.

In order to plot the real-time acceleration and spectrum on the user interface of the VI, a rolling DC offset filter had to be added. The necessity of this filter goes back to the operation of the signal conditioner. The signal conditioner is operating within its specifications if the DC offset of the signal is below 20 mV, which unfortunately for these measurements corresponds to 20,000 micro-g. This is several orders of magnitude higher than the measurements, especially when trying to measure a "quiet" floor. To add to the complication, this DC offset is not completely steady state as the name implies and typically had a frequency on the order of 0.02 Hz. This might seem like it is a trivial problem that could be resolved with something like a Bessel filter operating in real-time, but the mechanisms a filter like that would require a very large buffer or window length and negate the purpose of a real-time display to ensure that there is no unseen interference during the measurements. Therefore, a special DC offset routine was created that takes an average of the signal every 2.5 seconds (half the buffer) and uses that value, along with the previous value, to form a linear function that is subtracted from the signal. In effect, this subtracts most of the DC offset from the signal conditioner lagging 1.25 seconds. This approach adds an artificial signal, but it is below the frequency of consideration for this work (1 Hz). The good news is that, for post processing the acceleration data, there is no limit to the window length (other than

how much data was collected) which can allow for a small enough frequency width and long enough time signal to directly filter out this DC offset.

The filtered acceleration signal is now plotted on the user interface in units of 10 micro-g, and after giving the DC offset filter a couple of iterations the values are centered enough to clearly see the values each accelerometer is reporting. The plot shows data for 10 seconds and auto-scales so disturbances are visible.

In addition to plotting, the filtered data now goes through a set of Bessel bandpass filters set to third octave upper and lower frequencies from 1 to 125 Hz. Third octaves are further explained in the post processing Section 3.3. Each of these third octaves has a Hanning window applied to it before it is sent through a RMS amplitude FFT algorithm. The individual third octaves are recombined into a complete amplitude spectrum from 1 to 125 Hz. Note that this is not the true third octave spectrum, but the additional detail of finer frequencies helps during field measurements in determining where other disturbances are coming from. This spectrum is plotted every 5 seconds.

Since the measurements for this project were primarily taken in a real operating manufacturing plant and not a laboratory setting, a method for recording noise from other operating equipment was included in this VI. Basically, before (or after) a piece of equipment is turned on to be measured, the background noise in a spectrum is recorded by pressing a button on the interface. The recording makes a running average of six windows (typically 30 seconds) and displays this spectrum for each sensor on the user interface. Initially, this must run a full 30 seconds for the average to be a true average. This noise signal is then subtracted in frequency domain from the current measured spectrum, and this difference is plotted on the user interface. Although this is

effective above 4 Hz, the background noise experienced during actually measurements was typically above 30 Hz and on the order 20 micro-g and, therefore, not large enough to significantly affect results. Below 4 Hz, there is still too much noise from the DC offset to be useful at "quiet" conditions.

Finally, a button on the user interface allows for all three of these spectra to be recorded in a TDMS file, for each window. A counter also displays how many windows of data have been recorded to ensure that enough data has been recorded. Typically, both raw accelerations and spectra are saved for each test. Figure 3-4 shows a partial screen shot of the NI VI created for these readings.

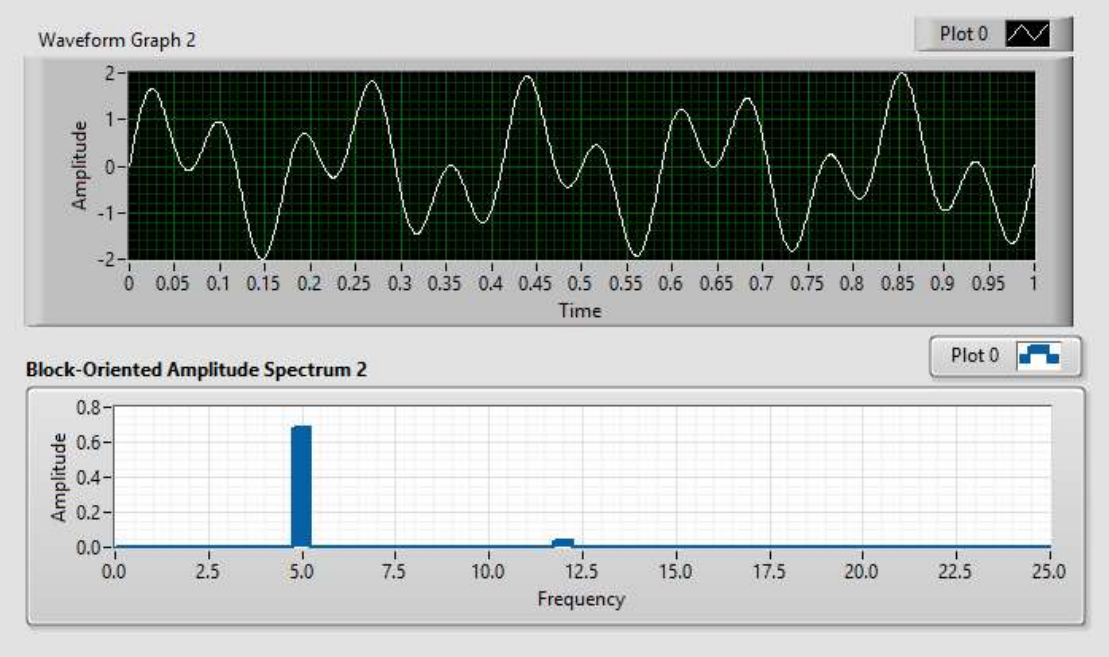

Figure 3-4: Screen Shot of the User Interface of the Virtual Instrument

It is important to mention that a program with this many components must be tested before it is used for actual measurements. To accomplish this, the "DAQ Controls" block shown in Figure 3-3 was replaced with a set of signal generators each with a specified amplitude and frequency. These generators were combined to form a

complex signal and run through the program. The outputs of the program were compared to the known inputs and shown to be identical. This verification was completed for multiple combinations of amplitudes and frequencies including a very low frequency very large amplitude signal to represent the signal conditioner's DC offset, and all cases processed correctly.

3.3 Data Post Processing Program

It is important to describe the signal processing scheme used to turn the raw acceleration data into third octave spectrums for these tests as there are multiple ways to interpret the acceleration data.

First, the TDMS file created by the NI VI was imported to Microsoft Excel simply by double clicking on the file with the National Instruments LabVIEW software not open and Microsoft Excel already active. The rest of the processing was performed using the software PTC Mathcad Prime 3.1.

Figure 3-5 details the basic flow chart of how the Mathcad sheet calculates and displays the results. A sample Mathcad sheet showing all of the detailed calculations is available in Appendix A.

The file name of the Excel data to be analyzed must be input at the top of the Mathcad sheet. After that, the remainder of the sheet is autonomous. Once the acceleration data is loaded, the first action is to apply correct units and conversions. Mathcad has the advantage of storing the units associated with a given variable and prevents errors of mishandled units or unit mismatch (for example, if acceleration is added to velocity, an error will occur and the addition will not take place). For these experiments, the values coming out of the NI VI are in Volts scaled by 10^5. Each

accelerometer has a unique calibration value supplied by PCB given in g per Volt. For this reason, the individual accelerometers were always attached to the same channel in the signal processing system. Note that sensor 1 is not always the closest sensor to the source and therefore did not always have the highest values. In other words, sensor 1 is always the sensor on channel zero of the NI VI. The values now with units of acceleration are stored in a single matrix "acc". These raw unfiltered accelerations are then directly plotted for each sensor to look for any irregularities, such as extremely high absolute acceleration values indicating the sensor was not properly settled before measurements were taken.

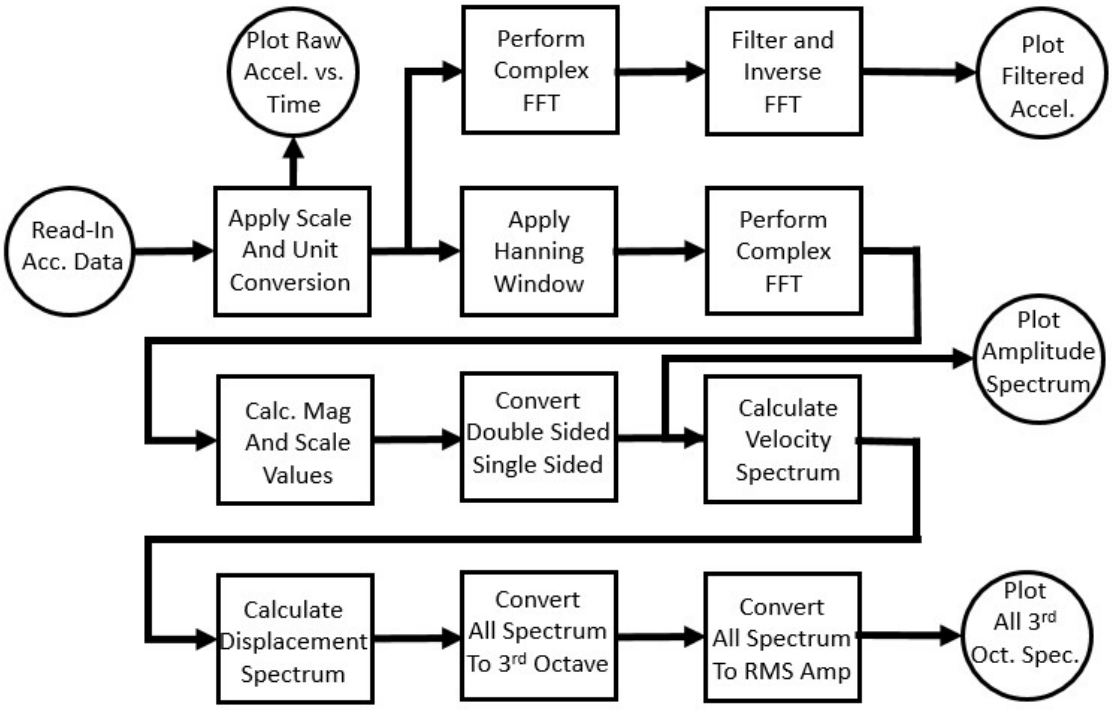

Figure 3-5: Flow Chart for Post Processing Program

At this point, the acceleration follows two paths. The simpler path takes the signal and preforms a Discrete Fourier Transform of complex data using the Singleton method, noted "cfft" in the sheet. The results of this function are given by:

$$c_j = \frac{1}{\sqrt{n}} * \sum_{k=1}^{n} v_k * e^{i\left(\frac{2\pi j}{n}\right)*k} \quad \textbf{(3-1)}$$

where *n* is the number of elements in vector *v*.

For filtering, the complex amplitude values at frequencies outside of the band being considered here, 0.8 to 150 Hz, are simply replaced with zeros. The remaining complex amplitude values are run back through the inverse function of the Discrete Fourier Transform to create a now filtered time signal. A section of this acceleration information is plotted against time to allow for closer inspection of the time portion of the signal. Note that the data at either end of the time scale will be distorted and not useful.

The other path the acceleration data flows through is slightly more complicated and is the path much more important to this work. In this path, a Hanning window the width of the entire data set is applied to the acceleration data. Next the same discrete Fourier Transform is performed on the windowed acceleration data. The magnitudes of the complex values are scaled by one over the square root of the number of samples. The vector of scaled magnitudes that comes out of the transform is symmetric about the Nyquist frequency and therefore must be converted to a single sided vector from zero frequency to the Nyquist frequency. The amount of frequency (df) associated with each element of this single sided vector is simply the sampling frequency divided by the number of samples ran through the transform. At this point, the peak acceleration spectrum can be plotted. The acceleration magnitudes can now be readily converted to

velocity and displacement spectrum by dividing each magnitude in a circular frequency (f) by the angular frequency (ω) and the angular frequency squared (ω^2), respectively.

Finally, these values must be further modified to compare them to third octave RMS values. To convert the spectrum where each amplitude has a constant "width" of *df* to a width that varies depending on the third octave center frequency, first the center values of the third octave frequencies from 1 to 125 Hz were calculated. Now all of the amplitudes between the low and high cutoff frequencies of each third octave are summed and assigned to the center frequency. Finally, to convert these amplitudes to RMS values, each amplitude is divided by the square root of two.

At the end of this sheet, the acceleration values for the third octave spectrum for each sensor are exported to a CSV file for further comparison with other tests.

Since this Mathcad program had multiple places for programming errors, another test Mathcad program was created to verify the proper operation. To do this, a set of ten sine wave functions all with different amplitudes, frequencies, and phase angles were combined into a single waveform. This combined sine function was sampled at 2 kS for 40 seconds and output to a XLS file that matched the structure of the files created by the LabVIEW software. This data file was run through the master post processing program to compare the spectrum with the known spectrum of the input sine waveforms. This test procedure was run several times with varying frequencies, particularly very low frequencies (0.02 Hz) and closely spaced frequencies. The tests verified proper operation.

3.4 General Test Preparations

There are some parts of the setup before taking accelerations measurements that are the same for every test.

First, each individual accelerometer needs to be mounted to the concrete slab. Although for the level of vibrations and the frequencies considered for these tests, simply setting the accelerometer on the floor would suffice, temporarily mounting the sensors prevents unexpected movement and makes securing the cabling easier. For this, beeswax was used. Beeswax is recommended by PCB and other sensor manufactures (e.g. Endevco) because it has the following advantages: (a) high purity forms are readily available and (b) it is easy to install and clean up when finished. Endevco even publishes the following equation for determining the resonant frequency of the wax:

$$f_n = 3.13\sqrt{\frac{AE}{tW}} \qquad \textbf{(3-2)}$$

where A is the contact area, E is the wax modulus of elasticity (5 x 10^4 psi), t is the thickness of the wax, and W is the mass of the sensor in pounds. For these tests the wax thickness was significantly below 0.1 inches, resulting in a natural frequency above 10 kHz, far above the need to include this consideration in these calculations.

To apply the wax, a small piece of wax was cut from a beeswax block and placed into a stainless steel quarter cup measuring cup. Wearing standard work gloves, the wax was heated using a standard air heat gun similar to a high powered hair blow dryer until all of the wax turned to a liquid. The wax was then heated for an addition 10 seconds and poured into a mold slightly larger than the sensor mount. Very quickly, the mount without the sensor installed was pressed into the liquid wax. Since the sensor

mount quickly spreads out the wax, it hardened nearly instantly. This allows for any small voids to be filled in the concrete, and it makes the sensor secure enough to avoid any inadvertent movement. To remove the sensor mount and wax, first the accelerometer was removed and safely stowed. Using a standard putty knife, the mount was pried up and the wax effortlessly scraped off the floor and mount. The wax was discarded as it turns out to be very effective at removing dirt from the floor as well.

The sensor mount plate and wax mold were made from quarter inch thick Lexan. The mount plate had a twofold purpose. The plate separated the sensor from the mounting wax, and it provided electrical insulation to help reduce any possible signal ground loops. The plates were cut to 1.5 x 1.5 inch squares and had a 10-32 threaded hole in the center.

Once the sensor plates were secured with wax in the desired locations and the locations clearly recorded on a scaled drawing of the test area, the sensors were screwed down onto the plate. Red electrical tape was placed around each sensor to make the sensor easier to see on the floor. Next, the signal cable that ran from the signal conditioner to the sensor was clicked into the BNC plug on the conditioner and then carefully screwed into the coaxial port on the sensor taking special care not to allow the center of the cable to rotate relative to the sensor; the coax cable end is very delicate. The cables were ran in such a way that there were no loops and only limited cable crossings. The cables were taped to the floor with colored electrical tape so that the cable could not move as cable movement can cause signal noise. Thereafter, the BNC cables connecting the signal condition to the NI CompactDAQ were installed noting the unfortunate labeling difference between PCB and NI that PCB starts numbering from

"1" and NI starts from "0". Just for clarification at this point, for this entire report and all of the programs and analysis sheets, the PCB standard is used starting at "1".

After all of the cabling was connected and secured, all of the devices, signal conditioner, CompactDAQ, and laptop were plugged into the same General Electric surge suppressor to ensure a common ground. The surge suppressor self-verified that the system was electrically grounded.

The locations of the sensor placement were chosen based on the relative magnitudes of the vibration source equipment after making some preliminary measurements. The sensors were spaced out in the available area, but close enough to the source to make accurate measurements. The precise sensor locations are described in Chapter 4.

3.5 Acceleration Measurement Verification

Since these experiments involve multiple complex components, such as sensors, signal processing hardware, data acquisition software, and signal processing software, it is necessary to perform a test with known results and verify that this entire measuring scheme correctly functions. The method PCB recommends for sensor calibration is to attach a "gold plate" sensor which is known to be accurate back to back with a sensor in question, apply a vibration and ensure that the two vibration signals are mirror images of each other. This would only partially test the system here and the sensors used were all brand new at the start of these experiments with certified calibration documents so a unique test had to be created.

A Delta scroll saw was chosen for this experiment because (a) it was readily available, (b) ran at a constant frequency, and (c) displacements on the arm could be

relatively easily measured. The saw used had a tenth horsepower eight pole inductive motor (switchable to four pole) that enables it to rotate at a stable frequency of slightly less than 15 Hz. The motor was directly coupled to the cutting arm assembly, and therefore the arm oscillated at the same known frequency of the motor. The relative displacements of the arm could be measured by manually rotating the electric motor and thus giving a known displacement. Finally, the arm displacements were clearly of an order of magnitude higher than any secondary vibration modes since the vibrating arm was made of steel with the intent of being rigid.

The setup involved creating a mount plate that could hold all three sensors on the single plate out of the same electrically nonconductive material used for the primary mount plates. This plate was attached to the upper saw arm using beeswax. The plate was manually pull tested and the saw ran at the higher speed for several minutes to ensure the mount plate would not separate from the saw during testing with the sensors attached. Figure 3-6 shows the saw used with the three accelerometers attached.

Figure 3-6: Scroll Saw with Sensors Attached

Before the test began, physical displacements were measured both vertically and horizontally. The terms vertical and horizontal refer to measurements from a fixed point, not the exact movement of the sensing element itself. The path of the sensors was assumed to be along the vector of the measured movement. The true movement is slightly more complex, but since the primary point of this test is to verify the overall operation of the combined measurement system and not exact calibration of the system, the vector path was deemed acceptable. As shown in Figure 3-7, a dial indicator was used to measure the vertical travel of each sensor. A caliper was used to measure the horizontal displacements from a fixed point near each sensor.

Figure 3-7: Vertical Displacement of Saw Arm Measurement

Table 3-1 shows the physical measurements of the sensor travel in inches. The RMS displacement amplitude of the vibration is half of the vector distance divided by square root of two. The RMS displacement value around 15 Hz is the quantity to compare against the output of the acceleration measurement system.

Table 3-1: Physical Measurements of Sensor Travel

Vertical (in)	Horizontal (in)	Vector (in)	RMS Disp. (in)
0.100	0.038	0.106	0.038
0.183	0.046	0.188	0.066
0.258	0.061	0.264	0.094

After all of the physical measurements were recorded, the saw was started and allowed to come up to speed. At this point, 40 seconds of steady state acceleration data were recorded following the same procedure used for all measurements in this report. The data was run through the same signal processing Mathcad routine used for all of the testing. Focusing on the RMS displacement spectrum shown in Figure 3-8 created from integrating the windowed acceleration value twice in the frequency domain, the RMS displacement magnitudes can be compared with the physically measured values from the 16 Hz third octave. The peak acceleration value for this motion occurred at 14.75 Hz and all of the nearby values fall into the 16 Hz third octave band, 13.92 to 17.54 Hz, which allows an easy comparison of a single value.

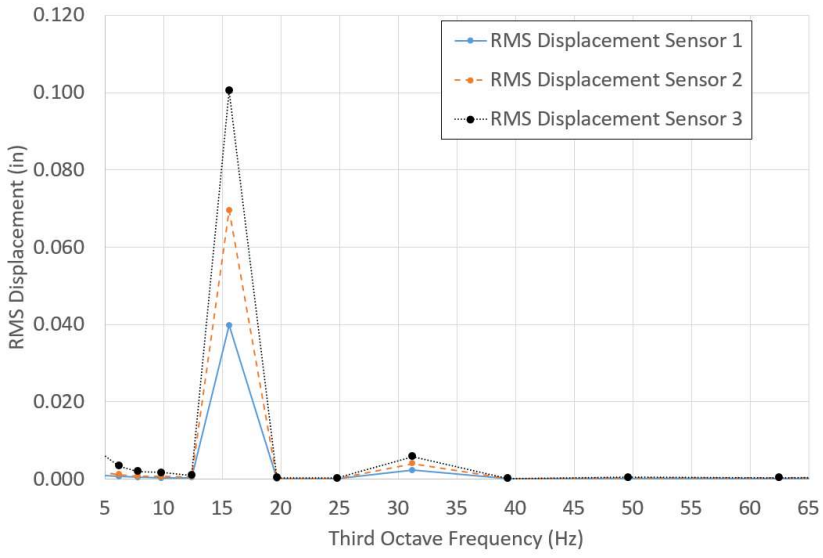

Figure 3-8: Third Octave Spectral Displacements

The comparison shows very good agreement between the physically measured and acceleration calculated displacement values. The percent differences are below seven percent for all three sensors and corresponds to absolute difference less than 1/64 inch, which is realistically the limit of accuracy to the physical measurement method used here as well as the specified broad band accuracy of the accelerometers. The frequency of the displacement motion, 14.75 Hz, is exactly where it was expected at a little less than 15 Hz accounting for the necessary field slip in the inductive motor. The second mode is clear as well at 29.5 Hz, shown in the 31 Hz third octave band in Figure 3-8, which is expected as the geometry of the saw has obvious motion in multiples of the motor rotational frequencies. In fact, although not visible in the displacement third octave figure, additional modes at multiples of the fundamental 14.75 Hz frequency can be seen from the acceleration spectrum. Figure 3-9 shows the standard spectrum (not third octave) for a single sensor showing the multiple modes.

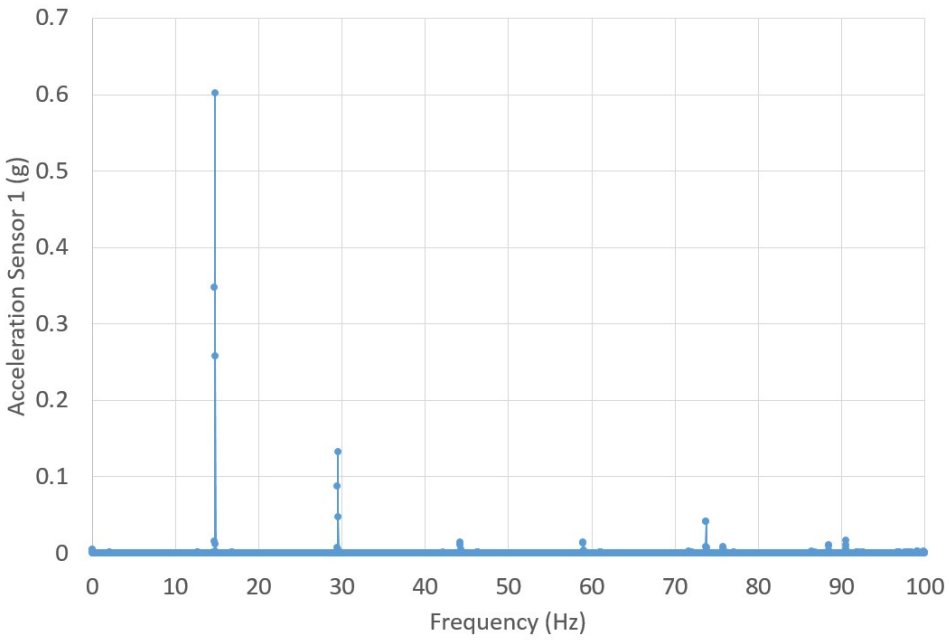

Figure 3-9: Acceleration Spectrum Values from Sensor 1

4. Individual Equipment Tests and Results

Chapter 4 contains the results of the measured attenuation of the vibrations created by various pieces of equipment that might be found near sensitive equipment.

4.1 Initial Test on Heat Exchanger

This section details the first field test of an actual piece of industrial equipment covered by this thesis. In addition to providing some vibration data, this test highlighted some areas of necessary improvement, particularly in the area of signal processing, sampling rate and sampling length. The hope in mentioning these challenges is that anyone trying to duplicate these experiments could save significant time and effort.

4.1.1 Heat Exchanger Test Description and Setup

The piece of industrial equipment under investigation in this section is a skid mounted heat exchanger system bolted directly to the eight inch thick concrete slab. This type of system can be found in many different types of locations and could be located near vibration sensitive equipment. The major components of the system are pumps, a plate heat exchanger, control valves and piping. The purpose of this particular heat exchanger system is perhaps a bit counterintuitive. Process chilled water is piped throughout this industrial building and supplies a cold side temperature around 45 degrees Fahrenheit, which is cold enough for most uses. However, there is still a lot of industrial equipment that needs cooling water, but for these types of equipment if the cooling water temperature is below the ambient dew point, condensation will occur with the worst case result of ruined equipment and at the very least a mess and slip hazard. So a heat exchanger system is installed to allow for controlled raising of the cooling

water temperature while still using the building cooling system. The point is, the need to regulate cooling water flow can result in a vibrating pump to be placed right next to vibration sensitive equipment, both installed on the same concrete slab.

There were a few differences in the test setup than what was described earlier in the general test preparations of Chapter 3. First, the sensors were not adhered to the floor with beeswax, but rather just set directly on the concrete. Second, the cabling to each sensor was not taped to the floor. Finally, there was no explicit consistency on how many samples were taken for each vibration test.

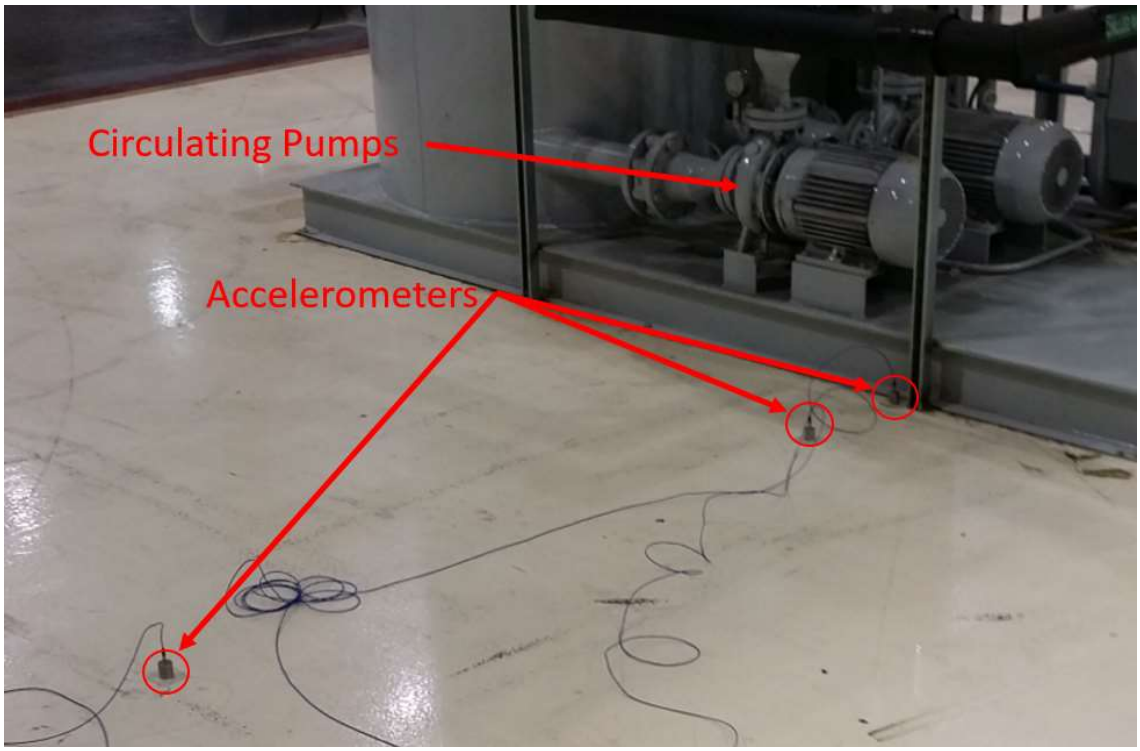

Figure 4-1: Vibration Tests near Heat Exchanger

The basic sensor placement is shown in Figure 4-1 along with the heat exchanger skid in the background. The water circulating pumps can be seen as well. Nine total sets of acceleration readings were taken. The first three sets had sensors located six feet from the skid, one foot from the skid, and directly on the closest edge of

the skid. The next three sets were taken at similar locations except the sensor on the skid was moved off the skid and placed directly on the slab next to the skid. This is the test shown in Figure 4-1. The final three sets of measurements were taken with one sensor on the edge of the skid, the next six feet from the edge of the skid and the third sensor eleven feet from the skid.

4.1.2 Initial Problems with Data Processing and Corrections

The first field test highlighted several issues with achieving meaningful results as the acceleration signals looked more like noise than useful information. Even though these problems were eventually resolved, the fact that they did occur and took significant effort to address, points to the need to include s background to help others avoid similar time intensive endeavors.

Figure 4-2 shows the velocity spectrum results initially calculated from the data. Although it may not be obvious, this interpretation cannot be correct. There simply is not a vibration of 1500 μ-in/s at 3 Hz for this location as that would easily be physically felt by a person, and there were no vibrations a human could feel during the test. The value of 100 μ-in/s at 60 Hz is possible as the pumps were two pole inductive motors turning near 60 Hz, but the low frequency noise throws the magnitude of that measurement into question.

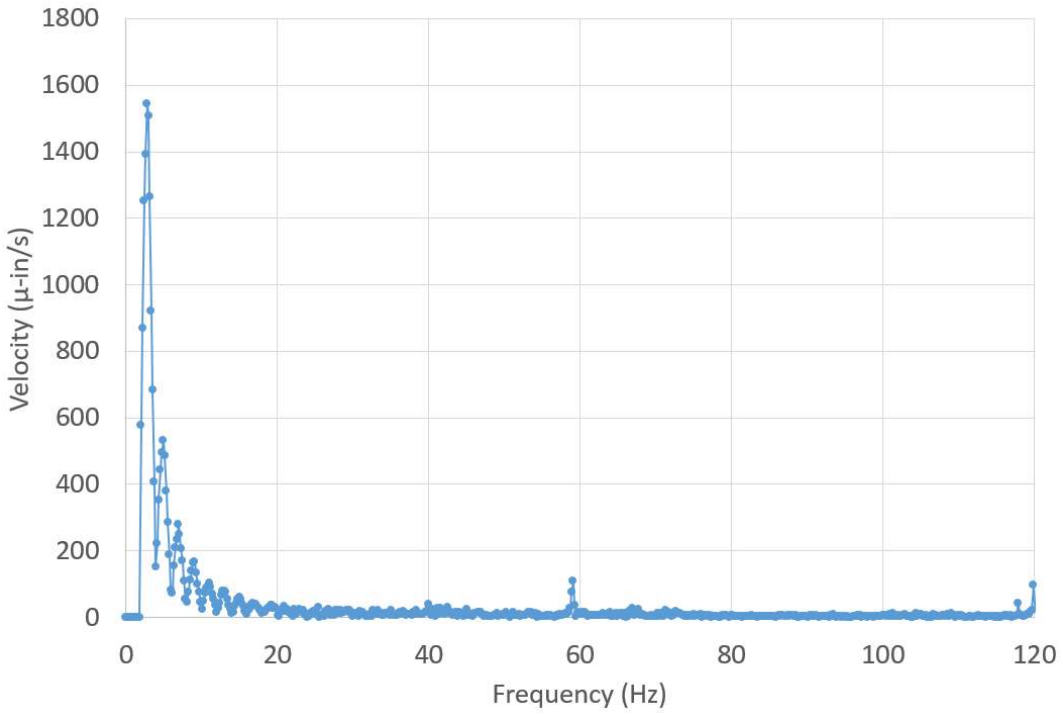

Figure 4-2: Example of Initial Velocity Spectrum

This interpretation was created not using the post processing program described in section 3.3, but rather eventually led to the development of that program. The process to create results like the ones shown in Figure 4-2 was as follows. First, a set of data of length 2^{13} samples was extracted from the middle of the overall data set. Since the sampling rate was 1612 samples per second, this amounts to about 5 seconds of data from the total of slightly less than 10 seconds. The average of the samples was calculated and subsequently subtracted from each sample to perform a DC offset. Next, a Fast Fourier Transform (FFT) was performed using the Cooley-Tukey algorithm. To attempt to filter the low frequency "noise," which was believed at the time to be caused by taking a measurement before accelerometer settling had occurred, the first 10 frequency data points, about 2 Hz and below, in the acceleration spectrum were forced to zero (this actually reduced the low frequency noise by a factor of 10). An inverse

FFT was perform on the modified acceleration spectrum to create a filtered time spectrum. Using the time domain data from the inverse FFT, a simple discrete integral was performed by multiplying each acceleration value by the time step and specifying an initial condition that made the data look the cleanest. Finally, another FFT was performed on the velocity time domain data to create the velocity spectrum as shown in Figure 4-2.

There were several problems with the aforementioned procedure that left the signal looking too much like noise. The problem here originates with the operation of the PCB signal conditioner. The signal conditioner sends a DC power signal on top of the measured signal and then separates the power portion of the signal from the measured signal and outputs only the measured signal to the NI analog to digital converter. In an ideal world, the signal conditioner would perfectly remove all traces of the DC power signal and output only the desired measured signal; however, this does not happen in the real world. The operating specifications of the PCB signal conditioner attempt to keep the DC offset below 20 mV, which for the measurements taken here corresponds to 20,000 μg. The frequency at which this DC offset varies depends on several environmental factors and for the measurements taken during these tests varied between 0.02 to 0.04 Hz. The lowest frequency under consideration here for sensitive equipment is 1 Hz with a magnitude of 63 μg. The initial method did not confine the slow moving DC offset to a tight single lobe and because the orders of magnitude between the measured signal and DC were so different, the DC offset leaked into the measured signal. Figure 4-3 shows the comparison between the initial

ineffective method and the final method on the exact same acceleration data set. Note that the final method does not incorporate a DC offset removal.

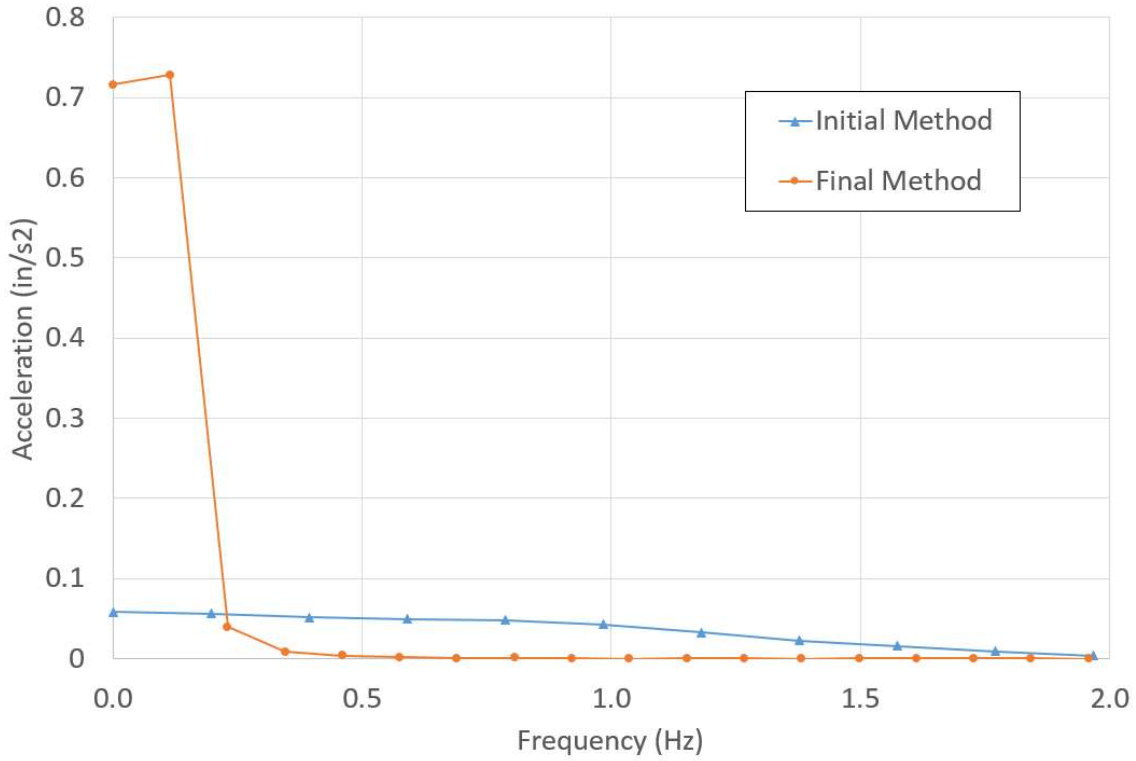

Figure 4-3: Initial Spectrum Method vs. Final Spectrum Method

Although it might not be entirely obvious the why the final method is significantly better (or even if it is better), the final method leaves a useful signal over the desired spectrum 1 to 100 Hz. The significance between the two methods becomes painfully obvious after recalling that sensitive equipment is more concerned with the velocity or displacement, and this acceleration is integrated to achieve velocity or displacement spectrums. In the frequency domain as shown in Figure 4-3, the magnitude of the velocity at each frequency is determined by dividing each acceleration magnitude at a frequency by the angular frequency (rad/s). Therefore, accelerations at lower frequencies have a higher impact on velocities and can overshadow the real measurement. For example, the 50,000 μ-in/s^2 acceleration observed at 1 Hz

corresponds to an 8,000 μ-in/s velocity, and a 50,000 μ-in/s^2 acceleration at 60 Hz, corresponds to only 130 μ-in/s. In a sense, the 1 Hz velocity noise is orders of magnitude greater than the measured 60 Hz value.

The improvements over the two methods are as follows. First, the length of the signal is not confined to powers of two, and, as can be seen in this case, it allows for a slightly higher resolution in the frequencies. Second, all of the DC offset is confined below 0.5 Hz which allows for an accurate real measurement at 1 Hz. With the initial method, even though the DC offset was less from the attempted direct removal, the DC offset still leaked out to 2 Hz in this case (and went even further in other cases). Third, since the final method is not confined to the length of the signal as a power of two, a longer sample of harmonic vibration source can be taken without having to double the sample length, which allows for higher resolution. In fact, if the data set is long enough to contain a cycle of the slow moving DC offset, the final method can assign it precisely to its frequency. Finally, although a Hanning window could have been applied to the initial method, which would have improved the analysis, but still not to the level necessary. (Applying a Hanning window has the effect of reducing the convolution effect of the FFT on the signal. When a finite length of data is extracted from a repeating set of data, the extracted set itself appears as a new signal at a period of the extracted length referred to as a window. This creates a convolution between the actual signal and the window. Apply a Hanning window, or similar window, to the measured data attempts to remove this convolution so the FFT returns the actual spectrum for the real data (Shin and Hammond 2008)).

For just a cursory mention, applying filters was attempted and abandoned for the final method described in section 3.3. For example, band pass filtering between 1 and 150 Hz using several types of filters in both real-time and frequency domain were tested. None of the filters were very successful at maintaining a useful measured signal at 1 Hz while eliminating the signal conditioner DC offset drift.

4.1.3 Final Results for Heat Exchanger Test

The good news is that a method was developed and tested, which allowed useful results, even of the initial data taken during this test. Figure 4-4 shows the velocity spectrum at varying distances measured from the edge of the heat exchanger skid. The velocity level at 6 feet can be compared to Figure 4-2 to visualize the processing improvement. For reference, the Vibration Criteria Curve at level C (VC-C) is shown in the figure, and it can be seen that within 6 feet from the skid, the vibration level has already dropped below the criteria for VC-C.

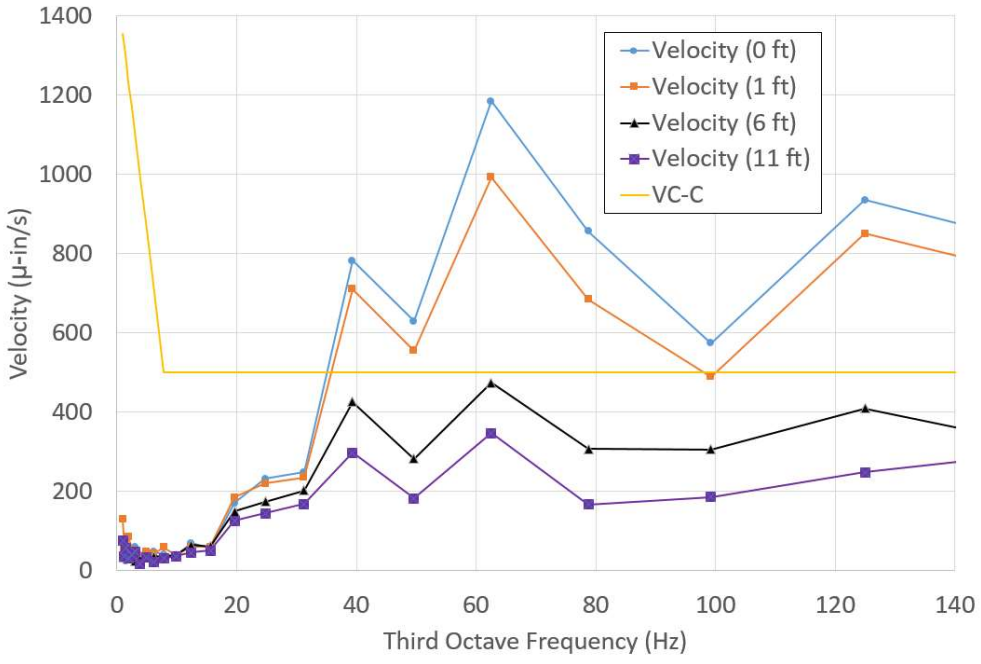

Figure 4-4: Third Octave Velocity Spectrum for Heat Exchanger

One of the key aspects to this work is the ability to predict how quickly a vibration attenuates with distance from the source. There were three methods considered for analyzing the data sets on a third octave band basis. The first method took the three acceleration measurements from a single test in a single band, and then performed a generalized function fit using the Levenberg-Marquardt method comparing least squared error to determine the coefficients A_1 and β of

$$A_r = A_1 \left(\frac{r_1}{r}\right)^p e^{[-\beta(r-r_1)]} \quad \textbf{(4-1)}$$

where A_r is the acceleration amplitude a distance r from the source, A_1 is the acceleration amplitude at a unit distance r_1 from the source, p is the reduction factor for geometric damping and β is the absorption coefficient.

For the heat exchanger skid, there are some assumptions that must be made to simplify the behavior. In order to use a geometric damping factor, p, of 0.5, the source must be considered a point source. The skid is on the order of 10 feet by 8 feet and the center was assumed to be 4 feet from the measurement point. This is opposed to assuming the source is a line source with a coefficient, p, of zero, which is more realistic for the measurements close to the skid, but not for farther from the skid.

Figure 4-5 shows the accelerations of the 62 Hz third octave band plotted with the fit of Equation (4-1) with fitted coefficients A_1 of 5.2 in/s and β of 0.12 ft^{-1}. The curve fit is somewhat good and technically has a Pearson's correlation of 0.999; however, that is a little misleading from the scales involved.

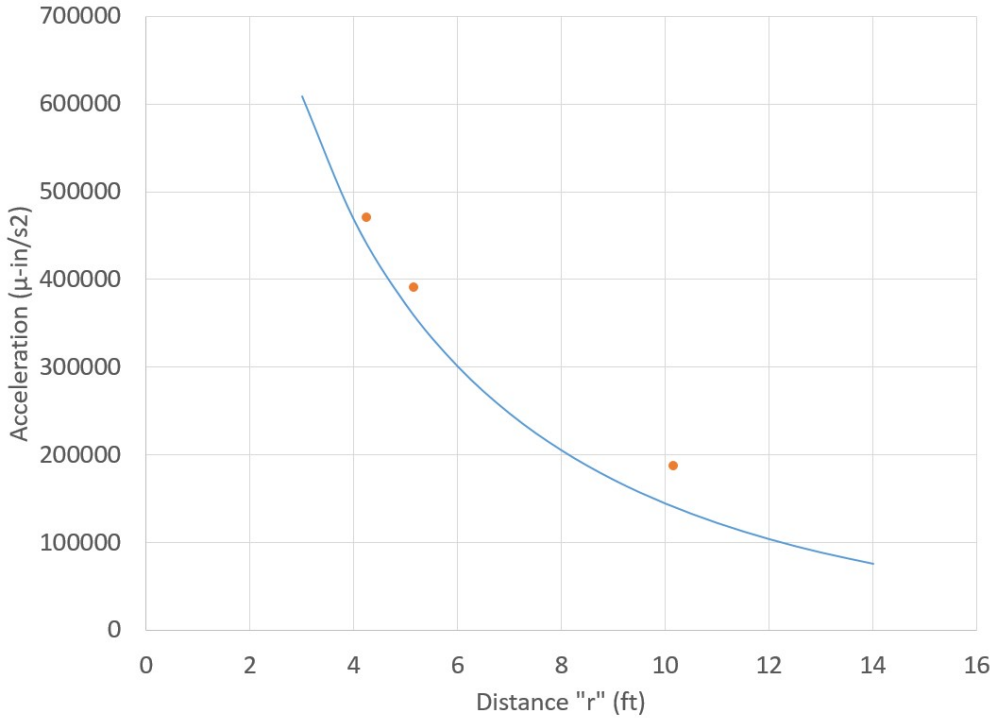

Figure 4-5: Acceleration vs Distance and Levenberg-Marquardt Curve Fit

After the coefficients A_1 and β are calculated for each third octave band and each test on a piece of vibrating equipment, the results of the coefficients were plotted together and averaged to determine the final coefficients A_1 and β. Only third octave bands with data above the noise level were used. Figure 4-6 and Figure 4-7 show the results for β and A_1, respectively. As can be clearly seen, there is significant scatter with these results. However, one issue with this specific set of data is that six of the nine data sets only had two accelerometer measurements since one of the accelerometers was sitting on the skid (unusable) and not the concrete slab. This caused the curve fitting function to not behave completely stable. The remaining tests for this project all had at least three data points which made the curve fitting function reasonably stable. Still the results are not infinitely variable and do capture some limits of the behavior.

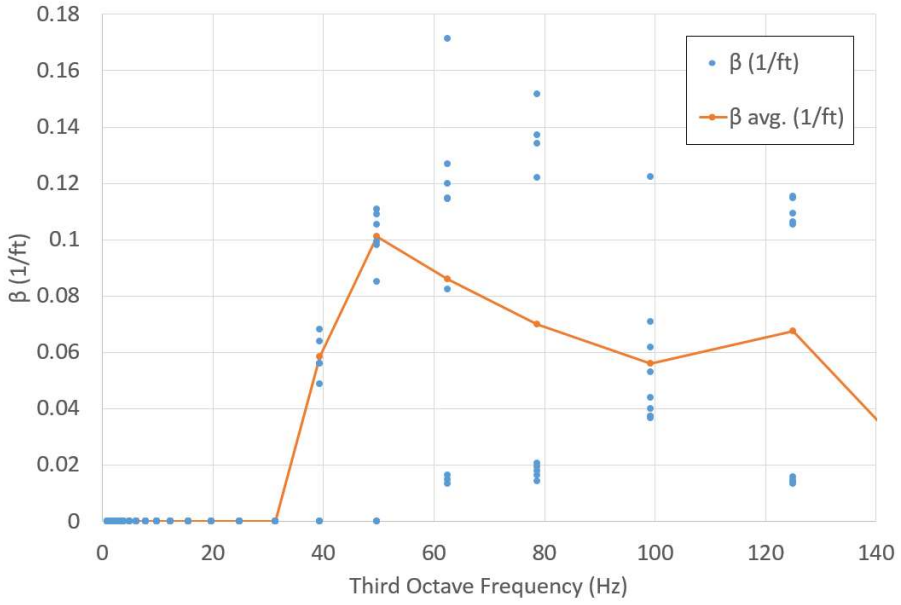

Figure 4-6: Individual Test β Measurement Spectrum

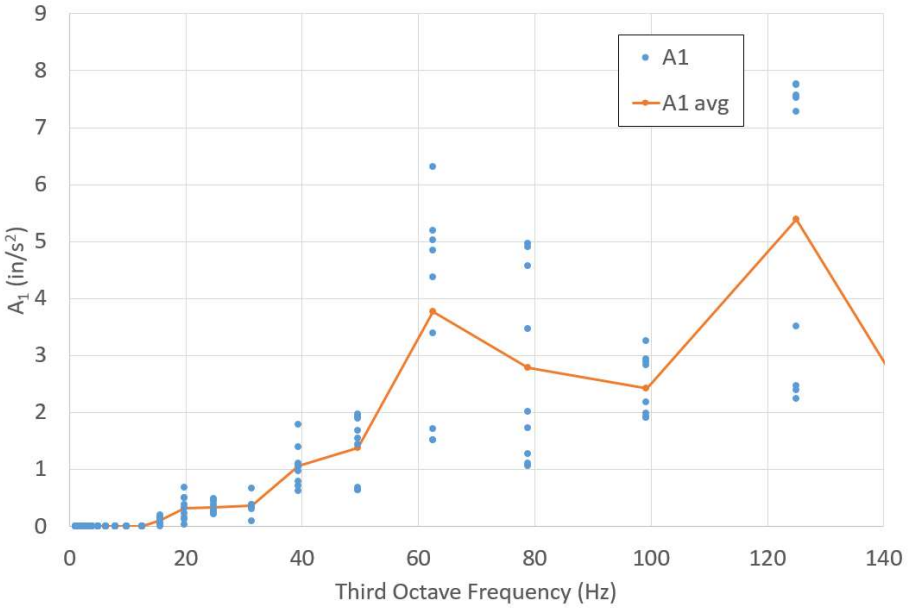

Figure 4-7: Individual Test A_1 Measurement Spectrum

The second method used for analyzing the decay in vibrations was to combine all of the acceleration measurements for a single piece of equipment at each third octave band and perform a Levenberg-Marquardt curve fit for the combined data to determine coefficients of Equation (4-1). Figure 4-8 shows the measured data from all nine tests

from the 62 Hz third octave. The curve fit function calculated β as 0.078 ft^{-1} and A_1 as 4.03 in/s^2.

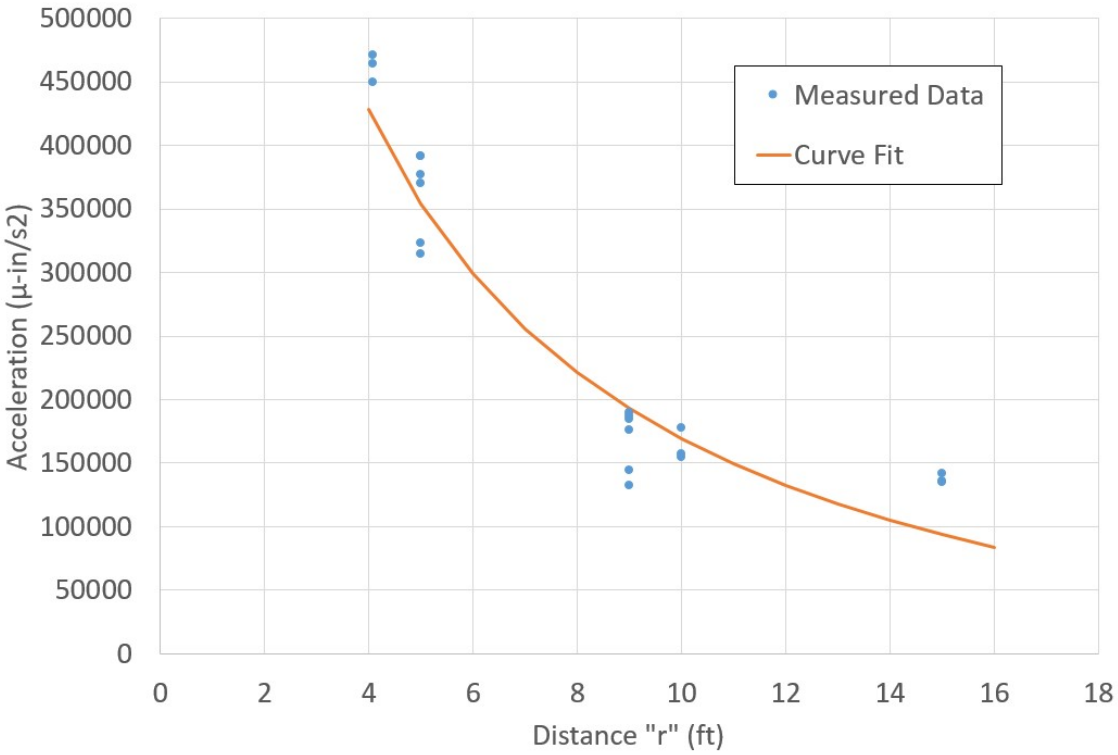

Figure 4-8: Acceleration Decay with Curve Fit from All Tests

Similarly, Figure 4-9 shows the acceleration third octave spectrum created from combining all of the test data before performing a curve fit. This provides a much more stable mathematical result than the first method described; however, since these measurements did not happen at the exact same time and the equipment providing the vibration source is real world industrial equipment, this second method can hide variability.

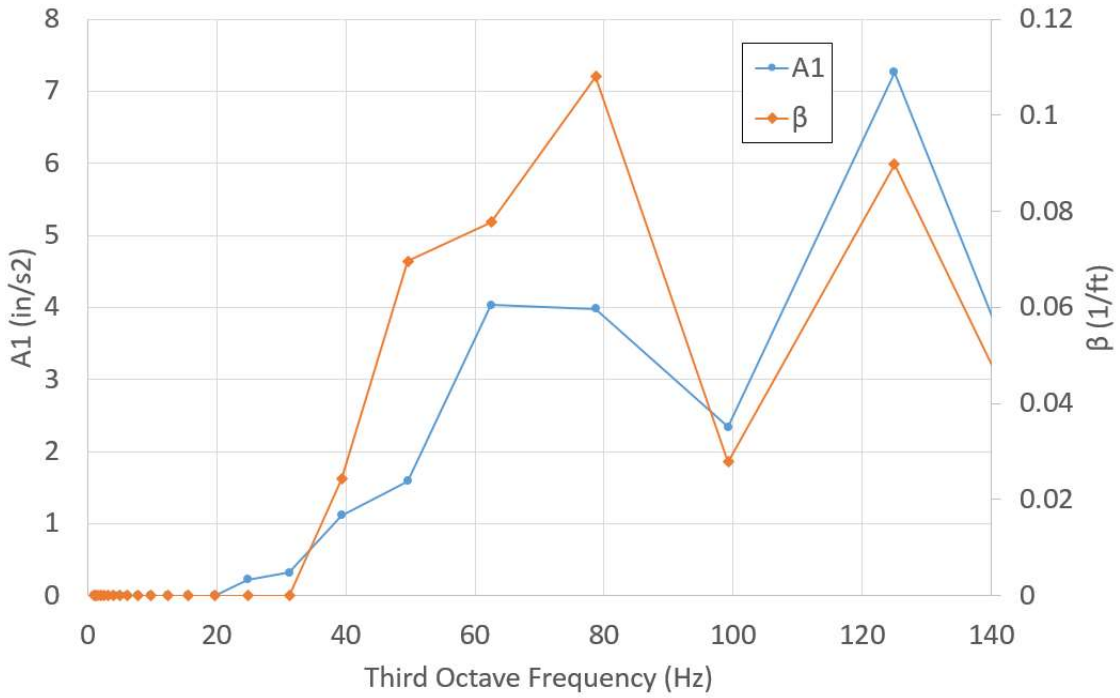

Figure 4-9: Combined Measurement Spectrum of β and A_1

The third method involved directly solving Equation (4-1) for β and using actual measurements for all values of r and A for each test at each third octave. This creates three values of β (sensor 1-2, 2-3 and 1-3) for each set which are combined, and the value of A_1 at the unit distance r_1 can then be back calculated. Figure 4-10 shows the calculated β values between the farthest two sensors, 2-3. Low acceleration values were omitted below the 40 Hz band. Once again, there is still significant scatter of the absorption values, but not unlimited variation.

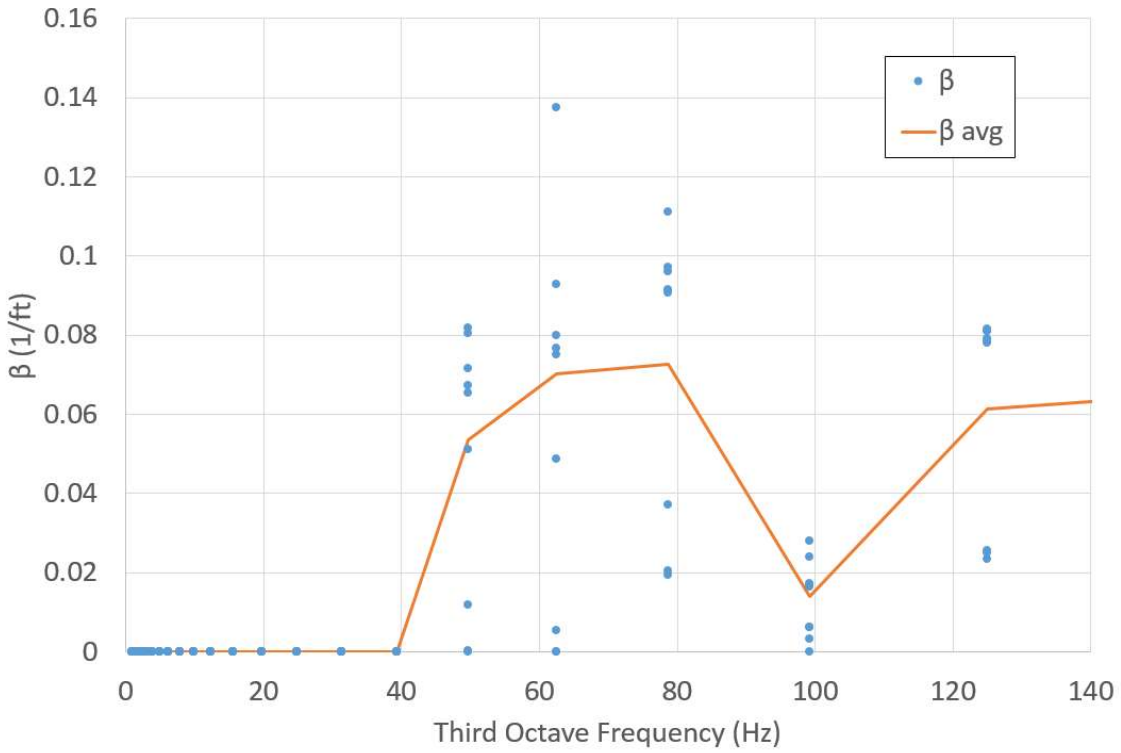

Figure 4-10: Direct Calculation of β in Third Octave Spectrum

Plotting the averages for the three different methods described here for the heat exchanger is shown in Figure 4-11. The three methods each have different assumptions, which affect the results, but the results show that the differences in β are not extreme. Unless otherwise specifically noted, the rest of the results reported later in this paper use the first method described for determining the average β and A_1. In a few instances, the third method was used to determine β, particularly where one of the three accelerometers was placed in a location that gave unusable information.

There is one trend that is obvious from this data that will similarly repeat for other locations. How the absorption coefficient varies with frequency is definitely not constant nor does it vary at a simple linear rate as several previous studies described in Section 2.3.3. Figure 4-11 appears to have two peaks showing as frequency increases to a point, the absorption coefficient increase, then it decrease, followed by increasing

again. Comparing these results to the values listed by Amick (1999), all of the values appear to be higher than expected and imply a more complex behavior. This behavior will be discussed more as more results are described.

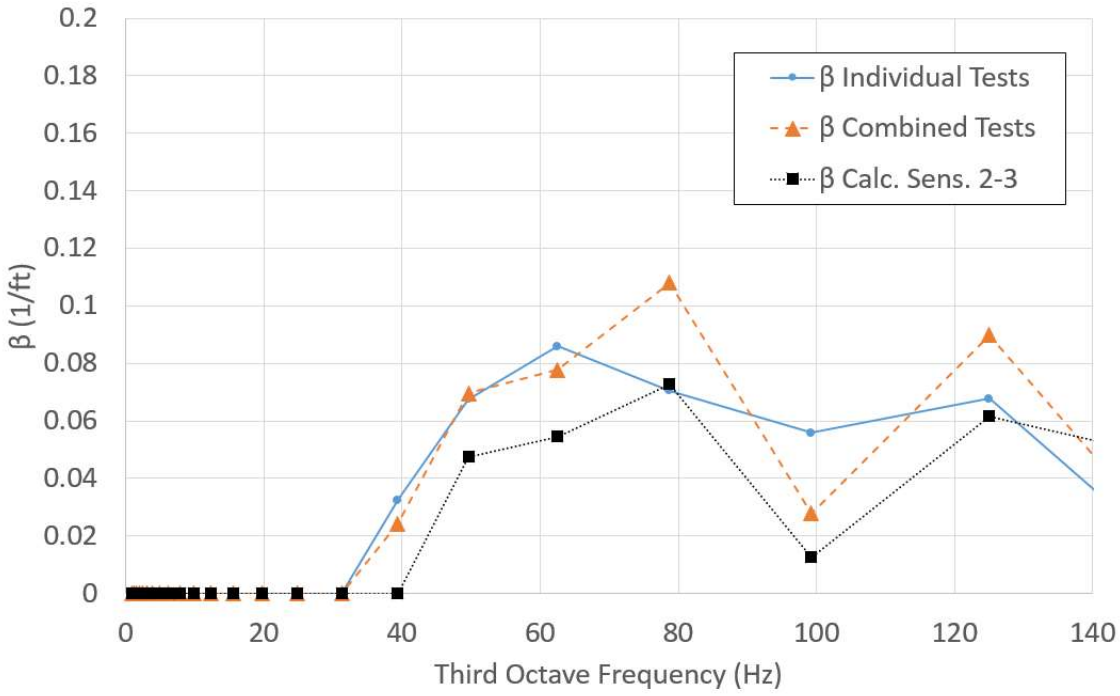

Figure 4-11: Combined Results of All 3 Methods for Calculating β

A final important aspect to consider for this test on a heat exchanger is the measured speed that the vibration wave travels. The acceleration time measurements from the furthest two sensors from the stand were compared to try to determine how much time passed as the vibration traveled. Since the vibrations caused by the pumps on the heat exchanger were not that large nor was it easy to determine exact peaks to compare, a short length of the data, about 0.1 seconds worth, was windowed with a Hanning window and run through a cross correlation function. Figure 4-12 shows the plot of the cross correlation function between two sensors against lag time. The idea is that the two signals will have higher correlations at a given lag time which indicates a

possible phase difference in the two signals. Although it is not perfectly clear, Figure 4-12 shows positive correlations, one at 0.0037 seconds and the other at 0.0118 seconds. Since the physical separation between the two sensors radially measured from the heat exchanger skid was 5 and 6 feet, respectively, a maximum possible velocity of the waveform is 510 and 1350 ft/s, respectively. However, this data is not completely clear and an argument could be made for selecting different lag times for determining phase velocity. A direct time domain figure of this method will be shown in section 4.2.1 where the vibration levels are higher and easier to see.

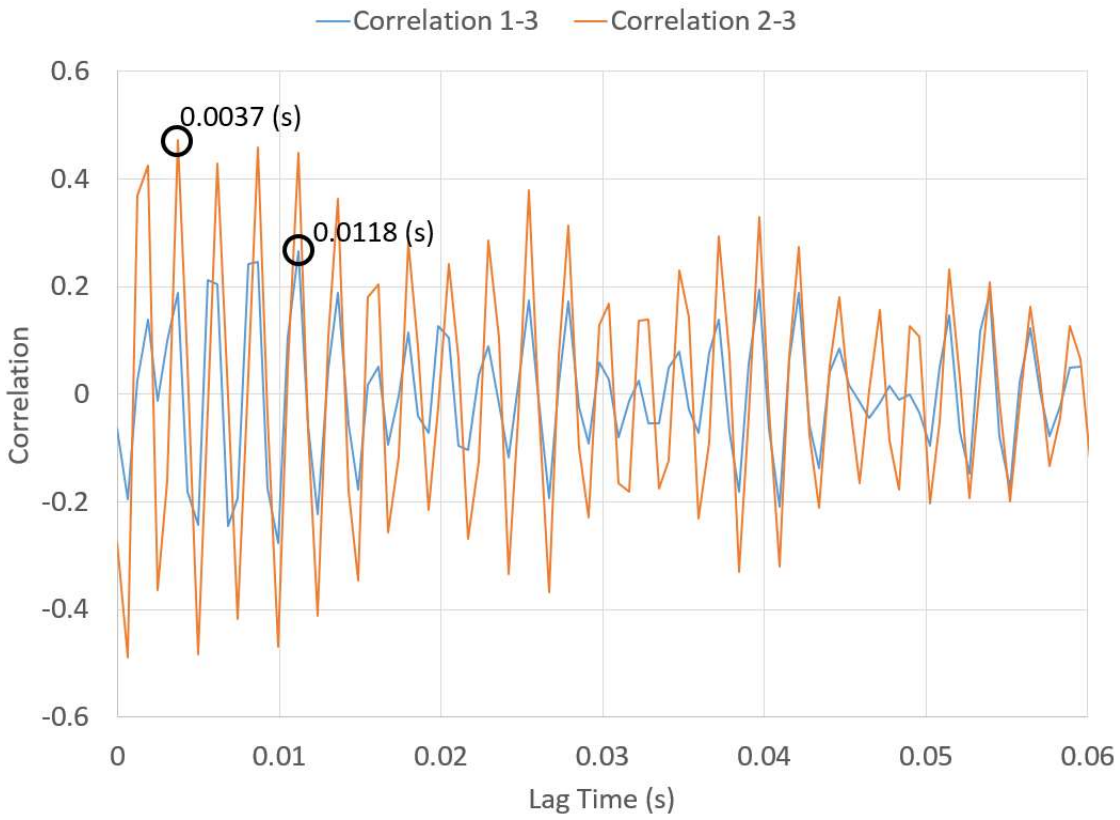

Figure 4-12: Autocorrelation between Sensors at Heat Exchanger

From looking at the acceleration spectrum (similar to Figure 4-4 but not reduced to third octave), it can be seen that a large amount of the acceleration is located at 59.0 Hz. Using the assumption that since a large amount of the acceleration oscillates at

59.0 Hz, a large percentage of the signal will repeat at this period, every 0.017 seconds. Although this was the first test and the distances between sensors were not that different, it can still be shown that by adding the lag time to multiples of 0.017 seconds and comparing the velocity results and looking for a velocity that is the same for both sets of sensors.

Table 4-1: Wave Velocity for Heat Exchanger

	Velocity 1 to 3	Velocity 2 to 3	% Difference
Lag	509	1343	62.1%
Lag + 1 Period	209	242	13.7%
Lag + 2 Periods	131	133	1.2%
Lag + 3 Periods	96	92	-4.5%
Lag + 3 Periods	75	70	-7.8%

Table 4-1 shows the possible velocities using this principle. Even with this messy signal, it is possible to see a pattern. As the calculated velocity for both sensor arrangements decrease indicating that multiple periods occurred between the sensors, the velocities become more similar until a point where they start to diverge again. This points toward a waveform velocity in the vicinity of 130 feet per second. To correlate this result, the same procedure was attempted at another high amplitude frequency, 118 Hz, and the results were identical. Unfortunately, the soil underlying this slab is known to be very stiff clay and 130 feet per second is on the extreme low end of possible values according to Wair and Dejong (2012). Most likely, this signal is too complex to determine an accurate phase velocity.

4.2 Small Scale Vibration Tests on Four Inch Slab on Grade

This section covers experiments performed in a small 1200 square foot metal building (approximately 36 feet x 36 feet) setting on a 4 inch concrete slab. The concrete slab rests on non-engineered (simply placed without specific profile) clay fill,

which is relatively soft compared to the compacted clay fill at the other test location in this report. This location has some ideal characteristics in that there are few ambient vibrations. Only the experimenter was present during these tests, and the building is a quarter mile from the nearest county mile section road. The only running equipment during each test was the equipment in question, as opposed to the other testing location where there was nearby running equipment. Also, the relatively soft slab allows for larger amplitude vibrations from a given piece of equipment to help see attenuation.

4.2.1 Description of Tests on Single Pieces of Equipment

These test were originally set simply to prove out the often sited Bornitz equation, Equations (2-10) and (4-1) in this paper, with the assumption that concrete has such a low absorption coefficient that only the geometric damping would be necessary in these relatively short distances. However, it was quickly evident that the attenuation of the vibrations occurred much quicker than simple geometric damping could explain, which led to more tests being necessary to attempt to explain the behavior.

The two main pieces of equipment tested were the 16 inch Delta scroll saw described in section 3.5 and an 8 inch Delta bench grinder mounted on a metal stand capable of variable rotation from 1800 rpm to 3600 rpm. These two pieces of equipment where chosen because they were readily available, they operated at consistent rotational speeds, they provided measureable floor vibrations, and they were easily moved from one location to the next. These pieces of equipment represent small ancillary equipment typically located in industrial facilities in all kinds of locations.

Sensors and cabling were mounted as described in section 3.4 on several different days. Figure 4-13 shows the layout of the equipment during tests. “L”

followed by a number indicate locations were the accelerometers where installed. "E" followed by a number indicate locations were the vibration source equipment was located. Measured radially from L1: L2 is 60 inches, L3 is 144 inches, L4 is 96 inches, L5 is 216 inches, E1 is 20 inches, E2 is 64 inches and E3 is 99 inches. Locations in the color red show the location that a rubber mallet struck the concrete during hammer blow tests described in section 4.5.

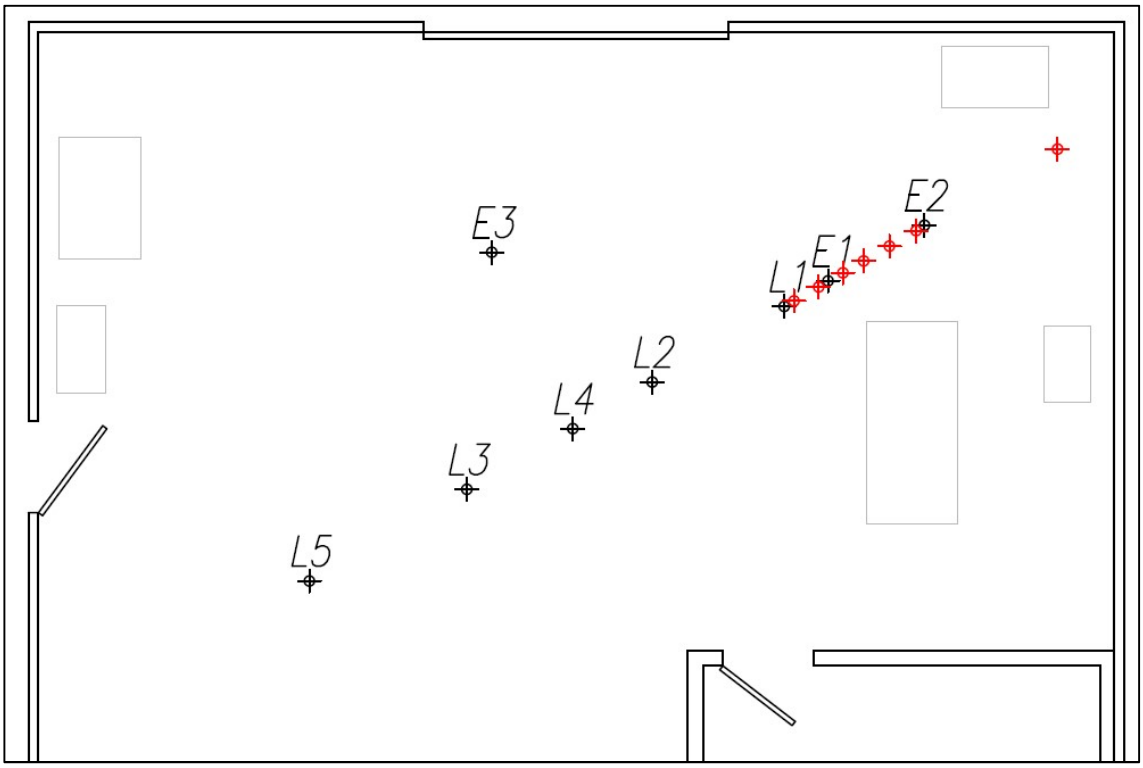

Figure 4-13: Equipment and Sensor Layout for Small Shop

4.2.2 Results of Tests on Single Pieces of Equipment

Using the method for determining β described in 4.1.3 with individual three accelerometer measurements, Figure 4-14 was created for the scroll saw running at two speeds and the grinder. Similar to the tests on the heat exchanger, the absorption values appear to be much higher than any of the previously reported values, as the highest value for any soil type listed, soft soil such as top soil, was 0.06 ft^{-1} at 30 Hz. The

grinder values appear to be lower than the saw values, but part of this was because the vibration signal was small and fell into the noise range of the measurement system.

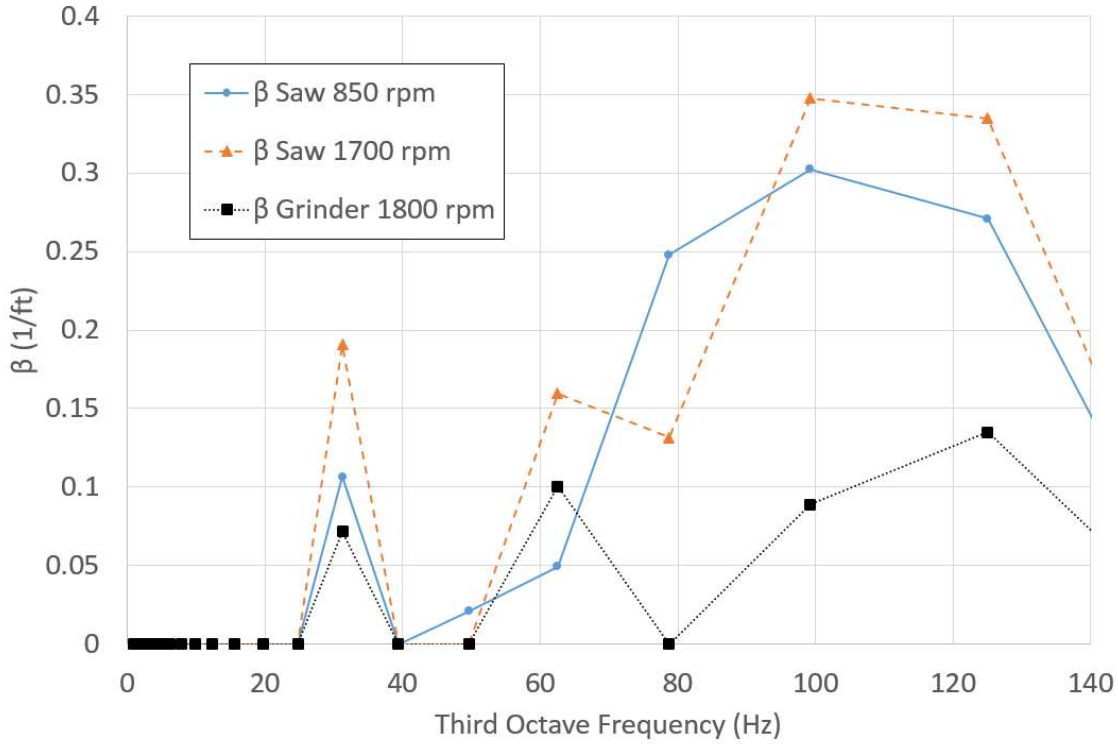

Figure 4-14: Average β for Individual Tests

To additionally complicate analysis, Figure 4-14 appears to have two similar peaks of β, but as can be seen in Figure 4-15, the complete drop off between 40 and 50 Hz comes from the fact that none of the equipment used here had vibration levels in those third octave bands. Another false correlation using Figure 4-15 could be made that β is simply follows the magnitude of the amplitude of the source vibration A_1. This correlation is shown to be false in Figure 4-20 in section 4.3 where the same saw was ran in a different location. There the A_1 values are similar, but the β values do not correlate at each frequency, particularly 60 Hz.

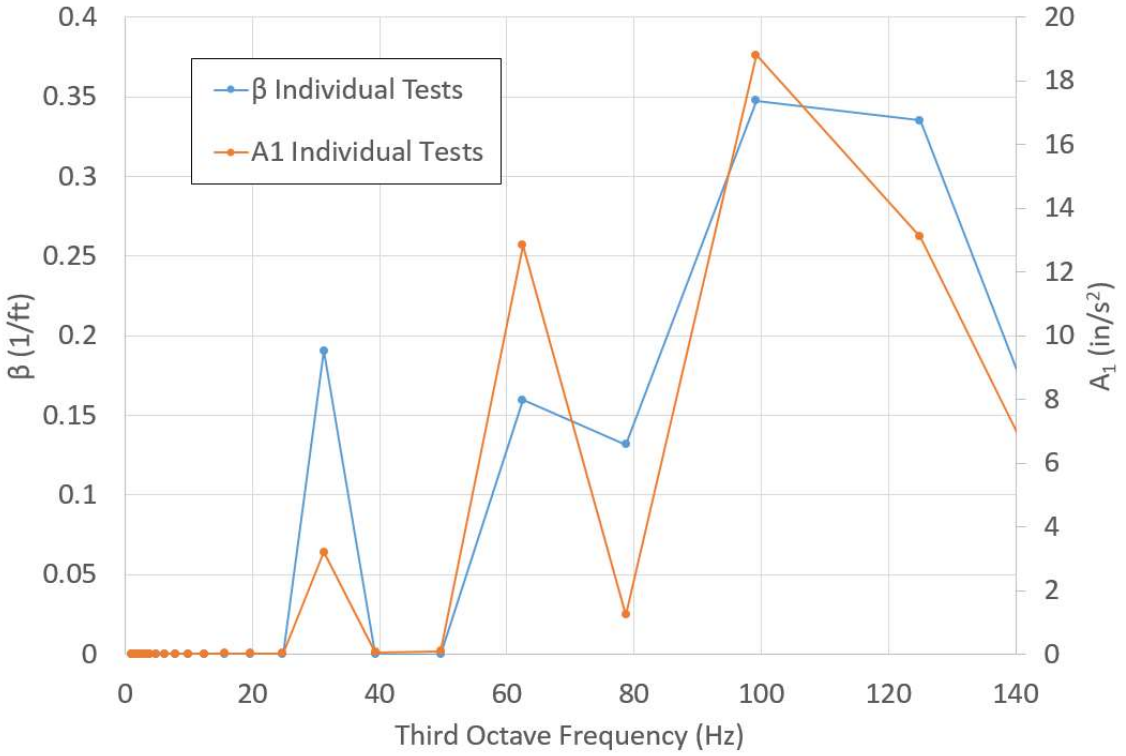

Figure 4-15: Scroll Saw Running at 1700 rpm

Following the pattern set up in the previous section, the vibration wave velocity was determined. The time domain acceleration data from each sensor is clear enough to make a direct determination of the lag time between the two signals as shown in Figure 4-16. This figure shows data from the scroll saw operating at 1700 rpm and sensor 1 was 5 feet radially away from sensor 2. Similar to the discussion in the previous section, it is not guaranteed that the peak circled on the sensor 2 data is the same peak as circled on sensor 1. The circled peaks correspond to a waveform velocity of 400 feet per second. If the correct waveform peak for signal was the next signal 2 peak at 0.0423 seconds, the velocity would be 175 feet per second. Similarly, the third peak would equate to 110 feet per second.

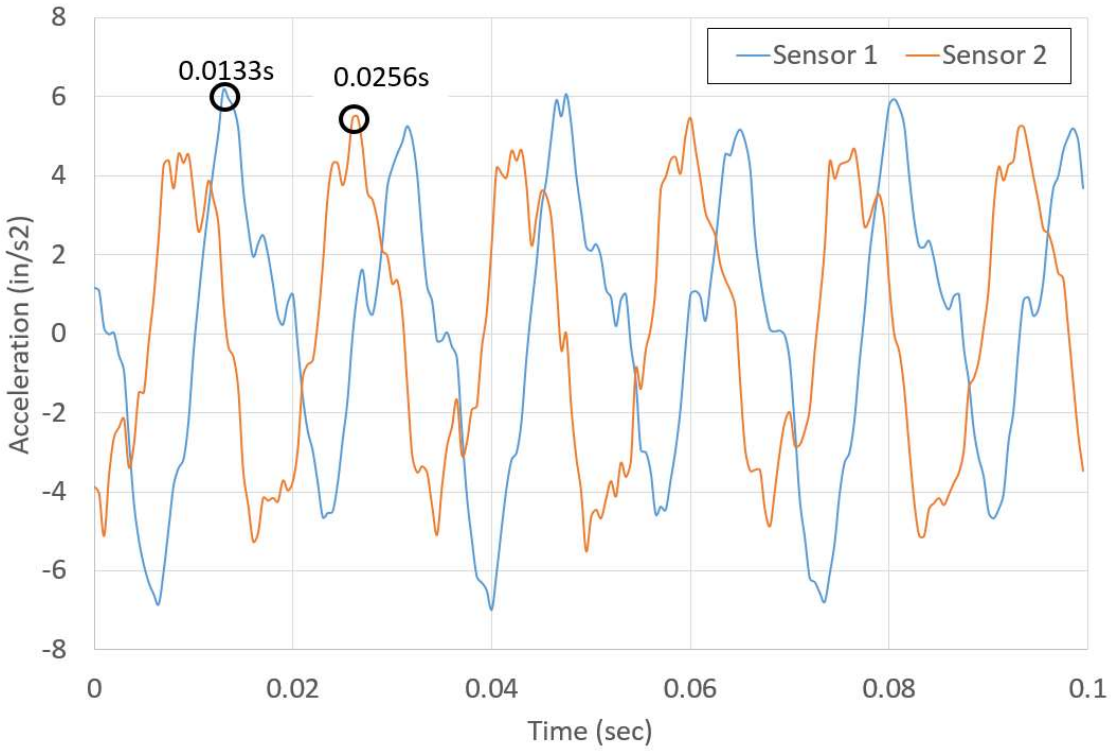

Figure 4-16: Acceleration Waveforms for Sensor 1 and 2 (Sensor 2 Scaled 5x)

Just like for the heat exchanger data (Section 4.1.3), a cross correlation was performed between the same two acceleration signals to more objectively determine the lag time between the two signals and is shown in Figure 4-17. This shows nearly an identical primary lag time of 0.0120 seconds between sensor 1 and 2, which corresponds to a maximum waveform velocity of 415 feet per second. The lag time cross correlation between sensor 2 and 3 is shown as well in Figure 4-17. Sensors 2 and 3 were 7 feet apart and a maximum velocity can be seen as 735 feet per second. Both of these cross correlations show very good correlation between sensors as the decay in correlation is constant showing that the waveforms are consistent across this duration.

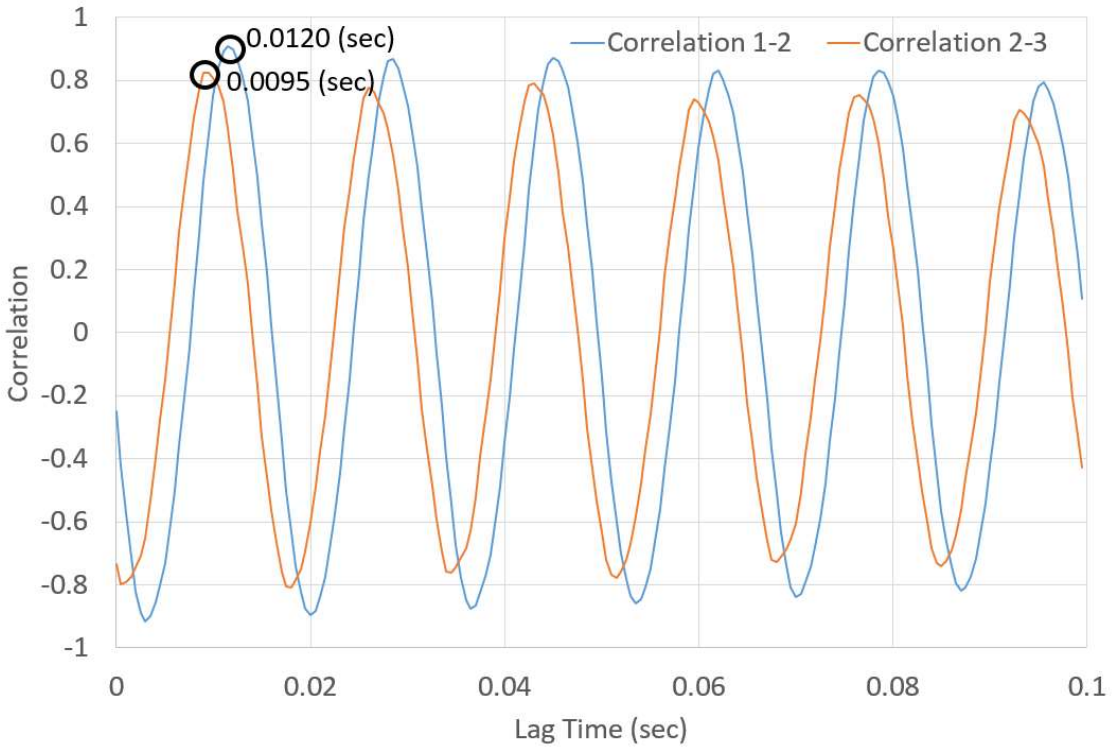

Figure 4-17: Correlation at Lag Times between Sensors

Since it seems odd that the velocity is as different as the maximum possible velocities shown, the effects of multiple periods must be considered to attempt to estimate the actual velocity of the waveform. Just like the results shown in Table 4-1 for the heat exchanger, the velocity seems to converge on a value near 145 feet per second.

At this point it is clear that one of the assumptions made before taking measurements that the surface waveform primarily traveled through the concrete slab cannot be correct. In the previous test case at the heat exchanger (Section 4.1.3), the maximum wave velocity was 2,000 feet per second but the correlation data was not conclusively clear. The minimum expected Rayleigh wave velocity in concrete is 5,000 feet per second and the maximum velocity measured during this test was a low as 400 feet per second. In fact, the velocity seems to converge on a value near 150 feet per

second, which is on the lower end of expected shear wave velocities for clay (Wair and DeJong 2012). This is the beginning of the realization that even though the source of the vibration is directly on the nearby concrete with no separation, the measured vibration waveform is not primarily traveling in the concrete. This idea is verified in section 4.6.1.

4.3 Tests of Vibratory Machines

Since the magnitudes of the equipment tested up to this point had decayed more rapidly than initially expected, vibration test were conducted in an area with industrial equipment with the highest expected vibration available. The equipment described in this section is commonly referred to as vibratory machines. This type of equipment is specifically designed to induce high vibrations to a bed of media. Production parts such as aircraft turbine blades can be placed in the media for cleaning or polishing. As the bed vibrates, parts move through the media from the induced motion of the vibrating media.

Although it is not likely that sensitive equipment would be placed in the direct vicinity of vibratory machines, they are sometimes installed in the same building resting on the same concrete slab as sensitive equipment. Therefore, it is important to understand how far these type of vibrations will travel before they attenuate below the level for sensitive equipment. In addition to that point, the higher magnitudes may behave differently and this needs to be investigated.

4.3.1 Description of Tests on Single Pieces of Equipment

The test locations for the vibratory area are shown in Figure 4-18. "E1" and "E2" are the location of the feet of the vibratory equipment shown. Each vibratory

machine has two feet and these feet are shimmed and bolted directly to the 6 inch thick concrete slab. There is no isolation foundation. The two vibratory machines are physical placed as mirror images with the sides opposing each other. The 50 horsepower inductive motor driving the vibration beds was located between the labels E1 and L1 for E1 and in the opposite corner for E2. E3 and E4 are the locations where the scroll saw described in section 3.5 was placed to correlate some of the results from section 4.2. The locations identified with "L" followed by a number show the locations where accelerometers were installed for measurements (there were only three sensors installed for any given test).

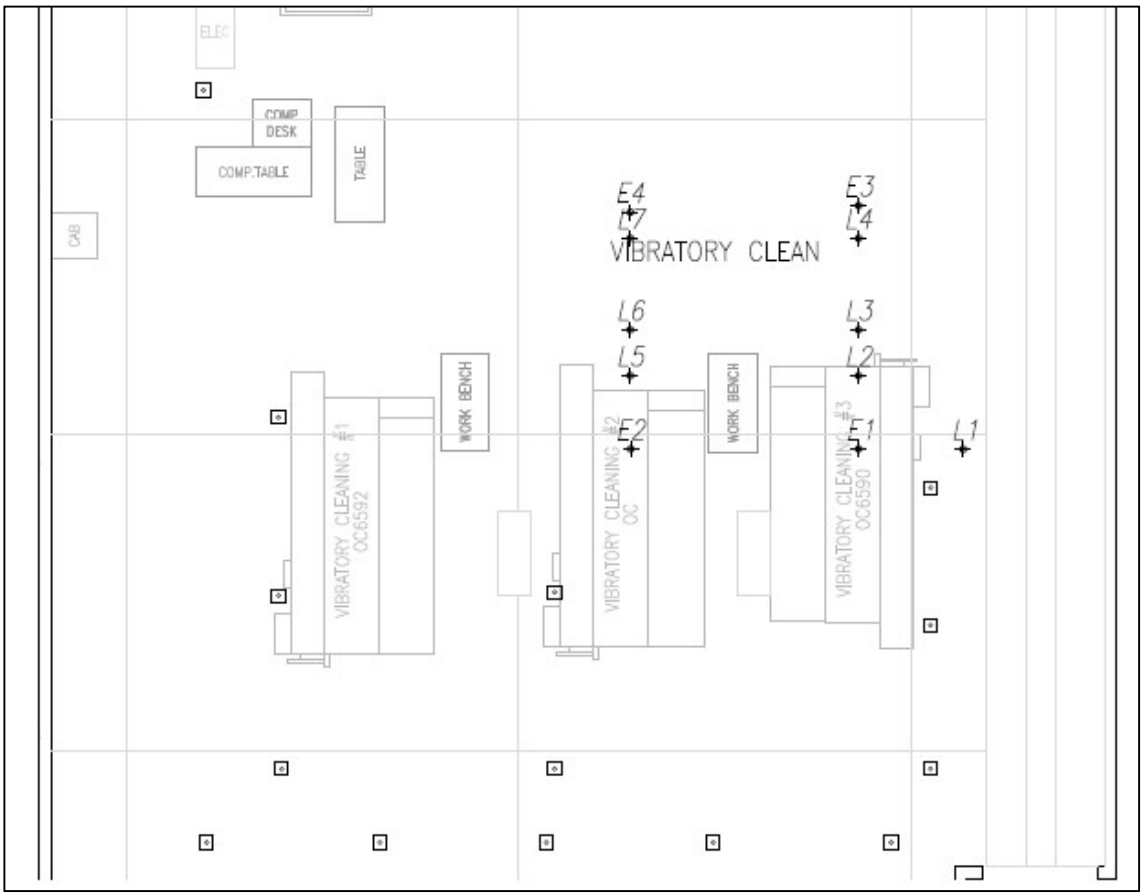

Figure 4-18: Vibratory Test Area Layout

For reference, L1 is 64 inches radially from E1. L2, L3, and L4 are 45, 72, and 129 inches from E1, respectively. E4 is 16 inches from L7 and E3 is 20 inches from L4. Although not shown in Figure 4-18, two addition similar pieces of vibratory equipment that were approximately 35 feet and 65 feet from the sensors were tested to make longer distance measurements.

4.3.2 Results of Tests on Single Pieces of Equipment

As somewhat expected, the magnitudes of the vibrations were relatively high for the vibratory equipment. Figure 4-19 shows the acceleration and absorption values in a third octave spectrum for the vibratory machines using the individual test readings averaged together. Note that the acceleration values, A_1, are similar across the spectrum even though the measurement were taken from two different directions from the machine orientation.

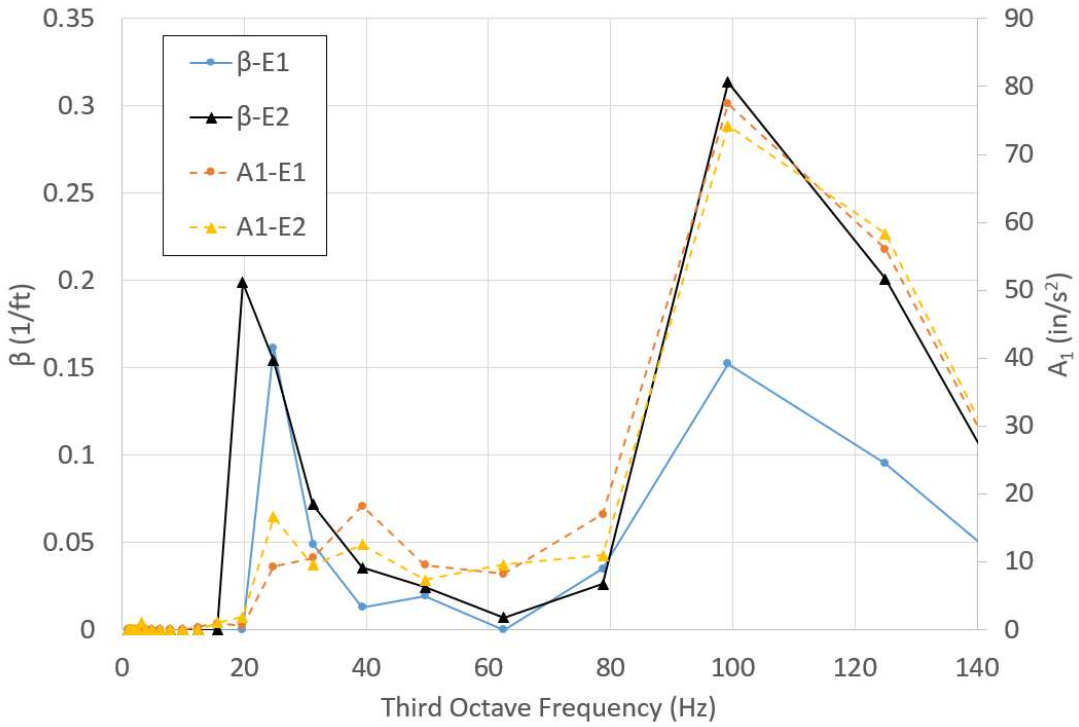

Figure 4-19: E1 Vibratory Third Octave Spectrum

Absorption coefficients, β, are similar at each frequency band, particularly below the 100 Hz third octave band. They likewise follow a similar pattern as the previous two cases in sections 4.1 and 4.2 in that there seems to be two peaks with a clear valley in-between the peaks. There could be a correlation between the A_1 amplitudes and β values, but it is less clear at the 30 Hz band. This helps transition to the scroll saw run in this location. If the absorption values are significantly tied to amplitude (at very high amplitudes the shear modulus would decrease as shown by Vucetic and Dobry (1991) and thus increase damping, but not expected at these strain levels), that correlation would have to be present at this location for the scroll saw.

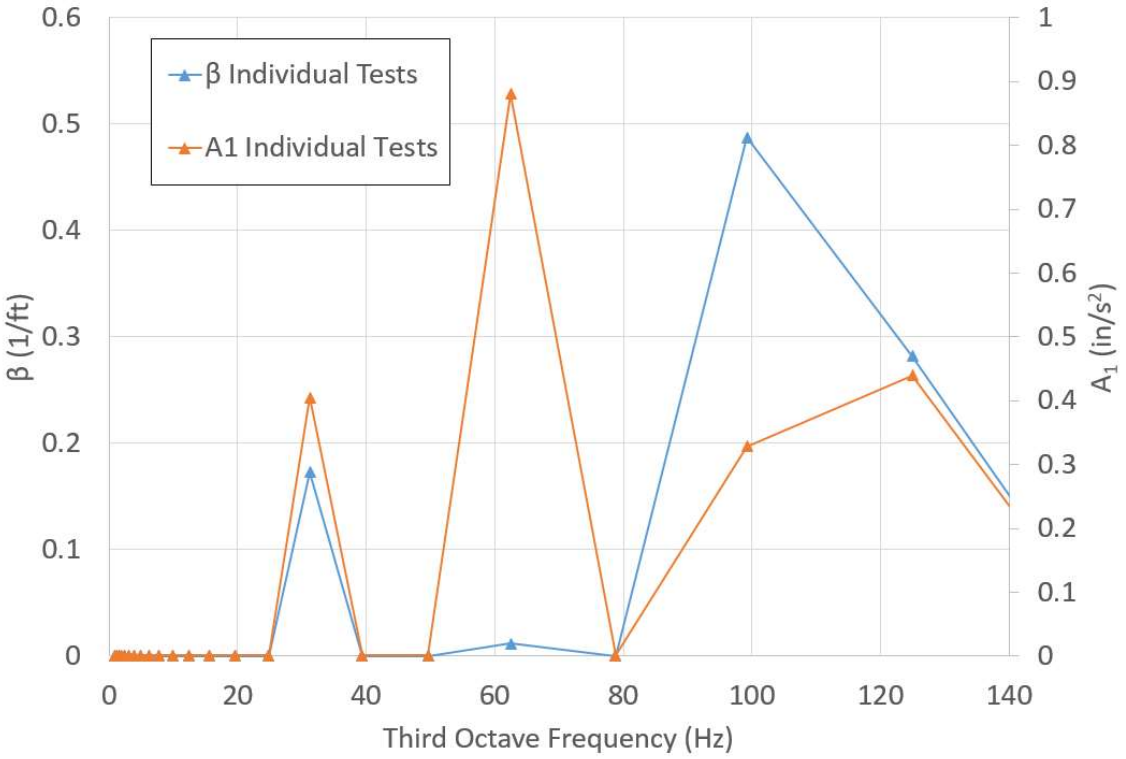

Figure 4-20: Scroll Saw Running at 1700 rpm in Vibratory Area

Figure 4-20 shows the fit to the Bornitz formula for the scroll saw running at 1700 rpm in the vibratory area. Conveniently, the primary operating frequency of 60 Hz, is precisely the frequency where the vibratory equipment showed the lowest

attenuation. This spectrum clearly shows that the lowest absorption is at the frequency of the highest acceleration values. Although this does not explain what is happening, it does help discount one of the possible cause of the peaks in absorption values being related to the magnitude of the acceleration.

To complete the comparison, Figure 4-21 shows only the absorption values in a third octave spectrum at this location for the three pieces of equipment discussed. As mentioned before, although not identical, the values follow the same pattern with respect to frequency and do not have an unlimited variance although the original hope was for less spread of the data.

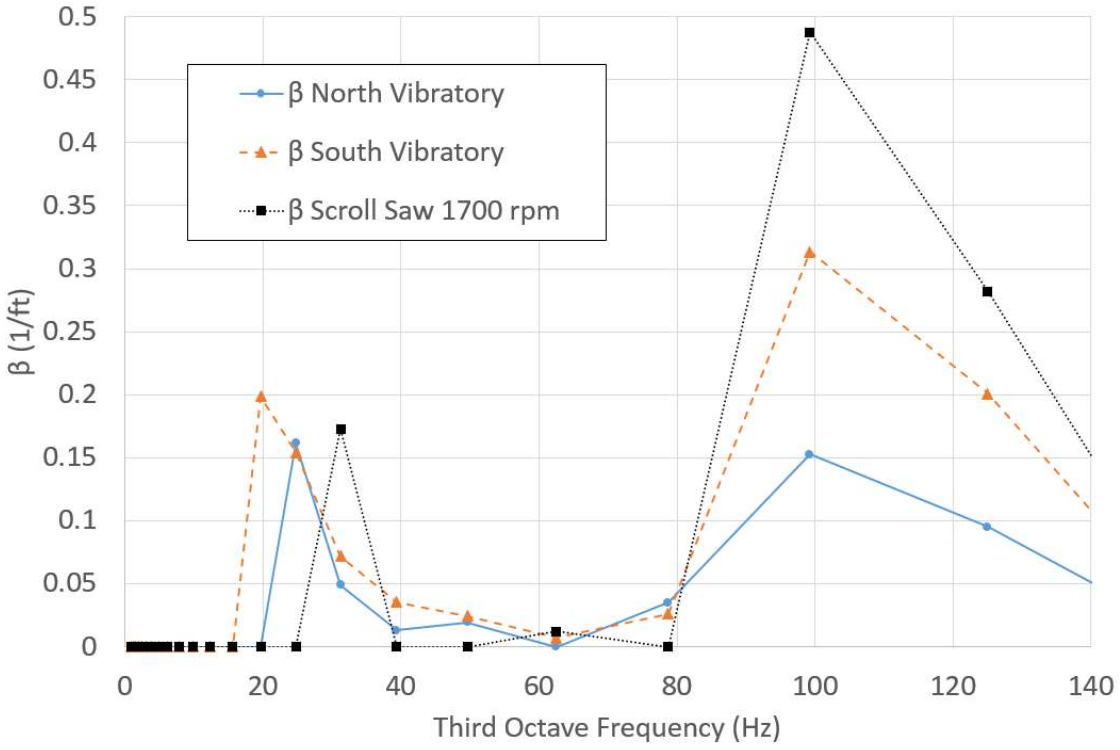

Figure 4-21: Beta Comparison for Three Equipment

Since at the time of these experiments the entire building was unoccupied, a couple of relatively long distance measurements were taken. The maximum distance measured for the other tests in the paper was on the order of 10 to 20 feet. Figure 4-22

shows measurements taken from two vibratory machines and compares them to the vibration levels of E1 at 3.75 feet with the vertical axis in logarithmic scale. The machine at 65 feet was similar in age to E1, but the machine at 35 feet was a newer model. Still, the 65 feet of distance reduced the acceleration magnitude significantly below the VC-C criteria.

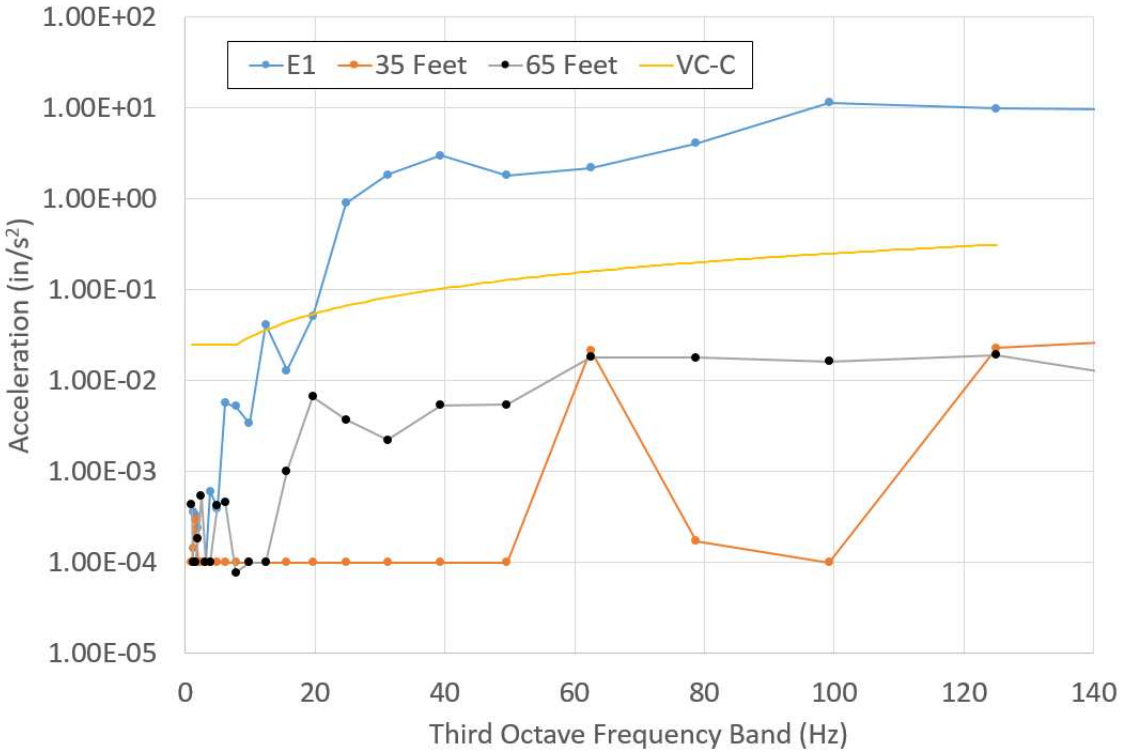

Figure 4-22: Long Distance Acceleration Measurements for Vibratory Equipment

Finally, a cross correlation between the sensor signals was performed to estimate the velocity of the waveform traveling during a test of the vibratory machine, which is shown in Figure 4-23. Unlike the results for the scroll saw in the small scale test in Figure 4-17, but similar to the heat exchanger in Figure 4-12, this result does not correlate that well. It does have a high correlation at a lag of 0.0015 seconds between sensors 1 and 2, which are 2.33 feet apart corresponding to a maximum velocity of 1550

feet per second. For sensor 2 and 3, which are 4.67 feet apart, the highest correlation is at a lag of 0.0020 seconds, indicating a possible velocities of 2300 feet per second.

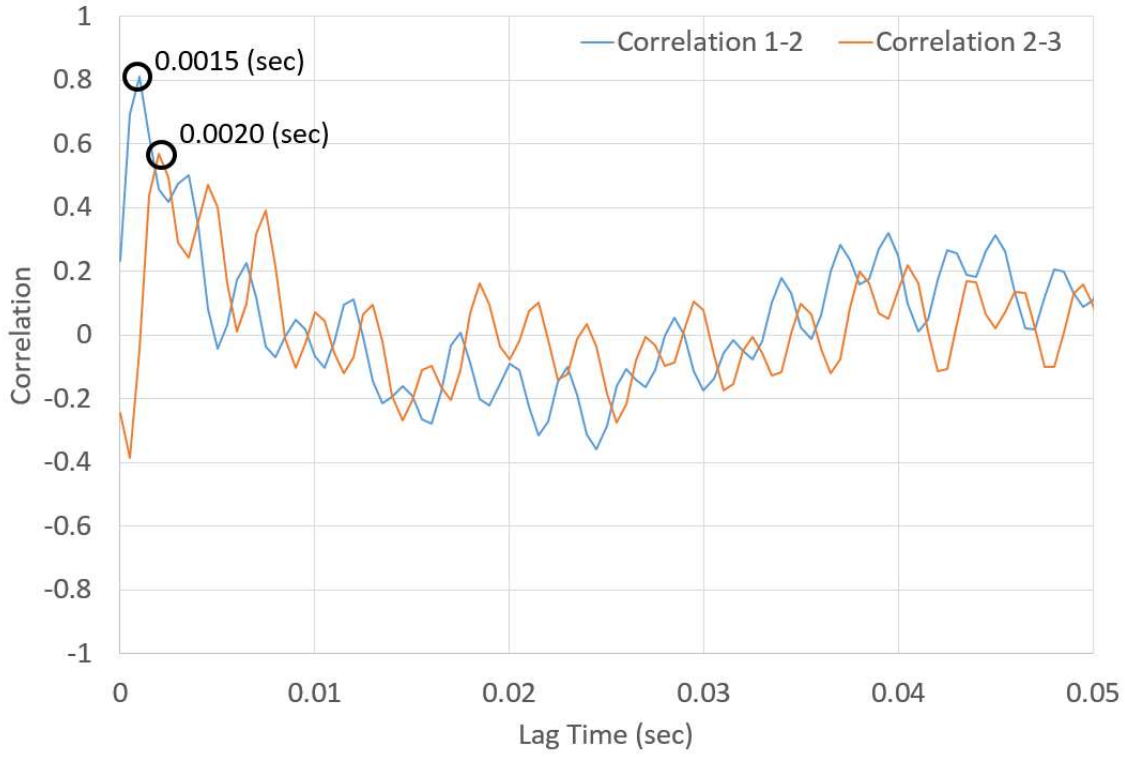

Figure 4-23: Correlation at Lag Times between Sensors for Vibratory Machine

As an additional check, the waveform velocity was determined using the data from the scroll saw since it produces clean waveforms. This produced an estimated maximum waveform velocity of 1,000. It is even clearer now that the waveform must be primarily traveling in the slower clay substrate as no measured velocities approach the velocity of a shear wave in concrete.

4.4 Tests of Equipment near LaserDyne Cutter

The final new location used for this report was near an actual piece of sensitive equipment, a LaserDyne cutter. This location was chosen for several reasons. First, "4x Diagnostics" (2015) performed a long term vibration study of the area before the LaserDyne cutter was installed. Second, it is highly relevant to the theme of this

research since the equipment is in the vibration sensitivity range under consideration here, around VC-C, but slightly different. Since the vibration study was performed, additional equipment has been installed nearby and the real world implication of these added pieces of equipment can be addressed.

4.4.1 Description of Tests on Single Pieces of Equipment

There were three basic types of vibration source equipment tested in this area. The first is what is called a compressed air booster pump. This device was actually installed specifically for the LaserDyne cutter by someone not considering the floor vibration limits. Figure 4-24 shows a picture of the booster pump.

Figure 4-24: Picture of Compressed Air Booster

One of the operations of the LaserDyne cutter requires compressed air at 300 psi on the order of 30 cubic feet per minute. To supply the volume of air at this pressure would require a significant air compressor with additional electric service and possibly a remote heat rejection system. However, in most industrial facilities, 100 psi

compressed air is supplied as a utility with significant capacity, and this is where the booster compressor comes into play. The booster works with two differing sized opposed pistons connected by a solid shaft. The larger piston uses the standard utility 100 psi compressed air to drive the smaller piston's air up in pressure to the necessary value. This provides a relatively inexpensive and reliable method to provide higher pressure air for a single piece of equipment. Nevertheless, the fact that the piston oscillates in a linear fashion with no counter balance means that it can apply noticeable vibrations. The point of this description is to explain one of the reasons a vibrating piece of support equipment can end up next to a piece of equipment that cannot tolerate high vibrations. The critical question here is: is the booster (there are actually two) too close to the LaserDyne, and, if it is, how far would it need to be relocated to bring the floor area back into specification?

The next piece of equipment tested in this location was what is termed here a "parts washer". In a sense, it is similar to a giant dishwasher about 7 feet wide by 9 feet long by 9 feet high. This parts washer had a 25 and 50 horsepower pump as well as the spray jets for vibration sources. This parts washer ended up near the LaserDyne more by coincidence as it sits on the border of two separately managed shops. There was simply enough floor space for it.

The last type of equipment was a simple drain pump installed to automatically pump industrial waste out of a tank. Drain pumps are common in many industrial facilities as gravity drains are not always close enough to be practical so liquid waste must be pumped away. Figure 4-25 shows a picture of the drain pump in the bottom and the back of the parts washers with its two pumps.

Figure 4-25: Picture of Back of Parts Washer and Drain Pump

The layout of the tests in this area is shown in Figure 4-26 and shows the combination of all layouts taking place over several days. E1 and E2 are booster pumps. E3 and E4 are the pumps on the parts washer. E5 is the drain pump. A true concrete expansion joint where the slabs are separated by about 1 inch is shown between building columns M101 and N101.

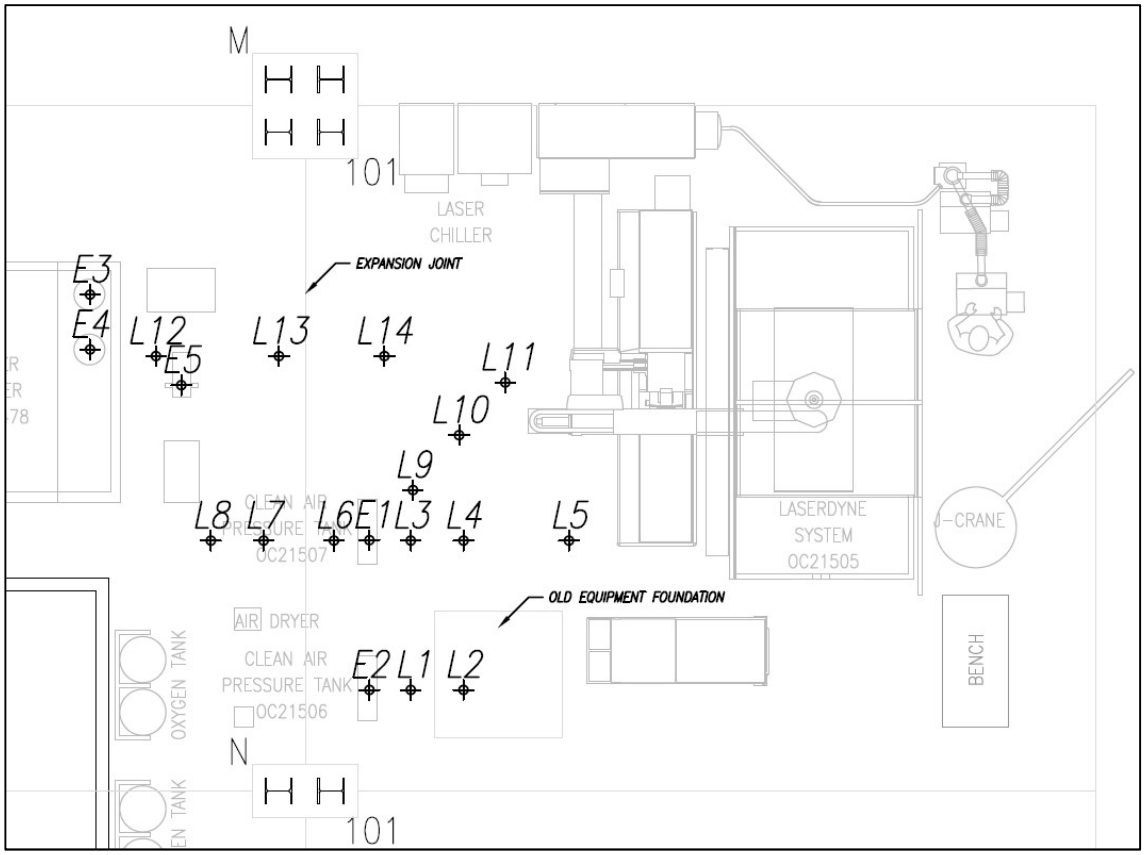

Figure 4-26: LaserDyne Area Sensor and Equipment Layout

The sensor locations are indicated by "L" followed by a number. Measured radially from E2: L1 is 19 inches and L2 is 42 inches away. Measured from E1: L3 is 19 inches, L4 is 42 inches, L5 is 90 inches, L6 is 16 inches, L7 is 48 inches, L8 is 72 inches, L9 is 30 inches, L10 is 62 inches, and L11 is 84 inches. Measured from E4: L12 is 42 inches, L13 is 90 inches and L14 is 137 inches.

4.4.2 Results of Tests on Single Pieces of Equipment

For the most part, the attenuation results for all of the equipment followed a similar pattern as in the other areas. Figure 4-27 shows the results for the booster pumps. Although at different frequencies than the other cases, there are higher and lower values of the absorption coefficient, β, across the frequency spectrum. These absorption values do not seem to be directly correlated to amplitudes to help eliminate

that as a possibility.

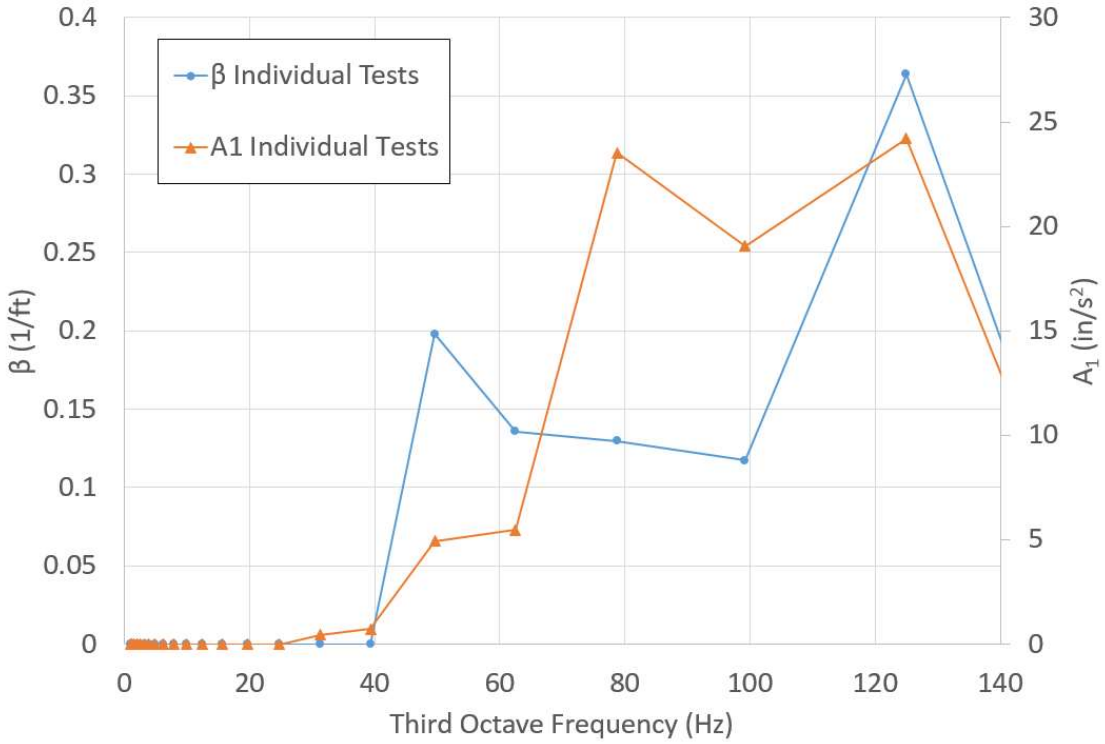

Figure 4-27: Booster Pumps Combined Results

While, this will be discussed more in depth in section 4.6.1 a trend was observed for acceleration measurements near the expansion joint. The values were consistently slightly higher than expected, and at some frequencies even showed increased magnitudes (the opposite of attenuation, increase in amplitude with distance from source).

It is convenient and perhaps interesting to initially touch on the answer to the question proposed in this section as to the effect of one of these boosters (the other equipment had much lower amplitudes and were further away) on the slab near the sensitive LaserDyne system. This will be covered more in depth in Chapter 5 as it is more important to cover the effects of all of the equipment, not just a single piece.

Figure 4-28 shows the results of the peak displacement spectrum for a two week period before any of the aforementioned equipment was installed. For reference, the allowable floor vibration for the LaserDyne machine is 80 μ-in peak below 10 Hz and 40 μ-in between 10 and 100 Hz. Even though this location is in operating industrial facility, this highlights the initial reasoning to avoid expensive isolation foundations. Clearly the location was originally well within specifications.

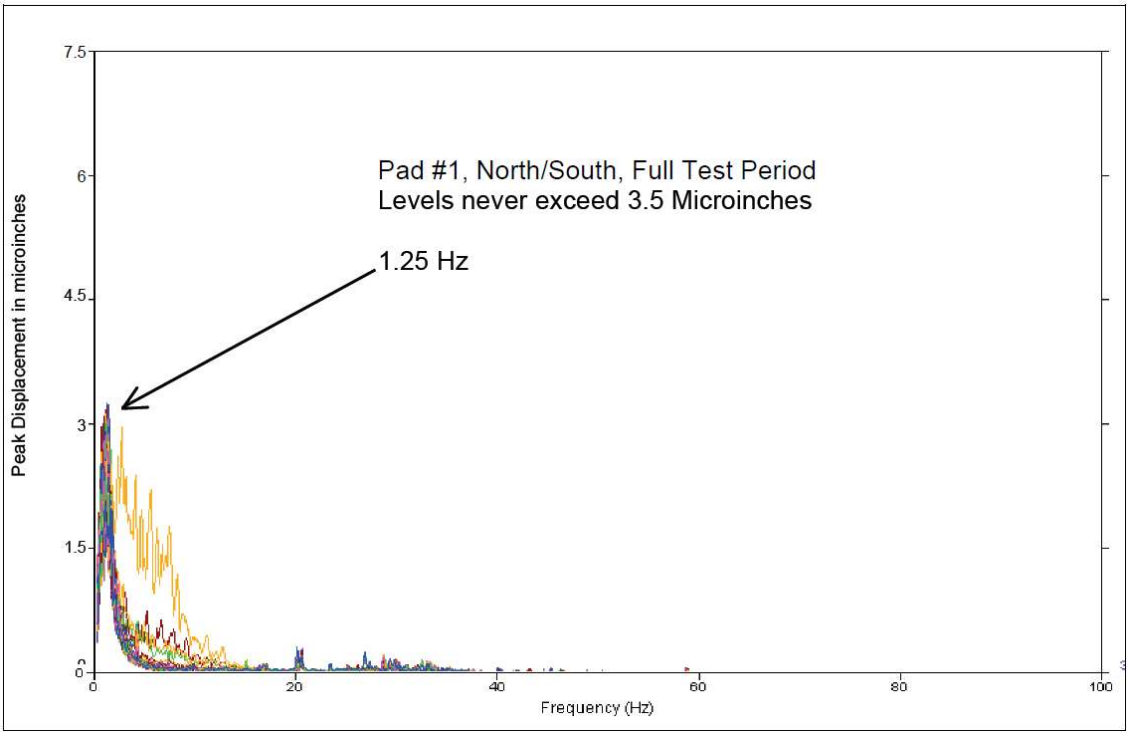

Figure 4-28: Floor Vibration Results from 4x Diagnostics (DeMatteo 2015)

Figure 4-29 shows the displacement spectrum for a single booster pump running. Clearly, this pump adds significant slab vibrations near the LaserDyne. However, the vibrations from this single piece of equipment do not exceed the specifications for the LaserDyne (although they do exceed vibration criteria level C). Therefore, considering a single booster located where it is now, the booster is not too close to the LaserDyne to pose a vibration concern.

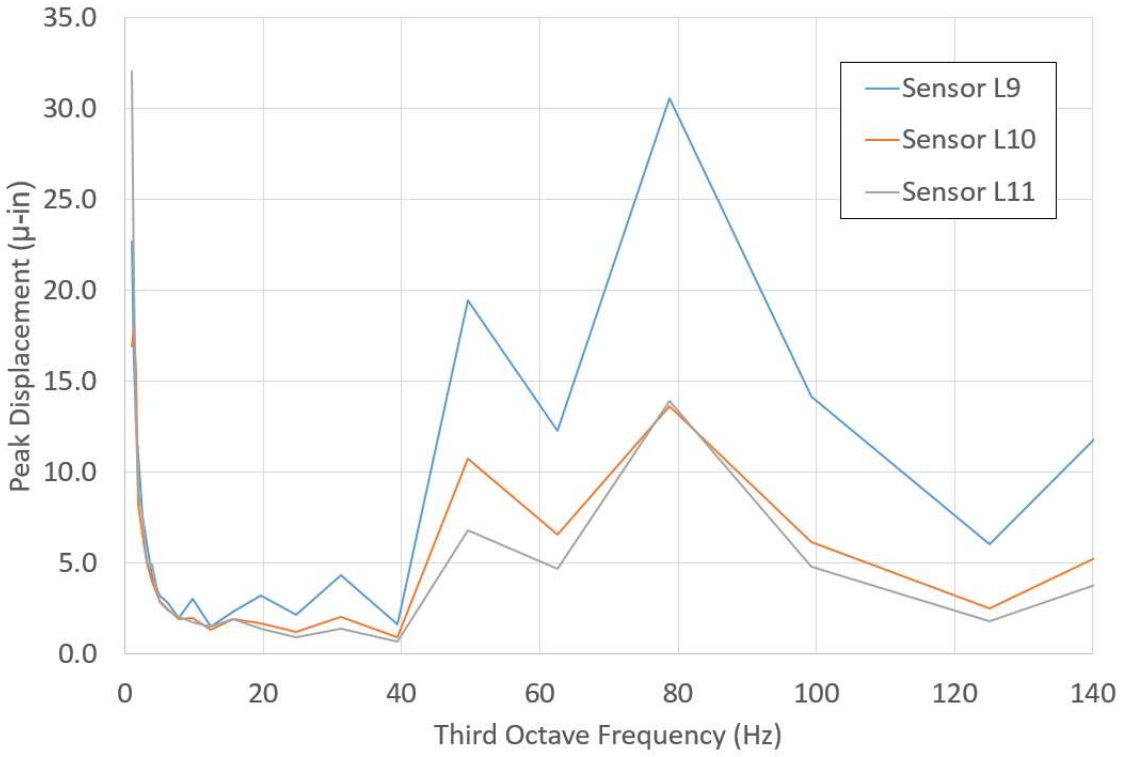

Figure 4-29: Displacement Spectrum for Single Booster

Finally, a cross correlation was run between sensors and a maximum possible phase velocity of about 1,000 feet per second was determined, similar to the area tested in section 4.3.

4.5 Hammer Blow Tests

In order to attempt to make sense of the varying absorption values, hammer blow test were performed in the same location as used in section 4.2. The idea behind the test was to see if shear waves reflecting off of a shallow known stiff layer were causing a resonance effect similar to what is described in section 2.4.1.

4.5.1 Description of Hammer Blow Tests

The setup up for this test consisted of mounting the three accelerometers spaced 8 and 10 feet apart following the standard procedure described in this thesis, shown as L1, L4 and L5 in Figure 4-13. The first accelerometer was mounted in the same

location as the first accelerometer for the previous experiments in this location. The tests themselves involved striking a rubber mallet at 3.5, 16, 24, 36, 60 and 120 inches from the lead sensor, L1, measured in a radial line from the three sensor setup. The sampling frequency was increase to 10 kS/s for these test to increase the resolution at the higher expected frequencies.

4.5.2 Results of Hammer Blow Tests

The results from these tests did not lead to any direct explanation as to the cause of the inconsistent absorption values; however, they did provide the lead that did. That lead is described below.

The first result analyzed was the acceleration amplitude spectrum. To do this, the time location of the initial acceleration was located. The signal was reduced starting approximately 20 data points before the onset of acceleration and continued for 2,000 points or about 0.2 seconds. This data was passed through a Hanning window followed by the same complex FFT described in Chapter 3. The only significant difference was that the signal was shorter, which led to a lower frequency resolution, *df*, of 5 Hz.

Figure 4-30 shows the results of a single hammer test located at 24 inches from the first sensor. The data does shows peaks and valleys which possibly could correspond to resonance occurring at a frequency near 60 Hz corresponding to the "valley" in the absorption, β, spectrum, which might mean that waves reflected from a shallow rock like layer are skewing the acceleration amplitude results. However, the same could be said for a frequency near 120 Hz, and that is not consistent with the absorption spectrum. This inconsistency calls into question the idea of reflected resonant waves.

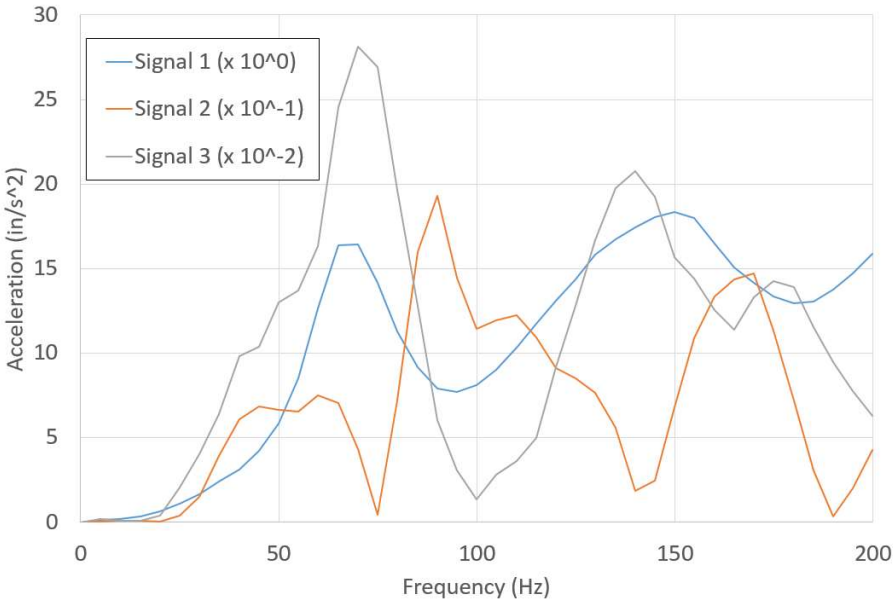

Figure 4-30: Hammer Blow Test at 24 Inches from Sensor 1

Figure 4-31 shows the acceleration spectrum for sensors L1 and L4 from two different tests which resulted in the hammer strike being 10 feet away from each sensor. If vibration reflection was a significant contributor to the surface waveform, it is expected that the spectra would be similar. However, they are nearly opposites.

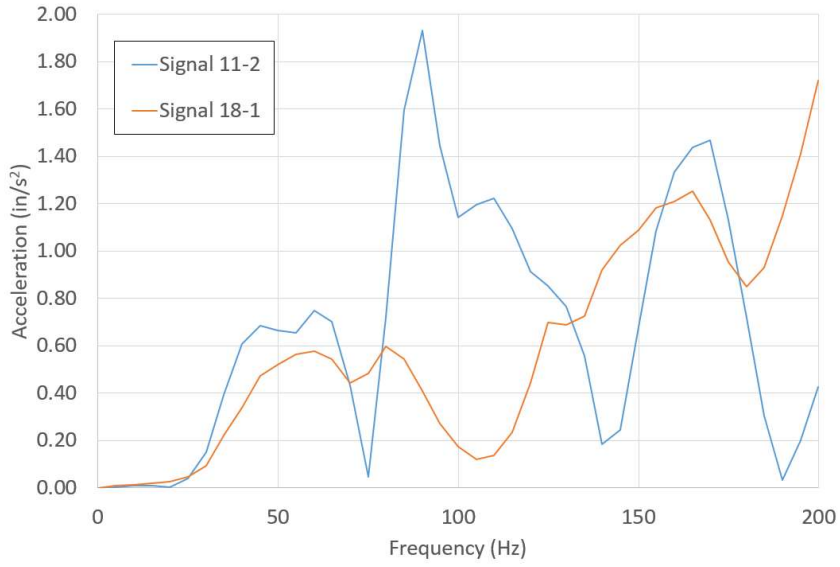

Figure 4-31: Comparison from Two Test from Equal Distance Sensors

Figure 4-32 shows the acceleration spectrum for all of the different locations of hammer strikes for a single sensor L4. The peaks in the accelerations clearly do not occur at frequencies to indicate a resonance effect, as the profile would shift as the distance from the source changed. However, there is a peculiarity that does seem consistent. At 75 and 140 Hz, there is an extreme consistent drop in acceleration. Referring back to Figure 4-30, it is clear that there was acceleration content at 75 Hz, both before sensor L1, and after sensor L5, but something is causing a complete attenuation of the vibration at this location.

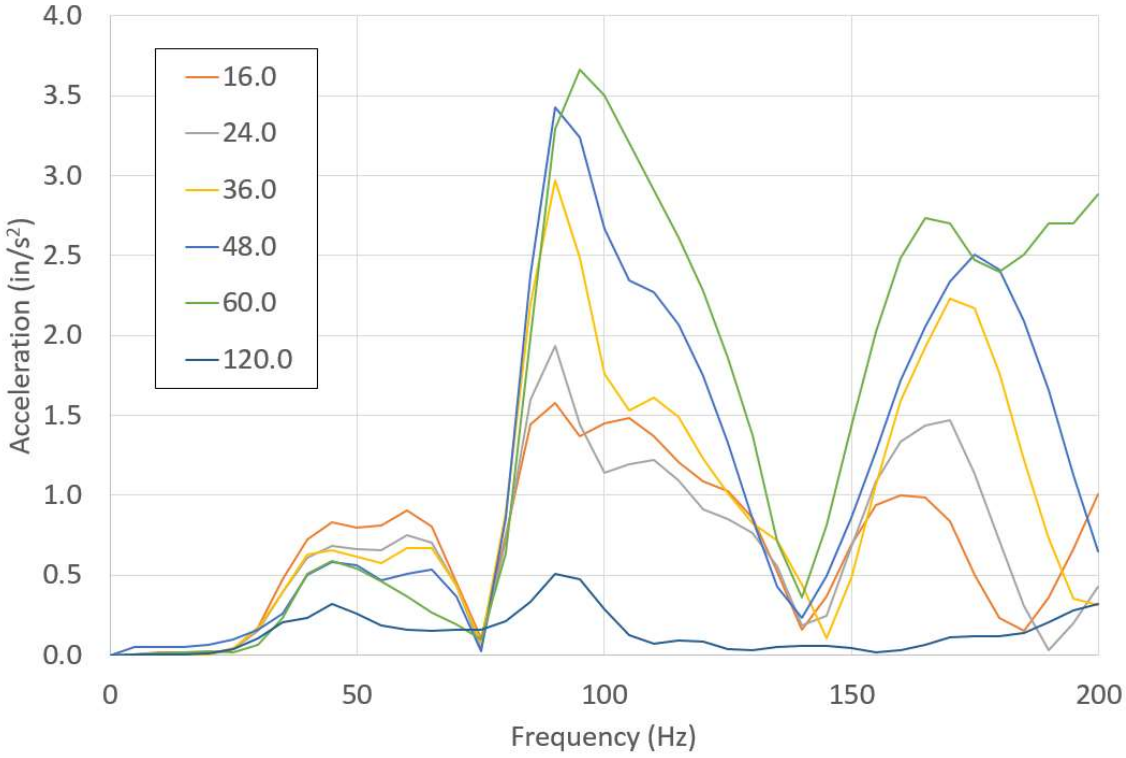

Figure 4-32: Combined Spectrums for One Location for All Tests

The final key to this puzzle that led to the most likely source of the absorption variation came from the time history of the hammer strikes. Figure 4-33 shows a typical time history between the sensor 1 at L1 and sensor 3 at L5 which are 18 feet apart. The sensor 3 values are scaled up by a factor of 250 to account for attenuation

and make a visual comparison possible. Looking at all of the tests carefully, the very first small amplitude part of the wave arrives at a somewhat consistent velocity of 6,000 to 7,000 feet per second, which corresponds to a shear wave velocity for concrete. However, the first large peak seems to travel at a consistent velocity between 2,600 and 3,000 feet per second, which does not correspond to the shear wave velocity of either medium.

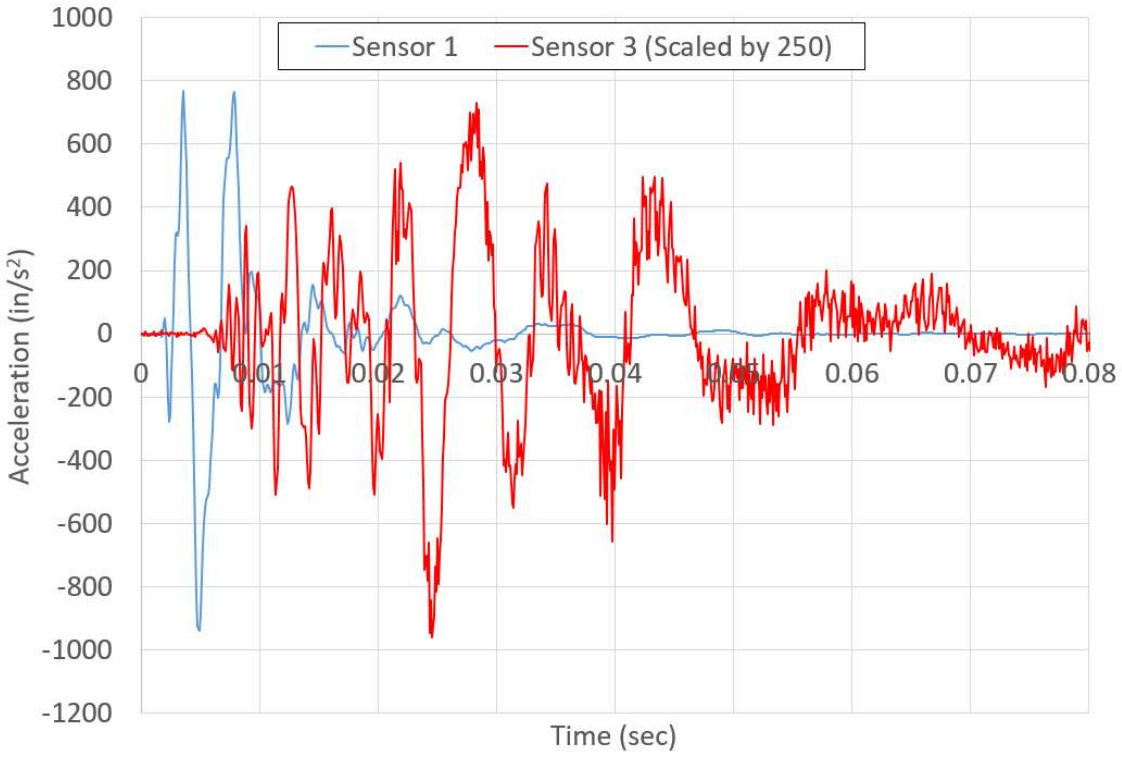

Figure 4-33: Acceleration Time History, Impact 5 Feet before Sensor 1

By carefully studying the profiles like the one in Figure 4-33, the vibration wave appears to have changed as it traveled from sensor 1 to sensor 3. The signal at sensor 1 has two clear positive peaks, then significantly damps to lower peaks. The signal at sensor 3 seems to have a repeating pattern of two peaks, but each successive set of peaks is at a lower frequency with similar amplitude. This seems to indicate that unlike the assumption of a Rayleigh surface wave, which travels at a velocity independent of

frequency, the velocity of the wave here appears to decrease with decreased frequency causing the wave to disperse over distance. Although this phenomenon is well known, it was not addressed in the researched articles dealing with measuring surface wave attenuation with regards to equipment nor in articles dealing with vibrations near sensitive equipment, and it was unknown to the author of this thesis up to this point. This line of thinking will be further discussed in next section.

4.6 Recommended Attenuation Model for Industrial Equipment

It is abundantly clear based on the attenuation results from the individual tests that the mechanism for how vibrations generated from equipment on a slab on grade decay is more complex than the Bornitz Equation (2-10). There does appear to be an overall increase in the absorption as frequency increases, which lends some justification to Amick's modification of absorption coefficient, Equation (2-12), increasing linearly with increased frequency. However, this does not explain the local peaks and valleys of the absorption at different frequencies. Yang's (1981) modification to include a body wave component does not seem to answer any of these questions either as the waveforms measured appear to be primarily surface type waves created from a surface source. Although, it is possible to adjust the geometric damping coefficient as Kim and Lee (1999) did on a frequency basis and align the absorption results for a single test or very similar test, those factors were different for every location for the results in this report. The mechanism for geometric damping is somewhat simplistic and is based on energy balance through an increasing vibrating mass with distance. For this reason, modifying the geometric damping to align results was deemed undesirable.

There is a line of thinking that does seem to more consistently address the measured absorption values for these experiments. This lead came from the apparent inconsistencies of the measured waveform velocities. For example, the velocity measurements for the scroll saw varied from a maximum possible velocity of 700 feet per second to a possible minimum of 120 feet per second, but in the same exact location, the hammer blow tests appear to have a surface wave velocity of over 2,600 feet per second. Up to this point, the surface wave was considered to act as a Rayleigh type wave which is considered non-dispersive. For a non-dispersive waveform, the phase velocity does not change with frequency. One explanation for why phase velocity appears to vary at a single location is that the waveform is dispersive, simply meaning that the waveform velocity is a function of frequency or more aptly wavelength. This highlights the first major point and is covered in the next section.

4.6.1 The Wave Travels through the Soil Not the Slab

To begin this sub section, it is interesting to note a question that has come up at times for installing sensitive equipment: is it better to, at the very least, cut a physical joint through the concrete slab surrounding a piece of sensitive equipment? The idea behind this is simple, concrete in and of itself transmits vibrations very well with low attenuation so why not create an air gap to stop this transmission? On the surface this seems an obvious good design decision; however, from the measurements taken in this report across a building expansion joint with a clear high impedance ratio similar to air, the best case result was no effect from the joint. For example, consider Figure 4-34.

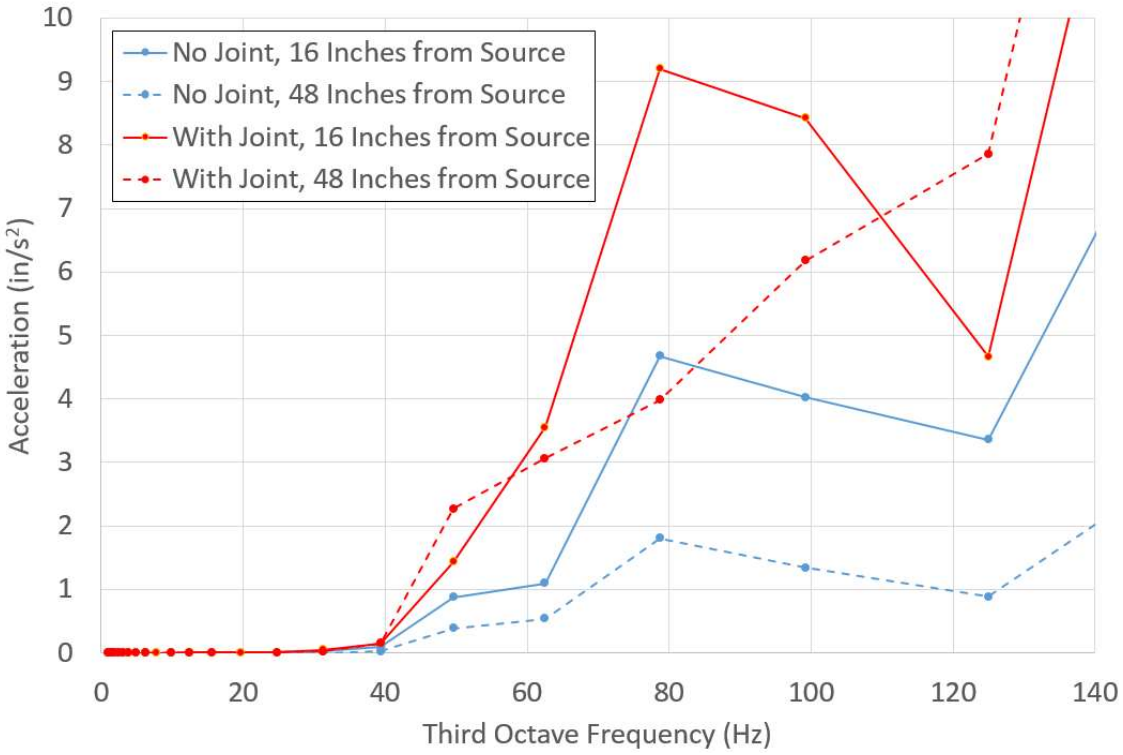

Figure 4-34: Vibration Differences through Expansion Joint

Figure 4-34 was created from the acceleration measurements of the booster pump E1 with sensors at L3, L4, L6 and L7. There is a building concrete expansion joint between L6 and L7, 13 inches from L6. The blue "no-joint" lines show the expected pattern where there is decay in every frequency band as the distance increases. However, the red "with joint" lines do not behave as expected. In the 50 and 125 Hz bands, the acceleration amplitude actually slightly increases. Although not shown, the third sensors L5 and L8 had similar acceleration magnitudes indicating that accelerations near a joint can be magnified. Most of the other bands have similar decay with distance, but in no way does the joint measurably help reduce the vibrations. There were similar results when measuring booster E2 from sensors at L1 and L2. L2 was inside an old isolated equipment foundation, isolated from the concrete slab that is.

It is also interesting in Figure 4-34 that the magnitudes of the vibrations in the wave direction that crosses the joint are nearly double those of the opposite direction not crossing the joint. All of the moving parts in the booster pump moved linearly in the direction perpendicular to the measurement vectors and although it is not provable with the available data, it is likely that the magnitudes would be similar if the joint did not exist at all. This could be explained that the joint reduces the stiffness of the slab, and this lower stiffness allows greater initial displacements in the slab, resulting in higher accelerations near a joint.

Taking both of these aspects into consideration, simply adding an air gap in a concrete slab with the intent to reduce vibrations is not advisable. But, this brings the question of: how do vibrations travel through this physical break? The majority of the vibration's waveform at the frequencies under consideration here must be traveling through the soil beneath the concrete slab. This is somewhat expected as the general solution to a Rayleigh wave as Richart et al. (1970) derived shows the expected depth a Rayleigh wave extends to be primarily a function of wavelength, and still has about a 20% magnitude at a depth of one wavelength.

This phenomenon, although not frequently documented with regards to attenuation of vibrations for the purposes discussed in this report, is well documented (Lefeavre et al. 1998). In fact, for years surface waves have been used to determine the characteristics of the medium in which they are traveling using the knowledge that the surface wave extends a known distance into the half space based on the wavelength. This leads to a similar experiment performed by Jones (1962). Although Jones was not concerned with how far vibrations traveled in a slab on a grade, he was concerned with

the theoretical background of a non-destructive test to determine the thickness of a concrete slab on grade using surface waves, in particular an existing roadway's thickness.

There are several key points from Jones's work and others like it that have application here. Focusing on the simplest case of a medium of finite thickness with a relatively high shear wave velocity (e.g. concrete resting on a medium of infinite thickness with a relative slow shear wave velocity like soil) several key behaviors can be seen. When the wavelength of the surface wave traveling on the concrete is small enough that all of the surface wave travels in the concrete, the surface wave travels at the expected phase velocity of a Rayleigh wave. For concrete, the calculated Rayleigh velocity is greater than 5,000 feet per second, and since this wave would entirely reside in the concrete, it would be non-dispersive, and the wavelength can be directly calculated. Assuming the highest frequency (resulting in the shortest wavelength) considered in this study of 125 Hz, the wavelength in the concrete would be on the order of at least 40 feet. It is not the purpose of this paper to determine precisely at what wavelength to concrete thickness ratio all of the surface wave would be traveling in the concrete, but suffice it to say the practical ratio is on the order of 0.5. In other words the concrete would need to be about 80 feet thick for this condition. For the acceleration vibration measurements in this thesis, the thickest concrete layer was 8 inches thick giving the smallest concrete to wavelength ratio of 60, which is much larger than 0.5.

With the same situation of concrete sitting on soil, when the majority of the surface waveform is traveling in the infinitely thick soil, the surface wave in the

concrete will travel at the phase velocity of the soil. The limits of the velocity of a Rayleigh wave traveling is soil are not as consistent as concrete, but assuming a value of 600 feet per second is reasonable and would equate to a wavelength of about 5 feet for the same 125 Hz frequency. Since the soil layer in this description is infinite, the wavelength to thickness ratio does not matter. However, it is important to remember that 5 feet is the smallest wavelength. Some of the acceleration measurements in this report were at 15 Hz and the soil velocity could be as high as 1,200 feet per second making a wavelength of 80 feet. Eighty feet is not a problem for infinitely thick soil, but in situ soil in the locations tested have multiple layers of varying thickness. Nonetheless, the vibrations at the frequencies considered for sensitive equipment clearly travel in the soil.

This idea of wave phase velocity on the concrete top layer traveling at the velocity of the layer underneath, may be a troubling thought as it seems that the concrete wave should propagate based on its own material properties. To make a simplified analogy that is not exactly what is occurring but is similar enough to demonstrate the behavior, consider two sine wave originating at the same point, traveling in a single direction along a line at the same frequency, but at different phase velocities. Next, consider a point some distance from the waveform origins. At this point, each wave will be oscillating at the same frequency as the velocity is not apparent at a single point; however, since the faster wave's "peak" would have arrived at this point before the slower wave's "peak", there will be a difference in phase angle between the two waves. Now, a real measurement at this point cannot distinguish between the two waveforms as the measured particle can only be in one place at one

time. The real measurement will show only the summation of the fast and slow waveforms. Figure 4-35 shows what this summation would look like where A1 is traveling faster than A2.

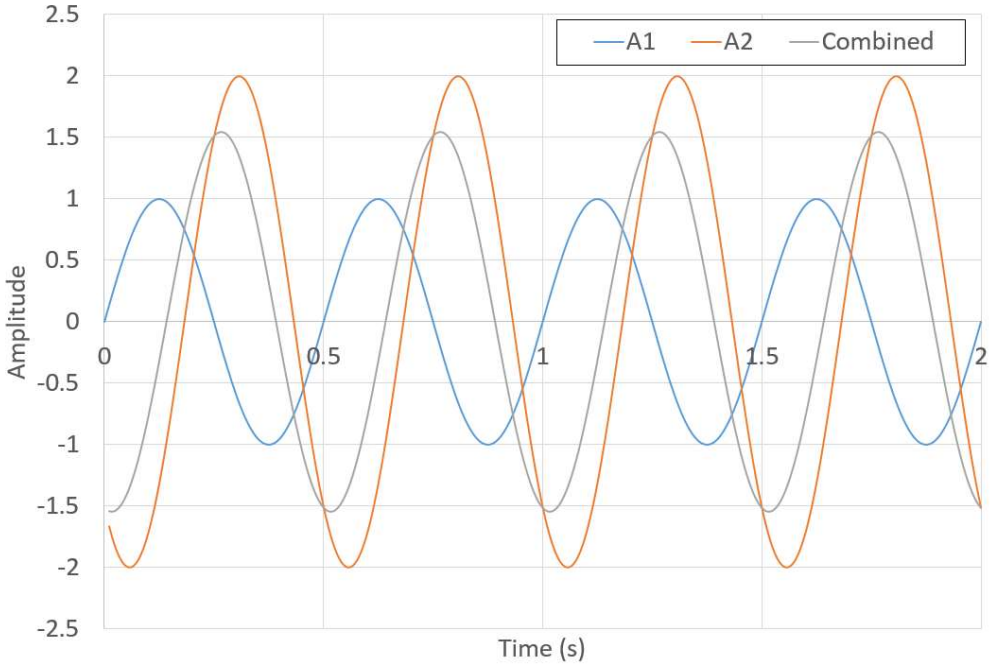

Figure 4-35: Sine Wave Analogy

The combined waveform oscillates at the same frequency of both of the individual waves, but has a shifted phase somewhere between the two original waves. To calculate the combined phase angle, the following equation from basic trigonometry can be used:

$$\phi_c = \text{atan}\left(\frac{A_1 \sin(\phi_1)\sin(\phi_1) + A_2 sin(\phi_2)}{A_1 cos(\phi_1) + A_2 cos(\phi_2)}\right) \quad \textbf{(4-2)}$$

The phase angle, ϕ_c, is dependent on the amplitude, A_1 and A_2, of each individual wave. If the amplitude of wave one, is significantly larger than wave two, the combined phase angle will simply be the phase angle of wave one and the phase angle of wave two will

have no impact. The amplitude of these simple sine waves is analogous to the level of energy of each surface wave traveling at each velocity in each medium.

To draw this analogy to a close there must be at least two point measurements to determine the velocity of the combined sine waves. The same principle will apply to the second point, and this effect will make the apparent phase velocity measured from peak to peak at points one and two dependent on the combined phase. In the real world example of the concrete on the soil, since the soil would have most of the amplitude, the phase angle would follow the soil and the apparent velocity would be the same as the soil waveform velocity.

4.6.2 Attenuation Models for Single Pieces of Equipment

One of the main aspects to this thesis is ability to predict the attenuation of vibrations sourced near vibration sensitive equipment. Up to this point, the raw acceleration measurements described in sections 4.1 to 4.4 have defied a consistent explanation. The values of the absorption coefficient have peaks at frequencies that are much higher than referenced documents (Amick 1999). Yet, there is a reasonable explanation if the line of thinking of surface wave dispersion is continued from section 4.6.1.

The point of section 4.6.1 was to provide a reasoning as to why the surface wave does not appear to be affected by the presence of the concrete slab, but there is more to the mechanics of surface wave dispersion that is applicable to these results.

At a certain frequency/wavelength, Jones (1962) described a change that occurs that he terms the transition from an upper branch of a curve to a lower branch and that, at this transition, attenuation is very high. He was making use of this behavior to help

determine the thickness of layers by forcing varying frequencies to travel across the surface of concrete. Additional work in acoustic microscopy has been more recently researched in this area (Lefeuvre et al. 1998), and term this high attenuation the "cutoff." Figure 4-36 shows this cutoff behavior on a small scale. As the phase velocity increases, the wavelength of the vibrations decrease (this was done at a constant frequency excitation), and a clear distortion of the attenuation can be seen at a given top plate thickness of 5 microns (the top plate or film in this case thickness was varied).

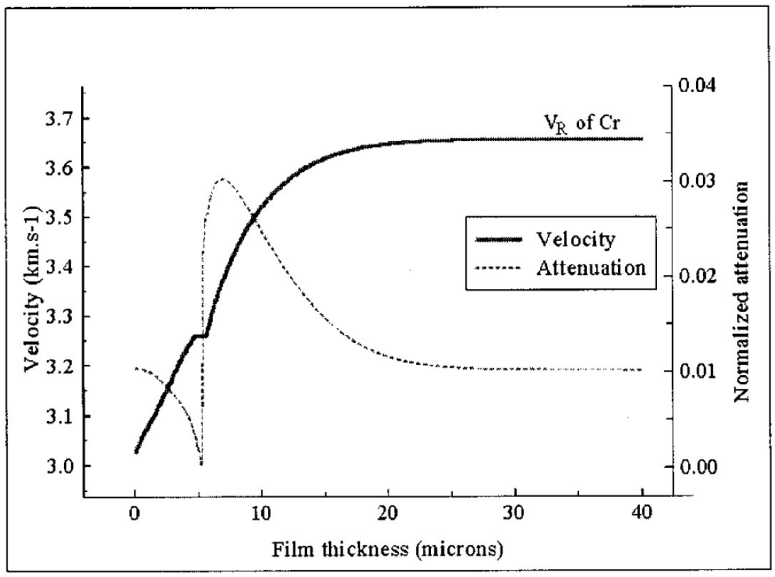

Figure 4-36: Graph Showing Cutoff (Lefeuvre et al. 1998)

The point here is not to determine precisely where the cutoff happens or use this information to determine concrete thickness or soil layer thickness, but to recognize that this cutoff will affect attenuation at specific frequencies more than other frequencies.

It is now time to move from the case of a fast thin concrete layer resting on an infinitely thick slow soil system to a fast concrete layer resting on a layered soil system with multiple slower surface wave velocities. Each of these layers will have its own

cutoff frequency, which would show up in the measurements taken here as increased absorption. As the vibration frequency decreases, the depth that the wave extends into the soil increases and is thus affected by deeper layer boundaries.

4.6.3 Recommendations for Absorption Values

The two fold behavior described in the previous two sections realistically describes the measured vibration behavior in these experiments. First, the majority of the waveform is traveling in the soil, and thus the absorption behavior is governed more by the soil behavior than the concrete. This explains partially why the absorption values overall are higher than expected. The documented values of soil are higher than the documented values of concrete. Second, there will be increased surface wave attenuation at frequencies that correspond to cutoffs of the underground soil layers.

With this behavior understood, it is now possible to make recommendations for absorption values in real world facilities. The most important realization is that the peaks in the absorption spectrum are most likely related to soil layering, which will vary from site to site and even in a single building. It is not advisable to take direct attenuation readings for a piece of equipment, relocate it, and expect the attenuation to be exactly the same since the soil layering will most likely be different. This holds true whether using the third octave spectrum used for this report or peak time domain values, since both are just different methods of processing at the same information. Another reason to not use the peaks in the attenuation spectrum is that, with modern industrial equipment, it is not a good assumption that the equipment will be operating at a constant frequency over its lifespan. Even for equipment currently driven by inductive constant speed motors, the increased prevalence of variable frequency drives

coupled with energy reduction initiatives creates a possibility that the operating frequency will be reduced, which could move the vibration spectrum out of high absorption values into lower values.

When the peak values absorption values are removed from the absorption spectrum, the values can be reasonably captured using the theoretical Equation (2-8) derived by Kramer (1996). Changing the name of k_2 to β and recognizing that shear wave velocity can replace density, ρ, and shear modulus, G, a more useful equation can be written as follows:

$$\beta = \frac{\omega}{V_s}\sqrt{\frac{1}{2(1+4\xi^2)}\left(\sqrt{1+4\xi^2}-1\right)} \qquad \textbf{(4-3)}$$

Equation (4-3) has two material properties that must be known or determined: the shear wave velocity, V_s, and the critical damping ratio, ξ. In a further simplification, for small ξ, the radical term simplifies to ξ, viz.

$$\beta = \frac{\omega \cdot \xi}{V_s} \qquad \textbf{(4-4)}$$

Note that this is not a new equation and is similar to Equation (2-13).

The damping ratio for small strains has been previously reported as shown in Figure 2-3. For these types of conditions, it is recommended to use a nominal value of 2.5% for the damping ration, ξ.

If possible, it is recommended to use two accelerometers spaced at a short distance (less than 2 feet) and measure the shortest lag times from the cross correlations between two stable acceleration signals to provide the maximum measured phase velocity to be used as the shear wave velocity for calculating Equation (4-4). If accelerometers are not available (note that they do not need to be as sensitive as the

sensors used here), Wair and DeJong (2012) provide guidelines on estimating the shear wave velocities of soils.

Using this method and normalizing the acceleration amplitudes from the third octave spectrums, a comparison was created. Figure 4-37 shows this comparison for the 30 Hz third octave band for all of the measurements from all equipment taken in the location described in section 4.2. Since the maximum calculated phase velocity varied between 400 and 800 feet per second, an average of 600 feet per second was used for this chart.

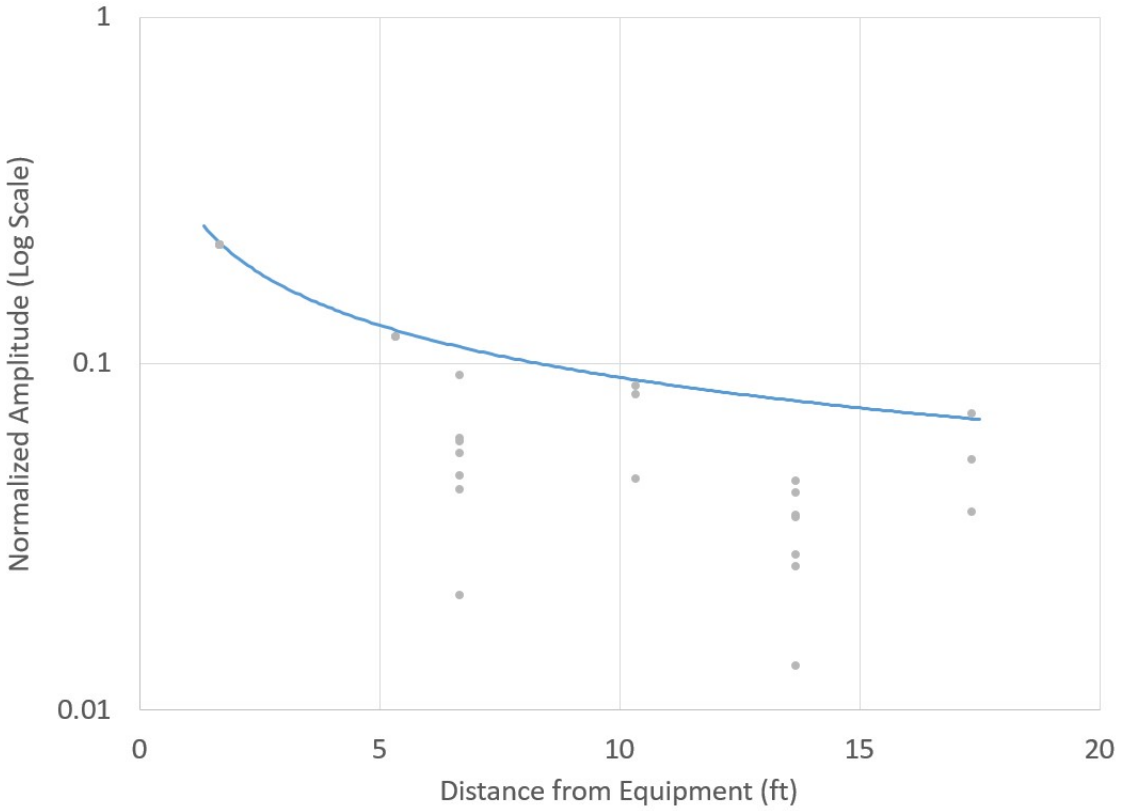

Figure 4-37: Normalized Accelerations vs. Distance for 30 Hz Band

A useful characteristic to using this theoretical absorption coefficient is that, for all of the frequencies where there was increased absorption from cutoff, the method is

consistently conservative. In fact, this method rarely under predicted the acceleration magnitudes, which is a useful characteristic in design.

4.6.4 Recommendations for Magnitude

The final aspect necessary to predict the effect of vibrating sources near a piece of sensitive equipment is knowing how much vibration energy is transferred from the vibrating source to the concrete slab.

For the simplest case, if the vibration source is already near its final installed location and standard accelerometers are available, a measurement of the acceleration can be directly taken near the equipment and then applied to Equation (4-1) using the method to determine β described in section 4.6.3. The accelerometer does not need to be overly sensitive because only the high magnitude vibrations will be measured and the lower values at a further distance from the source where a standard accelerometer may not be as reliable, will be calculated as previously discussed. However, the measurement does need to be somewhat close to the source, half of the equipment's width away, to limit the effects of possible high absorption values affected from waveform dispersion effects. It is possible that some equipment excites the ground non-uniformly, which was seen in several of the measurements taken; therefore, a second measurement the same distance from the equipment should be taken at a location perpendicular to the first measurement to note any differences related to direction.

A more common case is where a piece of equipment will be relocated from one location to a location near the sensitive equipment. Assuming modeling the connection between the vibrating equipment and the concrete slab as a single degree of freedom spring-damper is a fair representation, Equation (2-18) can be used. For the steady-state

vibration sources, the exponential decay portion of the equation can be ignored. The transfer portion of the equation can also be ignored. This assumption is realistic since the concrete slabs from one location to another will likely behave in the same way with respect to the excitation frequency. In other words, even though the stiffness will vary from one concrete slab on grade to another, the frequency ratio *r* will not very enough to change the behavior. In fact, the value of the transfer function is likely to be approximately 1 for the types of equipment described here, especially considering a majority are directly bolted to the concrete slab. This leaves only one value to vary from location to location, X_0, the equivalent static displacement.

By eliminating the transfer function and the transient portion, X_0 can now readily be converted to acceleration in the frequency domain by multiplying the displacement by the excitation frequency squared. The excitation frequency is a property of the equipment and will be the same at both locations allowing for a linear comparison of accelerations in the frequency domain. This allows for two possible methods to determine how the primary acceleration values will change for one location to another location.

The first method would be to simply apply the same static load in the known location and the future location, compare the deflections, and multiple the known acceleration spectrum by the ratio of deflections to create the initial magnitude of accelerations at the future location. Without a significant load or sensitive displacement measuring technique, this method is impractical.

The second method is to take a vibration source that can be easily relocated and measure accelerations in both locations. Just like with the deflections, create a ratio

between the two measurements and multiply this ratio by the known accelerations. The second method is likely to be more accurate and could even be applied over the spectrum to capture any effects ignored by the assumption of eliminating the transfer function.

The additional complication with vibration sources that produce a pattern that is directional will be address in the next chapter, which deals with combining multiple vibration sources surround a sensitive piece of equipment.

4.7 Summary

- Floor vibration caused by equipment operating in a steady state condition decay at varying rates from surface wave dispersion caused by layered concrete and soil.
- It is not possible to directly measure the attenuation of a piece of equipment in one location and expect the attenuation to be identical in another location even if the slab and underlying soil are similar as the subsurface conditions govern the behavior at the frequencies under consideration here.
- The attenuation of floor vibrations on the surface of a concrete slab can be conservatively modeled using the frequency dependent absorption values calculate from Equation (4-4).
- The majority of the vibration waveform travels through the soil at a depth greater than the waveform wavelength. Any attempt to isolate sensitive equipment from a vibration waveform must take this into account. For example, simple cutting an air gap in the concrete slab, in general, has no positive effect.

5. Multiple Equipment Results and Discussion

For a piece of moderately vibration sensitive equipment (VC-C) installed in an industrial facility near vibration source equipment, it is likely that there are in fact multiple pieces of vibration source equipment. It is therefore necessary to have a method for combining the vibrations from multiple sources and estimating their impact at the location of the sensitive equipment.

5.1 Theory for Combining Vibration Waveforms

The idea in this chapter centers on the premise that when two waves come together at a point location, their displacement amplitudes at any instant in time add together. Since the data in this report is primarily analyzed in the frequency domain, the magnitudes of the displacement amplitudes are related to the magnitudes of the acceleration amplitudes at each frequency by a factor of the angular frequency squared, i.e.,

$$|\text{Acceleration}(\omega)| = |\text{Displacement}(\omega)| * (\omega^2). \quad \textbf{(5-1)}$$

The relationship in Equation (5-1) is "simplified" because it ignores phase angle shift. In reality, the displacement and accelerations are 180 degrees out of phase; however, at each frequency the change is the same, and it is therefore possible to say the accelerations from two waves add together at a single point.

However, it cannot be said that the magnitudes of two waves added together can be unassumingly directly summed. Even if at one theoretical point, the peaks of the two waves arrived at this point at the exact same time (completely in-phase), that could not be true at adjacent points. In other words, on a floor space where a sensitive piece of equipment will be installed, there will be places where the waves from two sources will

be in-phase and out of phase. The trigonometric relationship that relates phase difference to adding two waves is as follows:

$$|A_c| = \sqrt{|A_1|^2 + |A_2|^2 + 2|A_1||A_2|\cos(\phi)}. \quad \textbf{(5-2)}$$

where A_c is the combined magnitude of the two waves that have a phase difference of ϕ in radians. A_1 and A_2 are the magnitudes of the individual waves. It may not be completely obvious, but if there is no difference in phase ($\phi = 0$), Equation (5-2) simplifies to $A_c = A_1 + A_2$. Conversely, if the waves are completely out of phase ($\phi = \pi$), Equation (5-2) simplifies to $A_c = A_1 - A_2$.

Even though it is possible to take the phase information from the FFT and determine a precise phase angle difference for each frequency at every location on the floor space, it is not useful for design purposes. There is no guarantee that the relative phase between two sources will remain constant at every frequency over the lifetime of a vibration sensitive piece of equipment and what is measurable today, may not be the same measurement tomorrow even. Subsequently, it is more important to work with the maximum values of the combined accelerations, and the assumption is that the maximum combined magnitude is in fact, the direct sum of the individual magnitudes.

Finally, since the research in this thesis is based on real industrial type equipment and not a calibrated waveform generator, it is unlikely that two pieces of equipment will operate at exactly the same frequency. In other words, one piece of equipment may operate at 59 Hz and another piece may operate at 58 Hz. Even though they are operating at similar frequencies, a fine resolution FFT can distinguish between the two frequencies, and they will show up in a fine spectrum on their separate corresponding frequencies. Since the primary method for defining the spectrum bands

was third octave intervals that simply summed all of the accelerations in that band, contributions from two pieces of equipment is generally expected to simply sum magnitudes.

5.2 Experimental Results

The setup for these experiments was the same as the setup described in Chapter 4 except, instead of a single piece of equipment operating, two pieces of equipment were operating. The procedure involved turning on one piece of equipment and recording the acceleration third octave spectrum, then doing the same for the other piece of equipment, and finally running both pieces of equipment simultaneously.

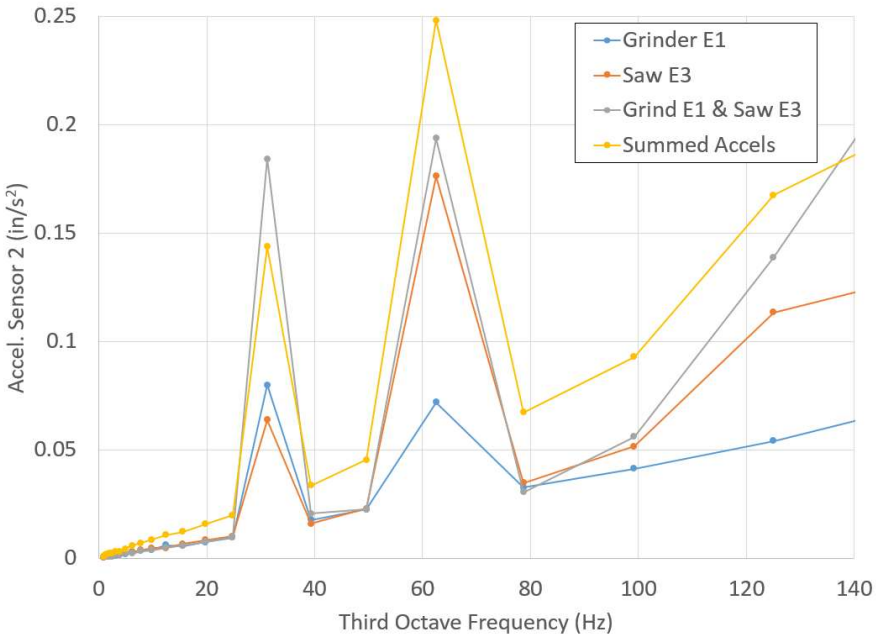

Figure 5-1: Accelerations for Two Sources at Different Locations

Figure 5-1 shows the results from a single accelerometer at location L2 as shown in Figure 4-13. With the exception of the 30 Hz band, all of the measurements line up as expected. The only offered explanation is that the grinder did not perform consistently between the time it was operated with the saw and the time it operating by

itself. From looking at the fine scaled FFT, both the characteristic frequency distributions can be seen for the saw and grinder separately and in the combined test. One peculiarity sticks out: the amplitude at 33.5 Hz increased and the amplitude at 67 Hz decreased for the grinder. Most likely, this is from inconsistencies in how the grinder runs.

In order to compare the data from multiple sensors and multiple tests at the same time, the measured accelerations from two pieces of equipment were divided by the summation of the accelerations from each individual measurement at each third octave frequency. In other words, if the measured acceleration is exactly the sum of the single measurements, the ratio would be equal to one indicating the measurements are constructive. If the value is below one, this indicates there is some interference between the acceleration waves of the equipment from phase angle differences. If the value is above one, this indicates inconsistences with this approach. Figure 5-2 shows the results of the vibratory equipment fully described in Section 4.3.

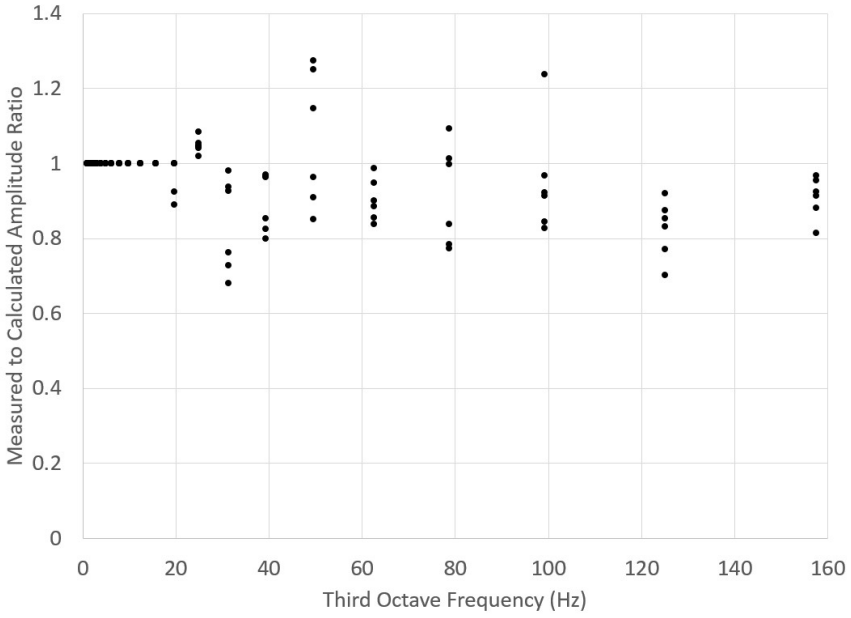

Figure 5-2: Calculated vs Measured Amplitude Ratio for Vibratory Equipment

Almost all of the data points perform as expected indicating that the simplified assumption of adding waves on a third band basis is acceptable. However, some of the values in the 50 Hz band are enough above one (~30%) to require further scrutiny.

Figure 5-3 shows the full spectrum in 0.025 Hz increments of the 50 Hz band for the data point in Figure 5-2 that had the highest ratio.

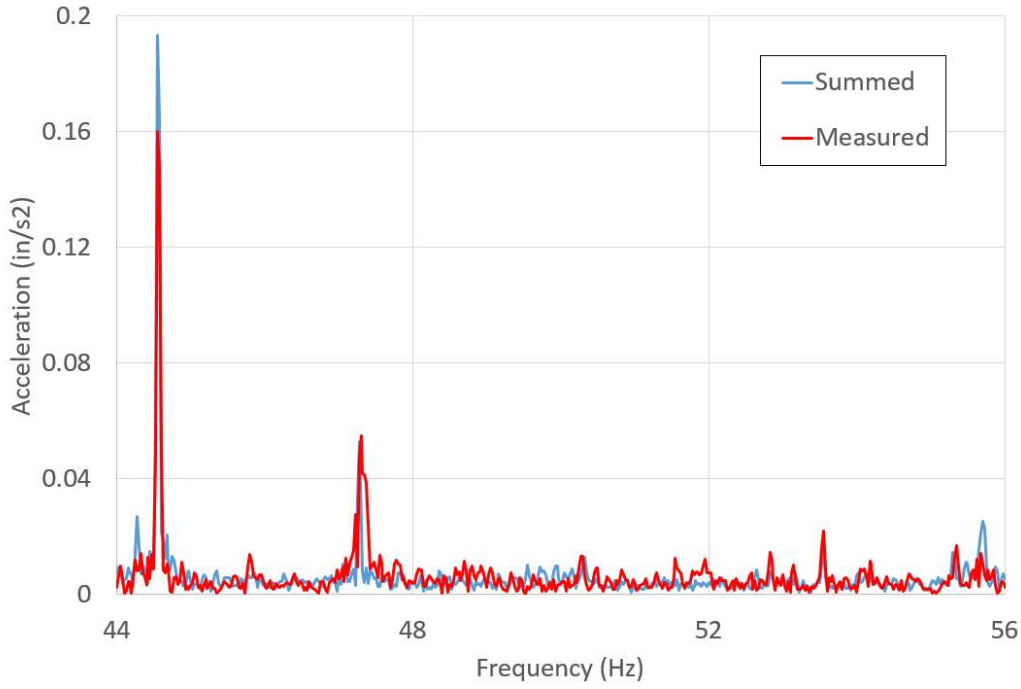

Figure 5-3: Fine Frequency Spectrum of 50 Hz Third Octave

The "Measured" data refers to the actual accelerometer readings taken while two vibratory machines were running. The "Summed" data is the values of each individual vibratory machine running added together for each frequency increment. Where the "Measured" values exceed the "Summed" values, this indicates a conservative value. For the five highest peaks, this is the case and this method provides ideal results. However, some of the smaller magnitude values are higher for the "Measured" case. Once again, since this is a real world machine with cleaning beads shaking around at somewhat random intervals, it is expected that the lower more random vibrations will

have more variance. It is viewed here that the more critical amplitudes are the large non-random specific amplitudes. Since this method accurately predicts or overestimates those, this deviation is not viewed as a significant problem.

One final set of results to consider is the equipment tested near the LaserDyne described in section 4.4. Using the same procedure that was used to create Figure 5-2, Figure 5-4 was generated. The results show that other than a couple of outliers this method performs well. One additional benefit to the data here are the low values. The values around 0.5 are from a test involving the two identical compressed air booster pumps. Since these boosters were identically running and running at their maximum speed, they have a higher likelihood of having very similar acceleration spectrum. This makes interference between the two waveforms more likely, and that interference shows up in a reduced combined acceleration measurement. This lends additional credence to the thought that summing magnitudes is a conservative approach.

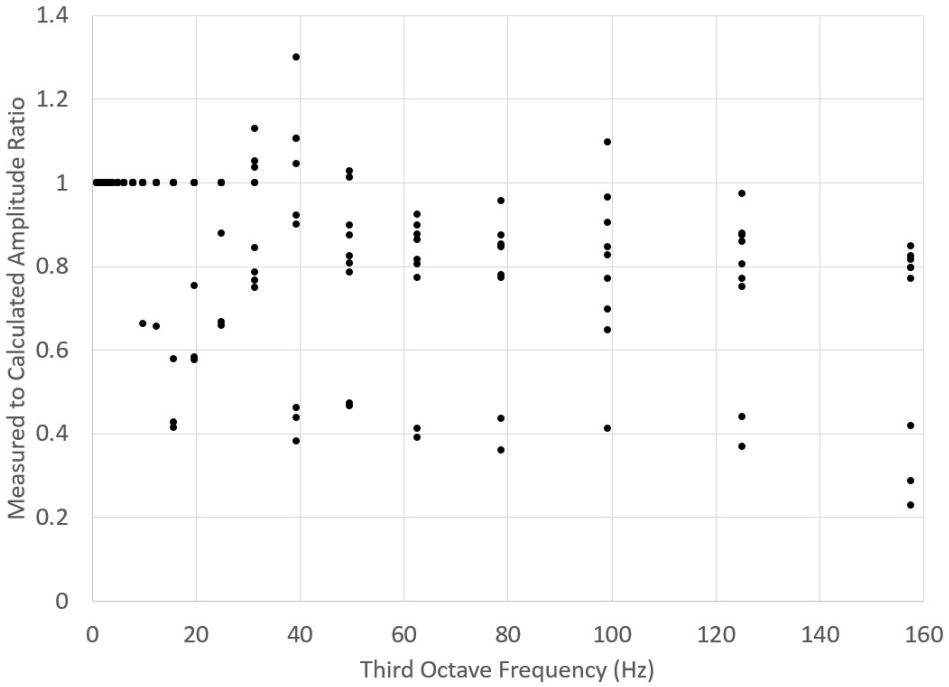

Figure 5-4: Calculated vs Measured Amplitude Ratio near LaserDyne

In summary of this section, although the precise behavior of multiple vibration waves combining is more complex and a function of both distance and frequency, it is a reasonable and conservative assumption to simply superimpose magnitudes from multiple waves at a single location.

5.3 Application

By combining the attenuation model created in Chapter 4 with the concept of equipment vibration magnitudes summing together, a prediction for the floor vibration for a given location can be created. To demonstrate the usefulness of the methods described in this thesis, an example will be worked through in this section to draw everything together.

The specific details in this example are partially idealized to simplify the presentation of the combined method for predicting slab vibrations in an industrial facility as well as use the measured data presented in this thesis. However, this is based on a real situation at a real industrial facility.

The vibratory equipment described in Section 4.3 is currently located in a 400,000 square foot facility that was originally designed to remanufacture jet engine turbine blades. Over the years, the demand for this type of turbine blade has reduced and the process to remanufacture them has changed. In fact, this building which used to be exclusively for this process is now home to completely different manufacturing processes, and the vibratory equipment is the last vestige to the turbine work in this building. Through a process improvement initiative that focused on reduced part travel time, it was determine to relocate three vibratory machines to another building near the chemical cleaning production line which is a process directly related to vibratory

cleaning. Unbeknownst to the team making the decision to move the vibratory equipment, the LaserDyne cutter, which is a vibration sensitive piece of equipment, is located in the same vicinity. After the decision to move the vibratory equipment becomes fully approved by management and general knowledge to plant personnel, concerns were raised that the vibratory equipment would affect the quality of the high precision aircraft parts produced on the LaserDyne.

This is why it necessary to have an accurate method to predict how industrial equipment vibrations combine and attenuate throughout an industrial plant. In this case, so much administrative energy has already been spent towards the benefits of relocating the vibratory equipment that simply canceling the move because it might cause a vibration problem is not possible. Additionally, moving the actual equipment and then testing the floor to determining the effect is excessively risky. However, if it can be shown that the planned location has a high likelihood of adversely impacting the LaserDyne, and even show locations far enough away that will suffice, it is more likely to overcome the already spent administrative energy. Furthermore, the planned location may be acceptable which could help quiet concerns. Figure 5-5 shows the planned location for the vibratory equipment.

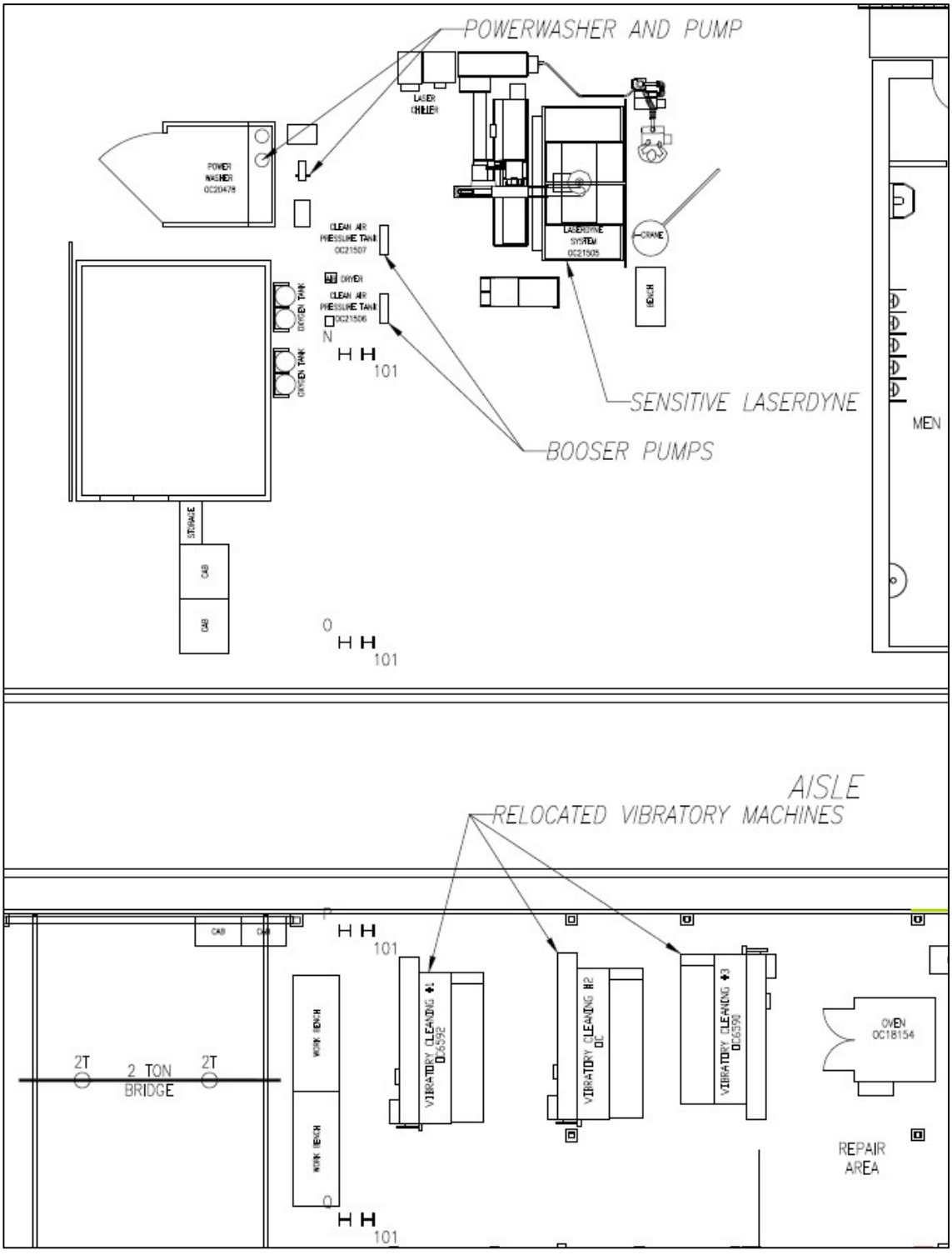

Figure 5-5: Equipment Layout Showing Relocated Vibratory Equipment

5.3.1 Determine Ambient Vibration Noise

The first step in the application of the methods described in this thesis to determine the total floor vibrations of a floor space is to ascertain the existing ambient floor vibrations with no nearby equipment running. The ambient vibration noise was already determined and used to separate the equipment portion of a measured vibration signal from the total signal as shown in the flow chart, Figure 3-3. Now, the ambient noise is the base vibration levels applied to the entire floor space under consideration.

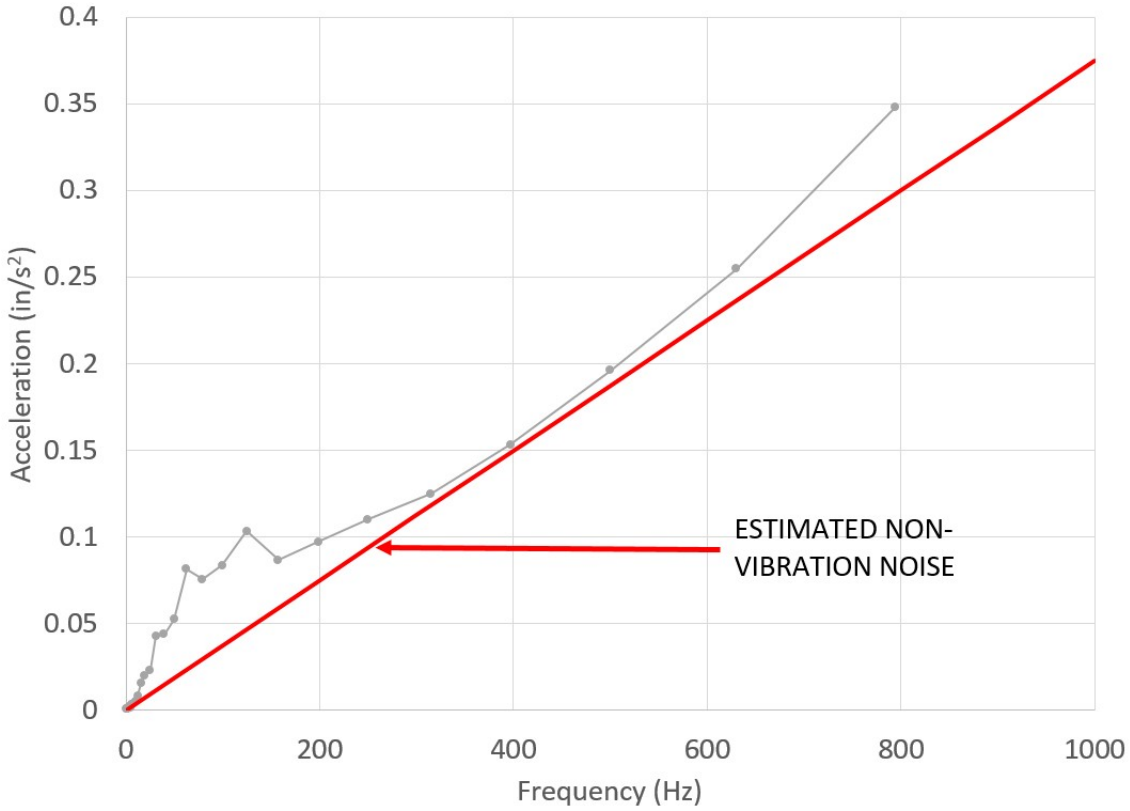

Figure 5-6: Raw Measurement of Ambient Noise

Figure 5-6 shows the ambient noise acceleration spectrum measured near the LaserDyne machine. One difference that needs to be applied here that did not need to be applied when taking measurements of vibrating equipment is to distinguish between actual vibration ambient noise and electrical signal noise. Previously, both needed to be

subtracted from a measurement, but now only the actual ambient vibrations are necessary. By assuming that the electrical noise will follow a Gaussian distribution, and that all of the higher frequency physical vibrations will have already attenuated by this location, a pattern can been seen in the third octave spectrum. By calculating the noise per frequency from the higher frequencies (above 300 Hz) as the average signal in each band, and subtracting that noise from the total signal, an estimated ambient vibration noise signal can be calculated. This result is shown in Figure 5-7.

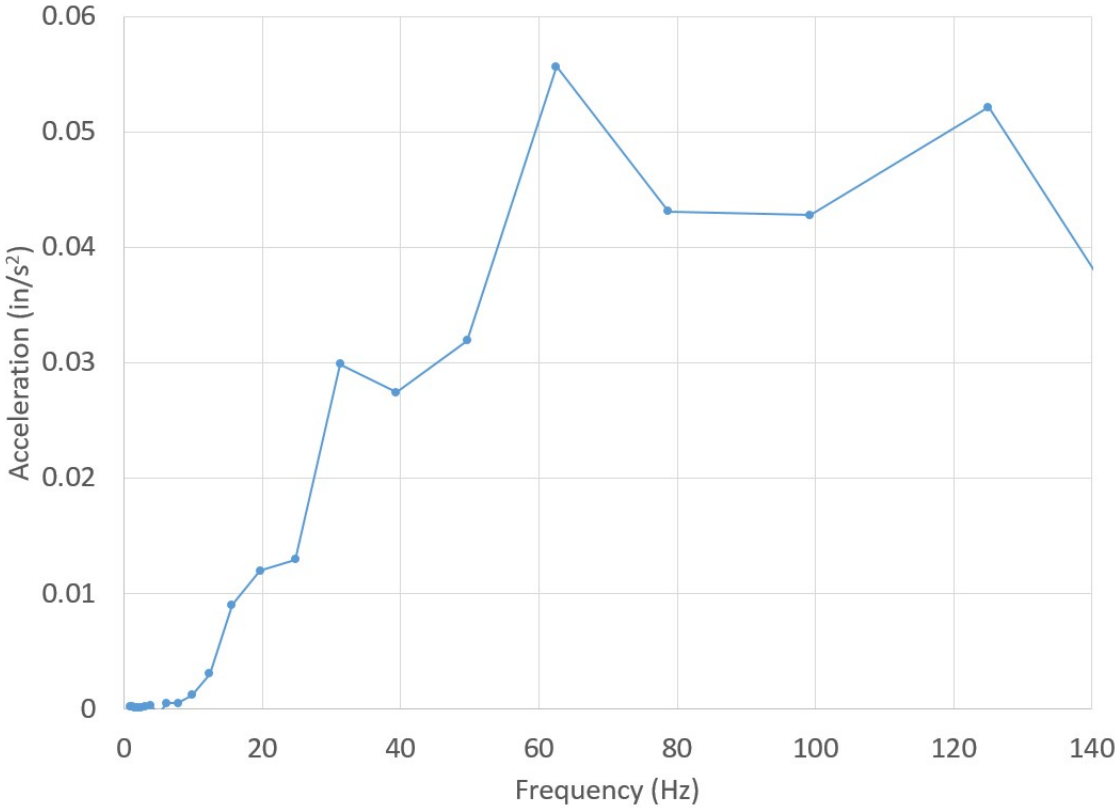

Figure 5-7: Ambient Vibration Noise with Electrical Noise Removed

The obvious aspect must be mentioned in that if the ambient vibration noise at a location is already above the specifications of the sensitive equipment, there is no need for further analysis with this method. However, in the case of the LaserDyne there is room for additional vibrations without violating the specification. For example, in the

62 Hz band, the LaserDyne can tolerate 0.5 in/s^2 acceleration vibration, which is an order of magnitude above ambient.

5.3.2 Determine Individual Equipment Models

Once the ambient levels are determined to be acceptable, the vibration attenuation models for each individual piece of equipment nearby the sensitive equipment must be determined. The core of the model is based on Equation (4-1) worked in discrete distances from the source in discrete third octave intervals. For this example, the critical damping ratio, ξ, was 2.5% and the measured shear wave velocity was 1,000 feet per second.

Table 5-1: Partial Spectral Acceleration Calculation at a Single Point

n	f_{ctr} (Hz)	β (1/ft)	r_{m1} (ft)	A_{m1} (in/s^2)	A_1 (in/s^2)	r (ft)	A_r (in/s^2)
9	125	0.0196	1.583	0.256	1.153	10	0.087
10	99	0.0156	1.583	0.313	1.399	10	0.109
11	79	0.0124	1.583	0.371	1.649	10	0.133
12	63	0.0099	1.583	0.077	0.341	10	0.028
13	50	0.0079	1.583	0.066	0.29	10	0.024

Table 5-1 shows the acceleration results of the calculations for 5 third octave bands for a single point location at distance *r=10* feet from the vibration source, in this case a compressed air booster. From the table, *n* is a counter for the third octave band, f_{ctr} is the center frequency for the third octave band, β is the absorption coefficient at the center frequency, r_{m1} is the location of a measured acceleration, A_{m1} is the measured acceleration magnitude at location r_{m1}, A_1 is calculated from Equation (4-1) at a unit distance of 1 inch, *r* is a point distance measured from the source, and A_r is the calculated acceleration magnitude at location *r*. The calculation required for this

method is not overly complicated; nevertheless, it is a significant bookkeeping endeavor.

There is one added complication. The amplitude of the vibration is sometimes dependent on the direction of the equipment's motion. For this model, it was assumed that the magnitude of the vibration varied from a minimum value to a maximum value separated by a right angle and varying in an elliptical pattern. For the booster pump described in section 4.4, there was a clear direction to the motion. Acceleration measurements were taken, and maximum and minimum acceleration amplitudes were determined. These values were fed into Equation (5-3) to determine values at angles between 0 and 90 degrees.

$$A_C = \frac{A_{min} \cdot A_{max}}{\sqrt{[A_{max} sin(\theta)]^2 + [A_{min} cos(\theta)]^2}} \quad \textbf{(5-3)}$$

The combination of these calculations can now be completed for a single piece of equipment on a floor space in third octave frequencies. Figure 5-8 shows the results of the calculation for a compressed air booster pump. In both graphs, the contours are acceleration in ft/s^2 and the vertical and horizontal axes are in feet. The graph on the left shows the acceleration in the 79 Hz third octave band, and the graph on the right shows the acceleration in the 125 Hz band. Notice that the higher magnitude vibrations are not always in the same direction. All third octave bands are calculated and retained for combination into the overall floor model.

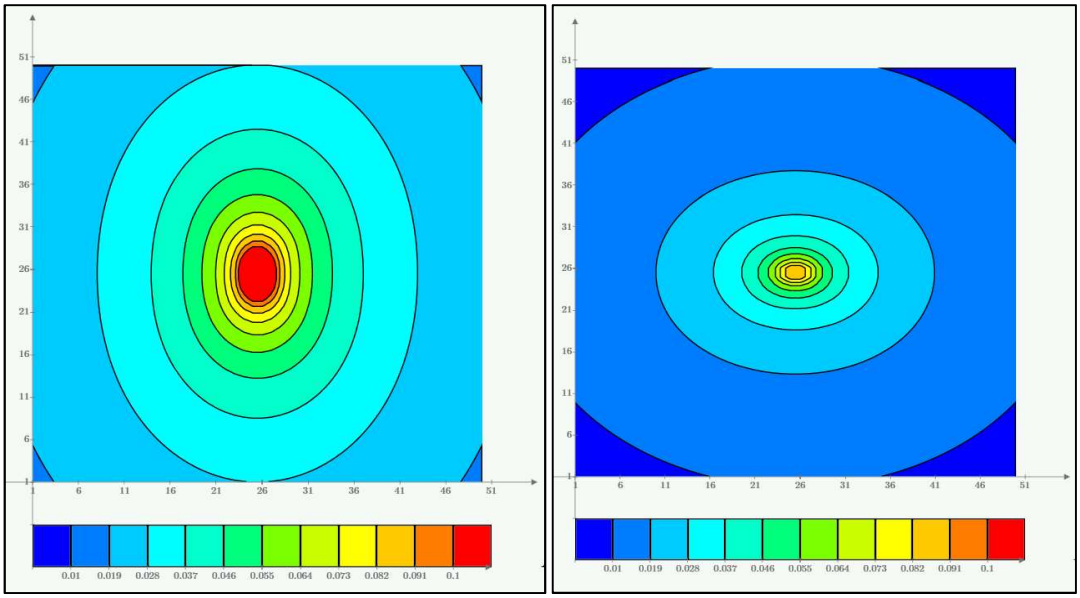

Figure 5-8: Acceleration Contours for Air Booster Vibration Model at 79 Hz (left) and 125 Hz (right) third octave bands

Relocating the vibratory equipment added additional parts to the model. First, from an analysis on the two different floor locations, the existing floor location was determined to be 80% as stiff as the proposed location. For this case it was assumed for simplicity that this would result in a frequency independent reduction in amplitude A_1 of 80%. Additionally, these vibratory machines are large and have two localized points for vibration sources. Each foot was treated independently, and then the acceleration values across the floor space were summed together for total model of a single vibratory machine.

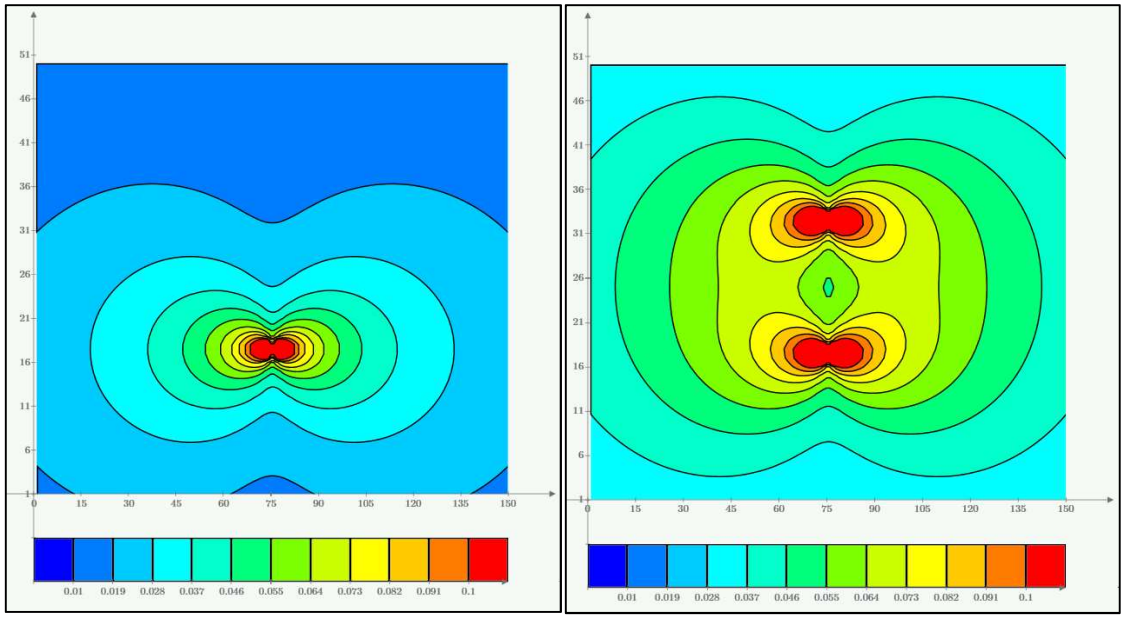

Figure 5-9: Acceleration Contours for Vibratory Machine: Single Foot (left); Both Feet (right)

Figure 5-9 shows the vibration model for a single vibratory machine for the 31 Hz third octave band. The contours are acceleration in ft/s^2, and the axes are in feet. The vibrations from the vibratory machines are highly dependent on the direction in which they are installed and have the tendency to travel further than the booster pumps because they have both higher magnitudes and lower frequencies with significant amplitude. This can be seen by comparing Figure 5-8 and Figure 5-9.

5.3.3 Build a Representative Floor Space

The remainder of the method is more or less an accounting exercise of tracking the vibration magnitude contribution from each piece of equipment at each discrete point on the floor. To accomplish this in this example, a total floor area of 100 feet by 150 feet was created in the form of a 100 column by 150 row matrix. Each element of the matrix represented a 1 by 1 foot point on the floor space. Each point had 30 levels

of values holding the acceleration magnitudes of each third octave band between 1 and 800 Hz.

Once the extent of the floor space to consider has been established, the relative location and orientation of each vibration source relative to the origin was determined. For this example, there were two air boosters rotated 90 degrees, one power washer, one drain pump, and the three relocated vibratory machines. The accelerations were then summed at each point location from each source in each third octave for the entire floor space.

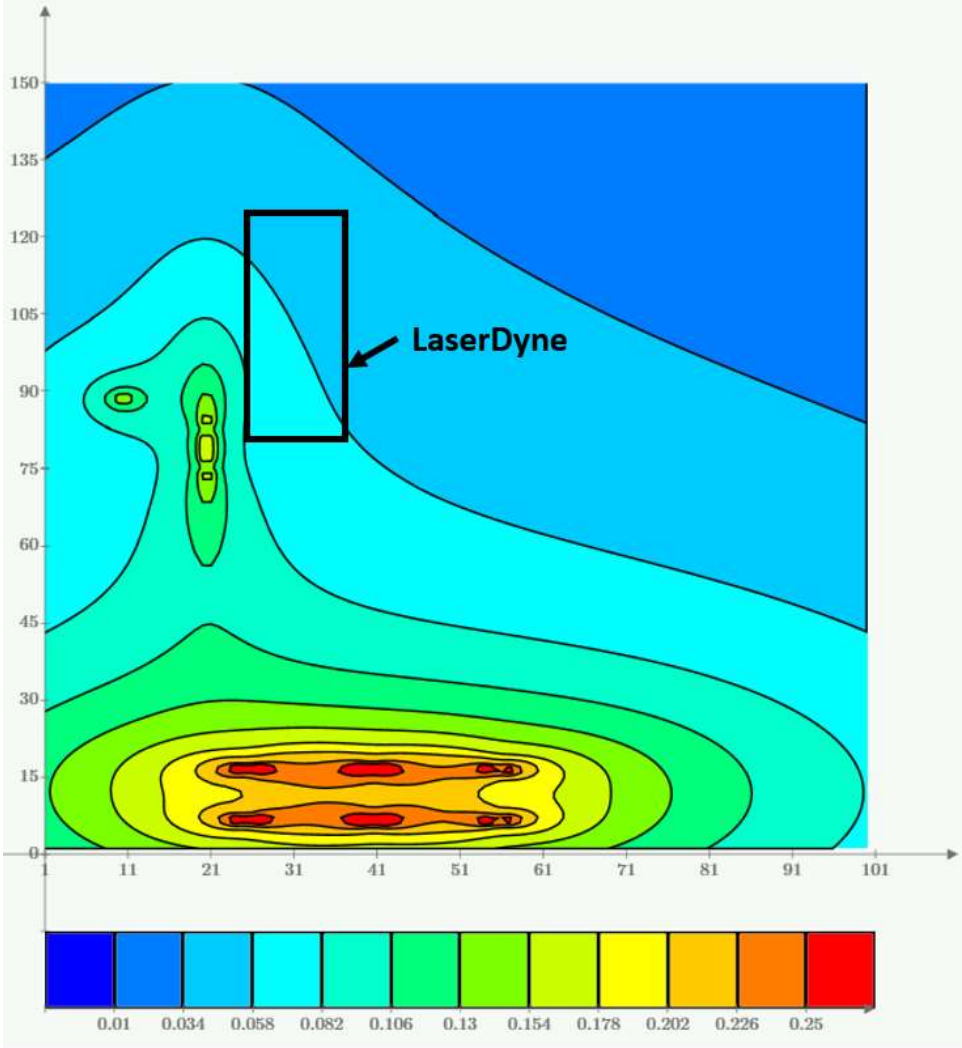

Figure 5-10: Acceleration Contours (ft/s^2) for 62 Hz Third Octave Band

The results at the 62 Hz third octave band from the aforementioned procedure are shown in Figure 5-10 along with the area of the vibration sensitive LaserDyne. The contours in the figure are acceleration in ft/s^2 and the axes dimensions are in feet.

Unfortunately, there is still one more necessary step before this information can be considered useful. At this point, it is not straightforward to see if the predicted vibrations are excessive or irrelevant to the operation of the LaserDyne since the amount of allowable vibration at each third octave varies and physically looking at each third octave band contour map correctly is problematic and time consuming. Nonetheless, it is only one more step in a calculation routine to compare all of values at a single time.

5.3.4 Compare Vibrations to Sensitive Equipment Specifications

The final step necessary to determine the effect of the relocated vibratory equipment is to compare the predicted accelerations to the LaserDyne specification. As previously mentioned, the manufacturer of the LaserDyne produced the vibration limits in terms of a displacement spectrum, 80 μ-in below 10 Hz and 40 μ-in above 10 Hz. This creates the necessity to convert the LaserDyne spectrum to an acceleration spectrum or convert all of the predictions to displacement spectrum. Mathematically, these conversions are equivalent, but it is computationally less demanding to convert only the specification as opposed to all of the floor space model. Additionally, the floor space model is based on measured acceleration values, and it is preferable to leave as much data in terms of the original measurement system as possible to reduce the possibility of a gross, non-obvious error.

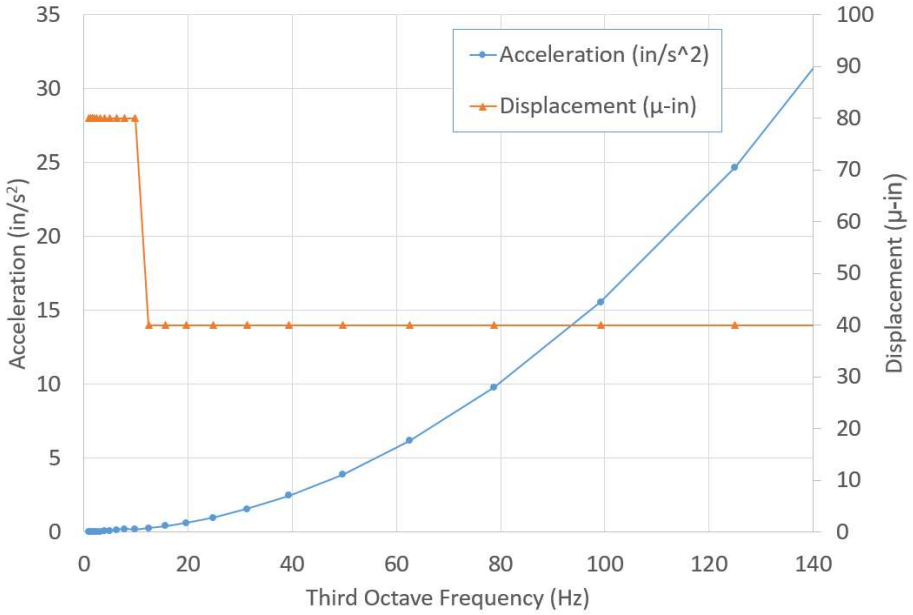

Figure 5-11: LaserDyne Vibration Specification

To ensure clarity of the conversion of the specification, Figure 5-11 was created to show the specification in displacement and acceleration spectra. By examining this figure, it is apparent why the manufacture provides the specification in terms of displacement instead of the more straightforwardly measured accelerations. The acceleration spectrum is more difficult to visually decipher across the spectrum, even if the acceleration was provided on a log scale. As a final side note at this time, the acceleration spectrum is the expected shape for sensitive equipment resting on a passive vibration isolator as the LaserDyne does. This is because as vibration frequencies increase beyond the natural frequency (typically between 1.5 and 8 Hz) of the isolation system, less of the vibration force (acceleration times mass) is transferred through the isolator as mathematically shown in Equation (2-19).

Now each acceleration in each band at each point location on the floor space can be compared to the acceleration specification. This was done in terms of the ratio of the predicted acceleration to the specified maximum acceleration. The results of this for the

62 Hz band is shown in Figure 5-12. The axes are the same as previously mentioned, but the contours are the ratio of the predicted to maximum specified accelerations.

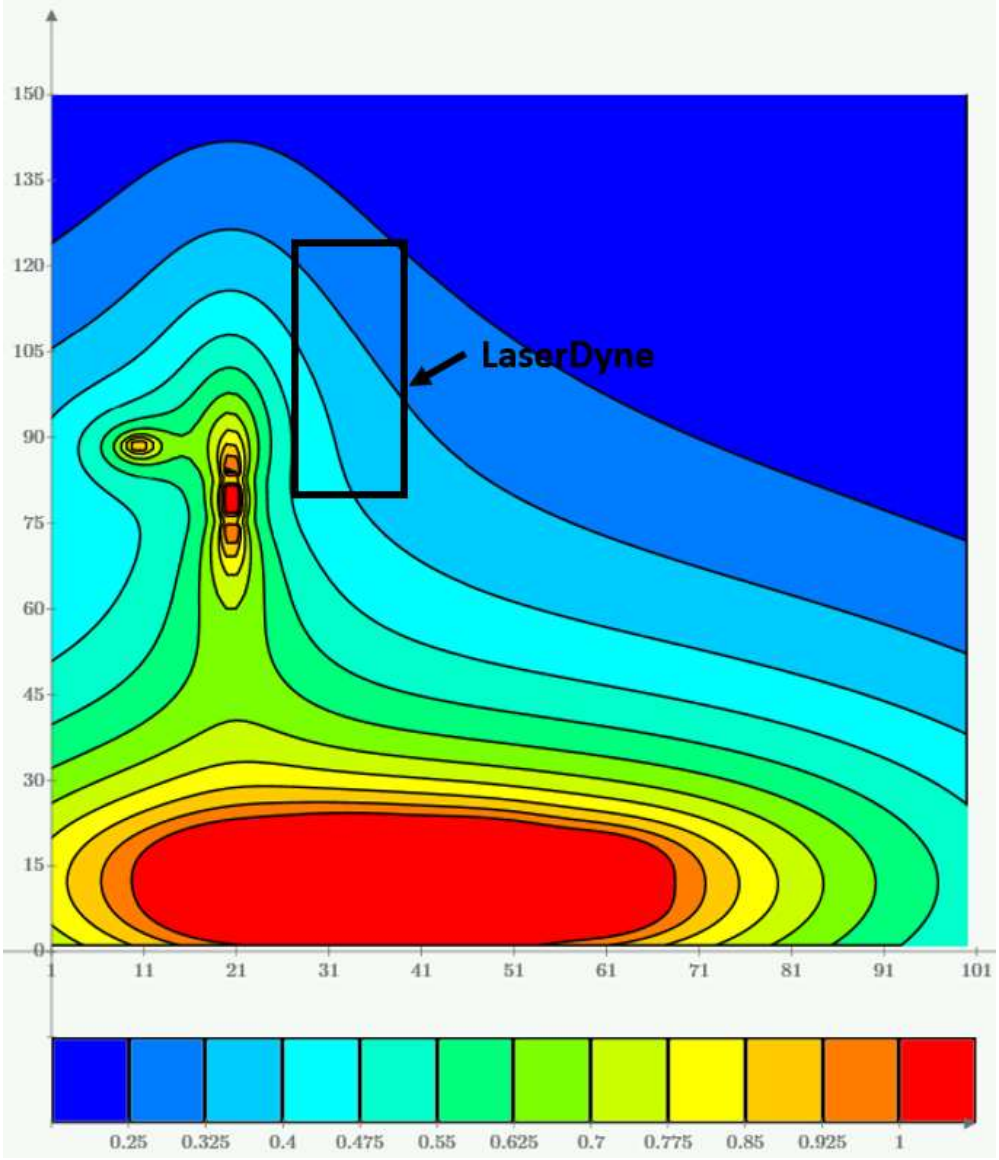

Figure 5-12: Ratio of Accelerations to LaserDyne Specification for 62 Hz Band

The results on a third octave basis are useful in helping to see where specific vibration levels are originating, but in terms of the limiting value, the highest ratio must be determined across all of the bands at each location. This final solution is shown in Figure 5-13 with the same units as Figure 5-12.

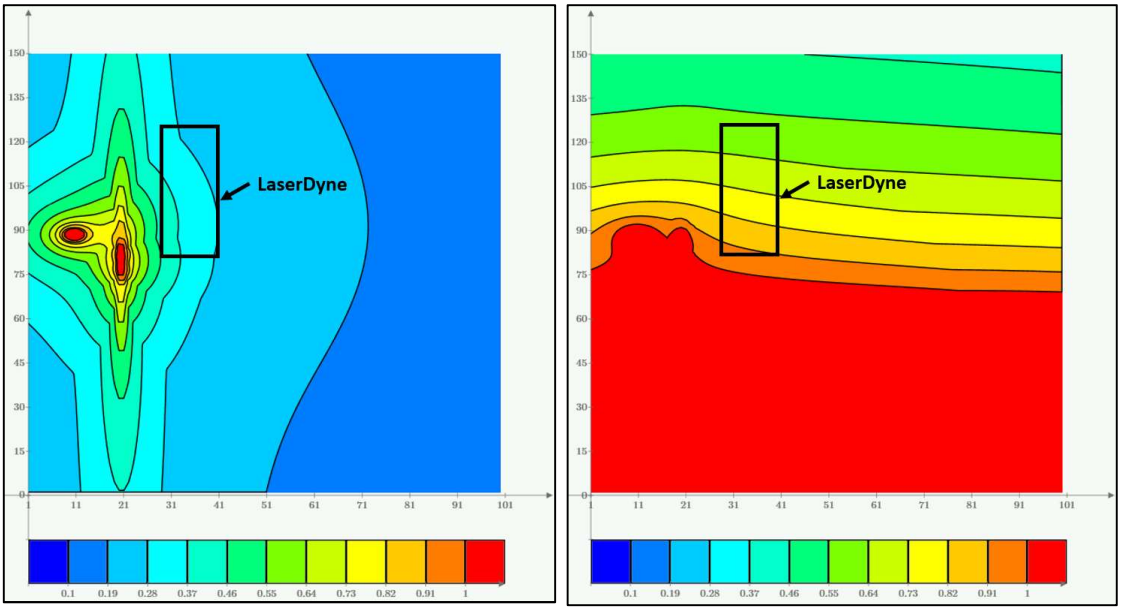

Figure 5-13: Maximum Ratio of Accelerations to LaserDyne Specification before Installation of the Vibratory (Left) and after Installation (Right)

As can be seen in Figure 5-13, the predicted accelerations at the edge of the LaserDyne are below the specified maximum levels. Still, most practicing engineers would probably elect to allow for a maximum ratio of 0.75 to 0.50 depending on how critical the operation of the LaserDyne, in this case, is to the overall operation.

There are a few of assumptions worth recalling at this final point with these results in mind. First, the assumed absorption coefficient is most likely lower at some frequencies than the actual absorption coefficient, meaning that these results are conservative in some of the frequency bands. However, the vibration levels of the vibratory machines (and the other equipment for that matter) were assumed to be consistent over time and these levels can change to some extent possibly reducing the safety factor. Finally, it is not beyond reason that when the final time comes to install the vibratory equipment, the actual installation is partially modified by field personnel unaware that the magnitude of the vibrations are direction specific. Rotating one of the

vibratory machines 90 degrees would put the vibrations at the LaserDyne above the specified values. All of these assumptions must be kept in mind when deciding how close is too close for vibrating equipment near sensitive equipment.

It is worthwhile to point out that, although the ambient vibration levels of the floor with none of the nearby equipment running are below the VC-C level, even with all of the existing equipment running the vibration levels at the LaserDyne would exceed the VC-C specification (not the LaserDyne specification). The addition of the vibratory equipment greatly exceeds the VC-C limits. This highlights the importance of knowing the actual sensitive equipment specifications, and indirectly shows how errors could be made during a general time study of a floor by not fully accounting for all possible vibration sources.

6. Findings, Conclusions and Recommendations

This thesis covered design considerations related to the installation of vibration sensitive equipment with nearby vibration sources. Specifically, a method was developed and experimentally tested to estimate the effects from multiple vibration sources at a location where vibration sensitive equipment is or will be installed.

6.1 Findings

One of the main findings of this thesis was that the measured absorption values for vibration attenuation sourced on a concrete slab vary significantly. This variation is not linear with frequency and is much higher at specific frequencies than is calculated from theoretical models. However, by assuming a viscous damping model for the underlying soil, a minimum value of the absorption coefficient was determined which provided a ceiling for all of the measured values.

In addition, even though the source of the vibration waves was on the concrete, the measured phase velocity of the vibration waves on the surface of the concrete was near the expected values of the underlying clay and not the concrete. A significant unexpected finding was that physical breaks in the overlying concrete slab have negligible positive effects in reducing vibration levels.

The final finding from the experimental data was that superimposing vibrations waves from multiple sources at a location produces a conservative value compared to the measured value. This was attributed to a majority of the surface vibration waveform traveling in the soil, which was consistent with all of the frequencies under consideration in this thesis (below 125 Hz).

6.2 Conclusions

Combining all of the aforementioned findings allows for the creation of a frequency dependent conservative vibration prediction model. To develop this method, a frequency dependent attenuation model was created based on the Bornitz equation using cylindrical geometric damping and a Kelvin-Voigt solid model with viscous damping for absorption. This model requires the estimation or measurement of the underlying soil shear wave velocity and critical damping ratio.

Compared with the experimental results, this model was conservative with respects to the absorption coefficient for the cases considered (and consequently vibration levels at a distance from the source). The absorption coefficient varied significantly at different sites, which was attributed to effects from different layered soil profiles resisting wave motion at specific frequencies. This effect is difficult to predict and left out of the attenuation model to allow for consistently conservative predictions.

These individual vibrating equipment models were combined on a floor space model to determine the vibration levels over the entire floor space. Experiments were performed to verify the accuracy of the approach used to calculate combined vibration sources. An example demonstrating the usefulness of the combined method was shown. The final result of the method is a contour map depicting locations with vibrations above the specification of vibration sensitive equipment.

In summary, the items laid out in this thesis can help engineers responsible for the installation and operation of vibration sensitive equipment make informed decisions on ground motion intensities from nearby vibration sources.

6.3 Recommendations

One area of additional research that could potentially increase the accuracy of the proposed method is the incorporation of the effects of the soil layers on the local attenuation. Such an approach could allow for the use of higher attenuation coefficients. Two questions that need to be answered are: (i) How wide is the range of frequencies where these high attenuation factors exist? (ii) How much variance in soil conditions (and attenuation factors) is there in a real facility, and are there situations where the higher attenuation coefficients could be used?

7. References

Albert, Donald G., Taherzadeh, Shahram, Attenborough, Keith, Boulanger, Patrice, and Decato, Stephen N., "Ground Vibrations Produced by Surface and Near-Surface Explosions", US Army Research Paper 176, 2013.

Amick, H., Wongprasert, N., Montgomery, J., Haswell, P. and Lynch, D., "An Experimental Study of Vibration Attenuation Performance of Several On-Grade Slab Configurations", Proceedings of SPIE, Society of Photo-optical Instrumentation Engineers, Vol. 5933, 2005.

Amick, Hal, Xu, Tao, and Gendreau, Michael, "The Role of Buildings and Slabs-on-Grade in the Suppression of Low-Amplitude Ambient Ground Vibrations", Proceedings of the 11th International Conference on Soil Dynamics and Earthquake Engineering, 2004, pp. 877-881.

Amick, Hal, "A Frequency-Dependent Soil Propagation Model", Society of Photo-optical Instrumentation Engineers Conference on Current Developments in Vibration Control for Optomechanical Systems, SPIE Vol. 3786, 1999.

Amick, Hal, Gendreau, Michael, and Bayat, Ahmad, "Dynamic Characteristics of Structures Extracted from In-sutu Testing", Society of Photo-optical Instrumentation Engineers Conference on Current Developments in Vibration Control for Optomechanical Systems, SPIE Vol. 3786, 1999.

Barkan, D. D., *Dynamics of Bases and Foundation*, translated from Russian by L. Drashevska, edited by G.P. Tschebotarioff, McGraw-Hill, 1962.

Bhatia, Krishna, Foundations for Industrial Machines: Handbook for Practicing Engineers, CRC Press, Rohini, New Delhi, 2007.

Cai, Chenguang, Zhou, Biao, and Li, Jingsheng, "Vibration Criteria for Vibration-Sensitive Laboratory Based on Intrinsic Microseism", Proceedings of the SPIE, Society of Photo-optical Instrumentation Engineers, Vol. 8916, 2013.

Dalmatov, B. I., Ershov, V. A., and Kovalevsky, E. D., "Some Cases of Foundation Settlement in Driving Sheeting and Piles", Proceedings International Symposium on Wave Properties of Earth Materials, PP. 607-613, 1968.

Das, Braja, Principles of Soil Dynamics, PWS-KENT Publishing Company, Boston, MA, 1993, pp.181-248.

Deckner, Fanny, "Ground Vibrations due to Pile and Sheet Pile Driving – Influencing Factors, Predictions and Measurements", Licentiate thesis, Division of Soil and Rock Mechanics, Department of Civil and Architectural Engineering, KTH, Royal Institute of Technology, Stockholm, 2013.

DeMatteo, Tony, "Bldg. 3001 at Post N-101 Vibration Study", 4x Diagnostics, 2015, pg. 12.

Dowding, Charles, Construction Vibrations, Prentice-Hall, 1996.

Forssblad, L., "Investigations of Soil Compaction by Vibration", Royal Swedish Academy of Engineering Sciences, Civil Engineering Sciences, Civil Engineering and Building Construction Series, no. 34, 1965.

Galvín, P. and Domínguez, J., "High-Speed Train-Induced Ground Motion and Interaction with Structures", Journal of Sound and Vibration, Vol. 307, 2007, pp. 755-777.

Gordon, Colin, "The Design of Low-Vibration Buildings for Microelectronics and Other Occupancies," Vibration Control in Optics and Metrology, Society of Photographic Instrumentation Engineers, Vol. 732, 1987, pp. 2-10.

Gordon, Colin, "Generic Vibration Criteria for Vibration-Sensitive Equipment", Society of Photographic Instrumentation Engineers Proceedings, Vol. 1619, 1991, pp. 1-12.

Günther, Roland H., O'Connell-Rodwell, Caitlin E., and Klemperer, Simon, "Seismic Waves from Elephant Vocalizations: A Possible Communication Mode?", Geophysical Research Letters, Vol. 31, 2004.

Gutowski T. G. and Dym C. L. "Propagation of Ground Vibration: A Review." Journal of Sound and Vibration, 1976, pp. 179-193.

Hong, S. U., Na, J. H., Kim, S. H., and Lee, Y. T., "Experiment on a Concrete Slab for Floor Vibration Evaluation of Deteriorated Buildings", Global Conference on Polymer and Composite Materials, 2014.

Hussein, M. F. M. and Hunt, H. E. M., "Modelling of Floating-Slab Tracks with Continuous Slabs Under Oscillating Moving Loads", Journal of Sound and Vibration, Vol. 297, 2006, pp. 37-54.

Jones, R., "Surface Wave Technique for Measuring the Elastic Properties and Thickness of Roads: Theoretical Development", British Journal of Applied Physics, Vol. 13, 1962.

Jones, Simon and Hunt, Hugh, "Predicting Surface Vibration from Underground Railways through Inhomogeneous Soil", Journal of Sound and Vibration, Vol. 331, 2012, pp. 2055-2069.

Jongmans D. and Demanet D., "The Importance of Surface Vaves in Vibration Study and the Use of Rayleigh Waves for Estimating the Dynamic Characteristics of Soils", Engineering Geology, Vol. 34, 1993, pp. 105-113.

King, K., Carver, D., Worley, D., and Bostwick, T., "Induced Ground-Vibration Study at Pueblo Grande, Phoenix, Arizona", U.S. Geological Survey, 1991, pp. 1-21.

Koroma, S. G., Hussein, M. F. M., Owen, J.S., "Vibration of a Beam on a Continuous Elastic Foundation with Nonhomogeneous Stiffness and Damping under a Harmonically Excited Mass", Journal of Sound and Vibration, Vol. 333, 2014, pp. 2571-2587.

Kramer, Steven, Geotechnical Earthquake Engineering, Prentice Hall, Upper Saddle River, NJ, 1996, pp. 144-181.

Lefeuvre, O., Zinin, P., and Briggs, G. A. D., "Leaky Surface Waves Propagating on a Fast on Slow System and the Implications for Material Characterization", Ultrasonics, Vol. 36, 1998, pp. 229-232.

Lefeuvre, O., Zinin, P., and Briggs, G. A. D., "Surface Wave Dispersion beyond Cutoff for a Fast Layer on a Slow Substrate", Applied Physics Letters, Vol. 72 Num. 7, 1998.

Nugent, Ramon, Zapfe, Jeffrey, "Designing Vibration-Sensitive Facilities near Rail Lines", Sound & Vibration, Nov. 2012, pp. 13-16.

Peng, S. M., "Propagation and Screening of Rayleigh Waves in Clay," Master's Engineering Thesis no. 386, Asian Institute of Technology, Bangkok, 1972.

Prakash, Shamsher and Puri, Vijay, "Foundations for Vibrating Machines," Journal of Structural Engineering. Special Issue, April-May 2006, pp. 1-39.

Richart, F.E., Woods, R.D. and Hall, J.R. Vibrations of Soils and Foundations, Prentice-Hall, Engelwood Cliffs, 1970.

Salyards, Kelly A. and Firman, Robert, J., "Review of Manufacturer Design Criteria for Vibration-Sensitive Equipment", Proceedings of the IMAC-XXVII, Society for Experimental Mechanics Inc., 2009.

Shin, Kihong and Hammond, Jospeph, Fundamentals of Signal Processing for Sound and Vibration Engineers, John Wiley & Sons Ltd, West Sussex, England, 2008, pp. 31-52 and pp. 57-139.

Suharsono and Samsudin, Abdul Rahim, "The Attenuation Effects of Surface-Wave Propagations on Rockmass using SASW Method", Geological Society of Malaysia, Bulletin 46, 2003, pp. 475-478.

Tedesco, Joseph, McDougal, William, & Ross, Allen, Structural Dynamics Theory and Applications, Addison Wesley Longman, Inc., Menlo Park, California, 1999, pp. 601-681.

Vucetic, M., and Dobry, R. (1991). "Effect of Soil Plasticity on Cyclic Response." J. Geotech. Eng., 117(1), 89–107.

Wair, Bernard R., DeJong, Jason T., "Guidelines for Estimation of Shear Wave Velocity Profiles", Pacific Earthquake Engineering Research Center, 2012.

Woods, Richard David, "Screening of Elastic Surface Waves by Trenches", Dissertation, University of Michigan, 1967.

Yang, S. J., "Attenuation of Ground Vibration Induced by Dynamical Machinery", First International conference on Recent Advances in Geotechnical Earthquake Engineering and Soil Dynamics, 1981.

Zhang, Jianfeng, Andrus, Ronald D., Juang, C. Hsein, "Normalized Shear Modulus and Material Damping Ratio Relationships", Journal of Geotechnical and Geoenvironmental Engineering, ASCE, 2005, pp. 453-464.

Appendix A: Sample Calculation of Third Octave Measurements

This appendix contains an example of the Mathcad Prime code used throughout this thesis to calculate the third octave spectrum values.

$file.name := \text{“signal\_7”}$ Excel file name where data is stored

$\text{ORIGIN} \equiv 1$ Set Matrix origin to 1 to conform to Excel notation

$scale := 100000$ Scale used in Labview Data Acquisition to avoid decimals in charts (10^5)

$sens.1.conv := 0.997 \ \frac{g}{V} \ \frac{1}{scale}$ Calibration of Sensor #1 from PCB

$sens.2.conv := 0.998 \ \frac{g}{V} \ \frac{1}{scale}$ Calibration of Sensor #2 from PCB

$sens.3.conv := 0.999 \ \frac{g}{V} \cdot \frac{1}{scale}$ Calibration of Sensor #3 from PCB

$data := \text{READEXCEL}(\text{concat}(\text{“.\”}, file.name, \text{“.xlsx”}), \text{“[2]”})$ Read in data from Excel

$sl := \text{strlen}(file.name) = 8$
$file.name.sig := \text{substr}(file.name, 0, sl)$
$file.name.sig.r := \text{concat}(file.name.sig, \text{“.sig.r.txt”})$
$file.name.sig.1 := \text{concat}(file.name.sig, \text{“.sig.txt”})$

Create file names to export csv values for later combined use

$\delta t := data_{3,2} \cdot s = 0.0005 \ s$ Read in dt for samples

$f_s := \frac{1}{\delta t} = 2000 \ Hz$ Sampling rate of DAQ

$Samples := \text{rows}(data) - 1 = 90000$ Number of Samples

$i := 1, 2 .. Samples$ Index for Samples

$data_1 := \text{submatrix}(data, 2, Samples + 1, 3, 3)$
$acc_1 := (data_1) \cdot V \cdot sens.1.conv$

$data_2 := \text{submatrix}(data, 2, Samples + 1, 4, 4)$
$acc_2 := (data_2) \cdot V \cdot sens.1.conv$

$data_3 := \text{submatrix}(data, 2, Samples + 1, 5, 5)$
$acc_3 := (data_3) \cdot V \cdot sens.1.conv$

Convert Raw Data to acceleration (raw data in Volts), and remove Headers

$t_i := (i - 1) \cdot \delta t$ Create a time array for the samples

$$dist := \begin{bmatrix} 20 \\ 80 \\ 164 \end{bmatrix} \cdot in = \begin{bmatrix} 20 \\ 80 \\ 164 \end{bmatrix} in$$

Locations of sensors in distance from center of vibration source

Plots of Raw acceleration data

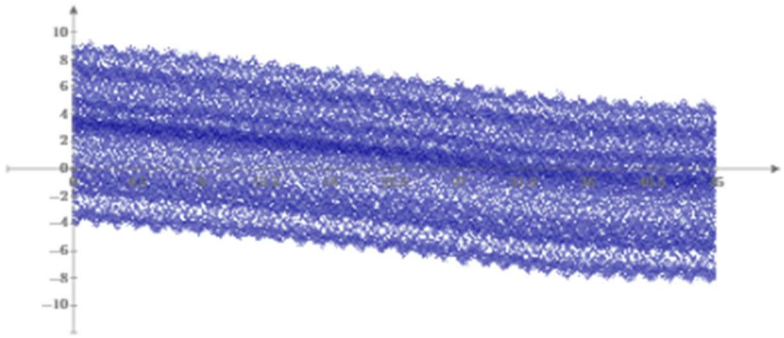

$acc_1 \left(\frac{in}{s^2}\right)$

$t\ (s)$

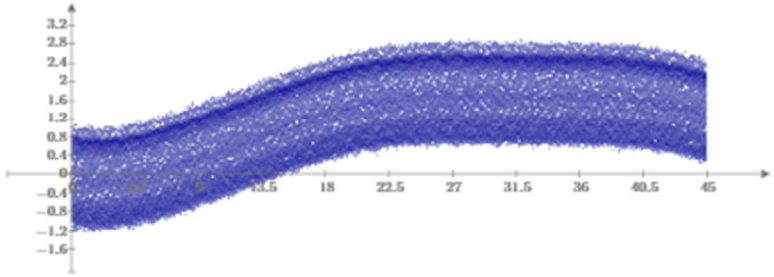

$acc_2 \left(\frac{in}{s^2}\right)$

$t\ (s)$

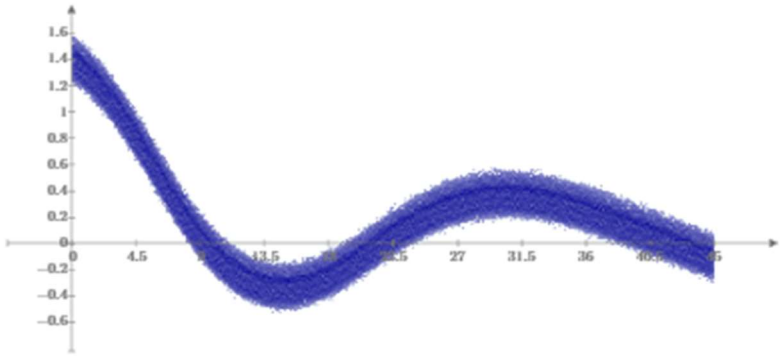

$acc_3 \left(\frac{in}{s^2}\right)$

$t\ (s)$

$hann := \text{hanning}(Samples)$ Create a vector of a hanning window

$acc.win_1 := \overrightarrow{acc_1 \cdot hann}$ Window the acceleration data

$acc.win_2 := \overrightarrow{acc_2 \cdot hann}$

$acc.win_3 := \overrightarrow{acc_3 \cdot hann}$

$acc.fft_1 := \text{cfft}(acc.win_1)$ Perform complex fft of windowed accel's

$acc.fft_2 := \text{cfft}(acc.win_2)$

$acc.fft_3 := \text{cfft}(acc.win_3)$

$acc.cfft.inv_1 := \text{cfft}(acc_1)$ Perfrom complex fft of non-windowed data to construct time domain filtered plot

$acc.cfft.inv_2 := \text{cfft}(acc_2)$

$acc.cfft.inv_3 := \text{cfft}(acc_3)$

$\text{length}(acc.fft_1) = 90000$ Length of the fft (same as length of data)

$k := 1, 2 .. \text{length}(acc.fft_1)$ Create an index for freq domain

$\delta f := f_s \cdot \frac{1}{\text{length}(acc.fft_1)} = 0.022\ Hz$ Calculate width of freq. in freq domain

$freq_k := (k-1) \cdot f_s \cdot \frac{1}{\text{length}(acc.fft_1)}$ Create vector of frequencies

$acc.fft.mag.half_{1_k} := \frac{1}{\sqrt{\text{length}(acc.fft_1)}} \cdot \left| acc.fft_{1_k} \right|$ Determine magnitude of accel's in freq domain (cfft scales by 1/sqrt(N))

$acc.fft.mag.half_{2_k} := \frac{1}{\sqrt{\text{length}(acc.fft_2)}} \cdot \left| acc.fft_{2_k} \right|$

$acc.fft.mag.half_{3_k} := \frac{1}{\sqrt{\text{length}(acc.fft_3)}} \cdot \left| acc.fft_{3_k} \right|$

Convert 2 sided frequency domain data into single sided (symetric about Nyquest)

$$acc.fft.mag_1 := \left\| \begin{array}{l} XX_1 \leftarrow acc.fft.mag.half_{1_1} \\ \text{for } k' \in 2,3..\dfrac{\text{length}\left(acc.fft_1\right)}{2}-1 \\ \quad \left\| XX_{k'} \leftarrow acc.fft.mag.half_{1_{k'}} + acc.fft.mag.half_{1_{\text{length}\left(acc.fft_1\right)-k'+2}} \right. \\ XX \end{array} \right.$$

$$acc.fft.mag_2 := \left\| \begin{array}{l} XX_1 \leftarrow acc.fft.mag.half_{2_1} \\ \text{for } k' \in 2,3..\dfrac{\text{length}\left(acc.fft_2\right)}{2}-1 \\ \quad \left\| XX_{k'} \leftarrow acc.fft.mag.half_{2_{k'}} + acc.fft.mag.half_{2_{\text{length}\left(acc.fft_1\right)-k'+2}} \right. \\ XX \end{array} \right.$$

$$acc.fft.mag_3 := \left\| \begin{array}{l} XX_1 \leftarrow acc.fft.mag.half_{3_1} \\ \text{for } k' \in 2,3..\dfrac{\text{length}\left(acc.fft_3\right)}{2}-1 \\ \quad \left\| XX_{k'} \leftarrow acc.fft.mag.half_{3_{k'}} + acc.fft.mag.half_{3_{\text{length}\left(acc.fft_1\right)-k'+2}} \right. \\ XX \end{array} \right.$$

Plots of windowed frequency domain data

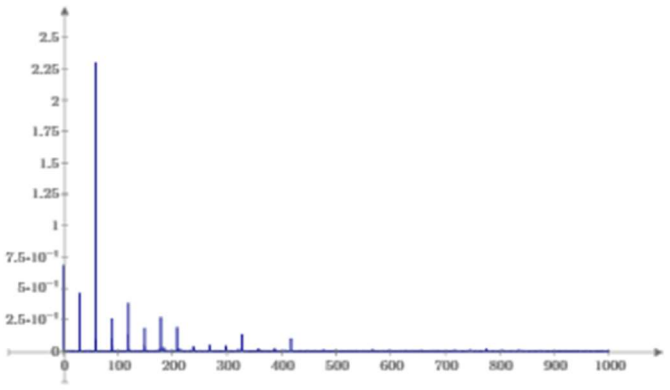

$acc.fft.mag_1 \left(\frac{in}{s^2}\right)$

$freq\ (Hz)$

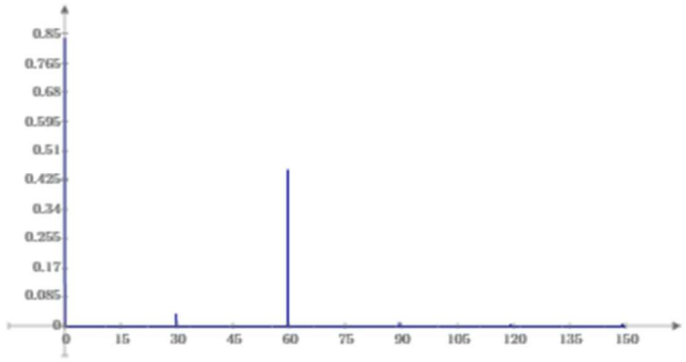

$acc.fft.mag_2 \left(\frac{in}{s^2}\right)$

$freq\ (Hz)$

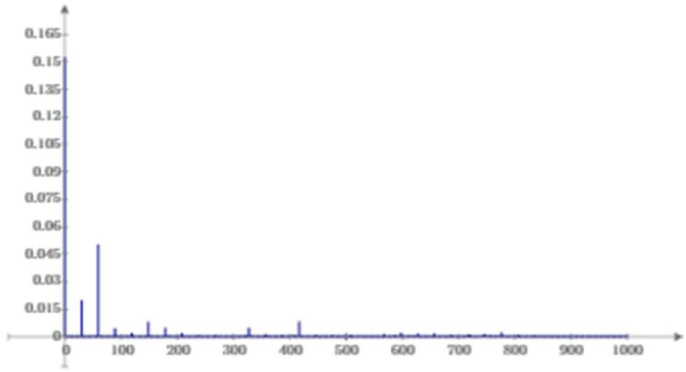

$acc.fft.mag_3 \left(\frac{in}{s^2}\right)$

$freq\ (Hz)$

$f_{low} := 0.8\ Hz$ $f_{high} := 150\ Hz$

$i_{low} := \frac{f_{low}}{\delta f} = 36$ $i_{high} := \frac{f_{high}}{\delta f} = 6750$

Create a frequency domain filter, to reconstruct the time signal.

$i_{low.2} := Samples - i_{low} = 89964$ $i_{high.2} := Samples - i_{high} = 83250$

$acc.fft.inv_1 :=$

for $i \in 1, 2 .. i_{low} - 1$

$acc_i \leftarrow 0\ \frac{m}{s^2}$

for $i \in i_{low}, i_{low} + 1 .. i_{high}$

$acc_i \leftarrow acc.cfft.inv_{1_i}$

for $i \in i_{high} + 1, i_{high} + 2 .. \frac{Samples}{2}$

$acc_i \leftarrow 0\ \frac{m}{s^2}$

for $i \in \frac{Samples}{2} + 1, \frac{Samples}{2} + 2 .. i_{high.2} - 1$

$acc_i \leftarrow 0\ \frac{m}{s^2}$

for $i \in i_{high}, i_{high} + 1 .. i_{low.2}$

$acc_i \leftarrow acc.cfft.inv_{1_i}$

for $i \in i_{low.2} + 1, i_{low.2} + 2 .. Samples$

$acc_i \leftarrow 0\ \frac{m}{s^2}$

acc

Frequency domain filter (double sided complex fft)

$acc.fft.inv_2 :=$

for $i \in 1, 2 .. i_{low} - 1$

$acc_i \leftarrow 0\ \frac{m}{s^2}$

for $i \in i_{low}, i_{low} + 1 .. i_{high}$

$acc_i \leftarrow acc.cfft.inv_{2_i}$

for $i \in i_{high} + 1, i_{high} + 2 .. \frac{Samples}{2}$

$acc_i \leftarrow 0\ \frac{m}{s^2}$

$$\left\| \begin{array}{l} \text{for } i \in \frac{Samples}{2}+1, \frac{Samples}{2}+2..i_{high.2}-1 \\ \quad \left\| acc_i \leftarrow 0 \frac{m}{s^2} \right. \\ \text{for } i \in i_{high}, i_{high}+1..i_{low.2} \\ \quad \left\| acc_i \leftarrow acc.cfft.inv_{2_i} \right. \\ \text{for } i \in i_{low.2}+1, i_{low.2}+2..Samples \\ \quad \left\| acc_i \leftarrow 0 \frac{m}{s^2} \right. \\ acc \end{array} \right.$$

$$acc.fft.inv_3 := \left\| \begin{array}{l} \text{for } i \in 1, 2..i_{low}-1 \\ \quad \left\| acc_i \leftarrow 0 \frac{m}{s^2} \right. \\ \text{for } i \in i_{low}, i_{low}+1..i_{high} \\ \quad \left\| acc_i \leftarrow acc.cfft.inv_{3_i} \right. \\ \text{for } i \in i_{high}+1, i_{high}+2..\frac{Samples}{2} \\ \quad \left\| acc_i \leftarrow 0 \frac{m}{s^2} \right. \\ \text{for } i \in \frac{Samples}{2}+1, \frac{Samples}{2}+2..i_{high.2}-1 \\ \quad \left\| acc_i \leftarrow 0 \frac{m}{s^2} \right. \\ \text{for } i \in i_{high}, i_{high}+1..i_{low.2} \\ \quad \left\| acc_i \leftarrow acc.cfft.inv_{3_i} \right. \\ \text{for } i \in i_{low.2}+1, i_{low.2}+2..Samples \\ \quad \left\| acc_i \leftarrow 0 \frac{m}{s^2} \right. \\ acc \end{array} \right.$$

$acc.f_1 := \text{icfft}\left(acc.fft.inv_1\right)$

$acc.f_2 := \text{icfft}\left(acc.fft.inv_2\right)$

$acc.f_3 := \text{icfft}\left(acc.fft.inv_3\right)$

Inverse the non-windowed, filtered data to reconstruct a time signal of each channel

$dt := 0.05\ sec$ $\quad dx := \frac{dt}{\delta t} = 100$

$t_0 := 5\ sec$ $\quad x := \text{ceil}\left(\frac{t_0}{\delta t}\right), \text{ceil}\left(\frac{t_0}{\delta t}\right) + 1 .. \text{ceil}\left(\frac{t_0}{\delta t}\right) + dx$

Scheme for only plotting a portion of the data

Plot time domain, filtered, non-windowed reconstructed accelerations

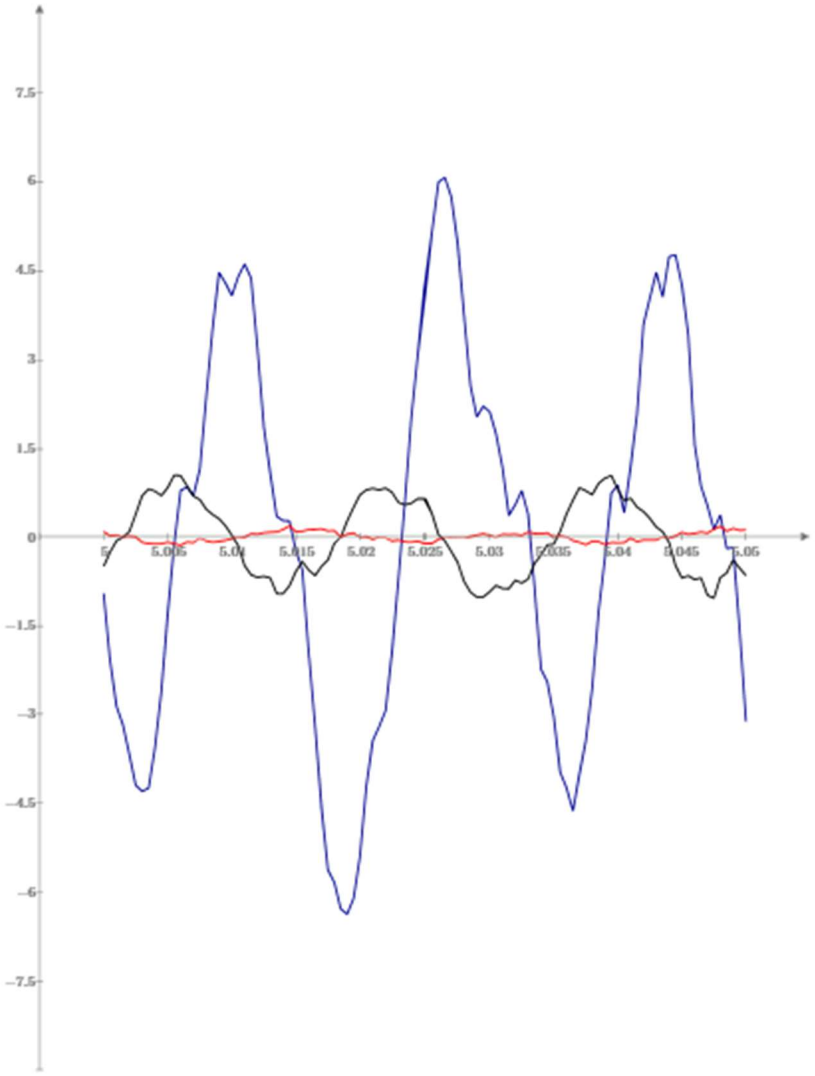

$\text{Re}\left(acc.f_{1_x}\right)\ \left(\frac{in}{s^2}\right)$

$\text{Re}\left(acc.f_{2_x}\right)\ \left(\frac{in}{s^2}\right)$

$\text{Re}\left(acc.f_{3_x}\right)\ \left(\frac{in}{s^2}\right)$

$t_x\ (s)$

$$Vel.fft.mag_1 := \left\| \begin{array}{l} Vel_1 \leftarrow 0\ \frac{m}{s} \\ \text{for } i \in 2,3..\text{length}\left(acc.fft.mag_1\right) \\ \quad Vel_i \leftarrow \frac{acc.fft.mag_{1_i}}{2 \cdot \pi \cdot freq_i} \\ Vel \end{array} \right.$$

Calculate the velocity spectrum from the acceleration data directly in the frequency domain, assume, the DC velocity is zero

$$Vel.fft.mag_2 := \left\| \begin{array}{l} Vel_1 \leftarrow 0\ \frac{m}{s} \\ \text{for } i \in 2,3..\text{length}\left(acc.fft.mag_1\right) \\ \quad Vel_i \leftarrow \frac{acc.fft.mag_{2_i}}{2 \cdot \pi \cdot freq_i} \\ Vel \end{array} \right.$$

$$Vel.fft.mag_3 := \left\| \begin{array}{l} Vel_1 \leftarrow 0\ \frac{m}{s} \\ \text{for } i \in 2,3..\text{length}\left(acc.fft.mag_1\right) \\ \quad Vel_i \leftarrow \frac{acc.fft.mag_{3_i}}{2 \cdot \pi \cdot freq_i} \\ Vel \end{array} \right.$$

$$Disp.fft.mag_1 := \left\| \begin{array}{l} Disp_1 \leftarrow 0\ m \\ \text{for } i \in 2,3..\text{length}\left(acc.fft.mag_1\right) \\ \quad Disp_i \leftarrow \frac{acc.fft.mag_{1_i}}{\left(2 \cdot \pi \cdot freq_i\right)^2} \\ Disp \end{array} \right.$$

Calculate the displacement spectrum from the acceleration data directly in the frequency domain, assume, the DC displacement is zero

$$Disp.fft.mag_2 := \left\| \begin{array}{l} Disp_2 \leftarrow 0\ m \\ \text{for } i \in 2,3..\text{length}\left(acc.fft.mag_2\right) \\ \quad Disp_i \leftarrow \frac{acc.fft.mag_{2_i}}{\left(2 \cdot \pi \cdot freq_i\right)^2} \\ Disp \end{array} \right.$$

$$Disp.fft.mag_3 := \left\| \begin{array}{l} Disp_1 \leftarrow 0\ m \\ \text{for } i \in 2,3..\text{length}\left(acc.fft.mag_3\right) \\ \quad Disp_i \leftarrow \dfrac{acc.fft.mag_{3_i}}{\left(2 \cdot \pi \cdot freq_i\right)^2} \\ Disp \end{array} \right.$$

Convert Spectrum into Third Octave spans

$n.max := 30$

Max n cooresponds to a center frequency of about 1Hz the limit of this study

$n := 1,2..n.max$

Index for calculating center frequencies of the third octave spectrum

$f_{ctr_n} := \dfrac{1000\ Hz}{2^{\frac{1}{3} \cdot n}}$

Calculate the center frequencies of the third octaves

$f_{low_n} := f_{ctr_n} \cdot \dfrac{1}{\sqrt{2^{\frac{1}{3}}}}$

Calculate the lower frequency of each thrid octave

$f_{high_n} := f_{ctr_n} \cdot \sqrt{2^{\frac{1}{3}}}$

Calculate the upper frequency of each third octave

$$acc.third.oct_1 := \left\| \begin{array}{l} \text{for } n \in 1,2..n.max \\ \quad Amp_n \leftarrow 0\ \dfrac{m}{s^2} \\ \quad \text{for } i \in 1,2..\dfrac{Samples}{2} - 1 \\ \quad\quad freq_i \leftarrow \delta f \cdot (i-1) \\ \quad\quad \text{if } freq_i > f_{low_n} \wedge freq_i \leq f_{high_n} \\ \quad\quad\quad Amp_n \leftarrow Amp_n + acc.fft.mag_{1_i} \\ Amp \end{array} \right.$$

Combine amplitudes by sumation between each third octave high and low cutoff frequency and attached to each "center" frequency

$$acc.third.oct_2 := \left\| \begin{array}{l} \text{for } n \in 1,2..n.max \\ \quad Amp_n \leftarrow 0\ \dfrac{m}{s^2} \\ \quad \text{for } i \in 1,2..\dfrac{Samples}{2} - 1 \\ \quad\quad freq_i \leftarrow \delta f \cdot (i-1) \end{array} \right.$$

$$\begin{array}{l}\text{if } freq_i > f_{low_n} \wedge freq_i \le f_{high_n} \\ \quad Amp_n \leftarrow Amp_n + acc.fft.mag_{2_i} \\ Amp\end{array}$$

$$acc.third.oct_3 := \left|\begin{array}{l}\text{for } n \in 1,2..n.max \\ \quad Amp_n \leftarrow 0\ \frac{m}{s^2} \\ \quad \text{for } i \in 1,2..\frac{Samples}{2}-1 \\ \quad\quad freq_i \leftarrow \delta f \cdot (i-1) \\ \quad\quad \text{if } freq_i > f_{low_n} \wedge freq_i \le f_{high_n} \\ \quad\quad\quad Amp_n \leftarrow Amp_n + acc.fft.mag_{3_i} \\ Amp\end{array}\right.$$

$$acc.third.oct.RMS_1 := \frac{1}{\sqrt{2}} \cdot acc.third.oct_1$$

Convert amplitudes to RMS values

$$acc.third.oct.RMS_2 := \frac{1}{\sqrt{2}} \cdot acc.third.oct_2$$

$$acc.third.oct.RMS_3 := \frac{1}{\sqrt{2}} \cdot acc.third.oct_3$$

$$n := 9,10..30$$

Counter to plot only the desired third octaves, 1 to 125Hz

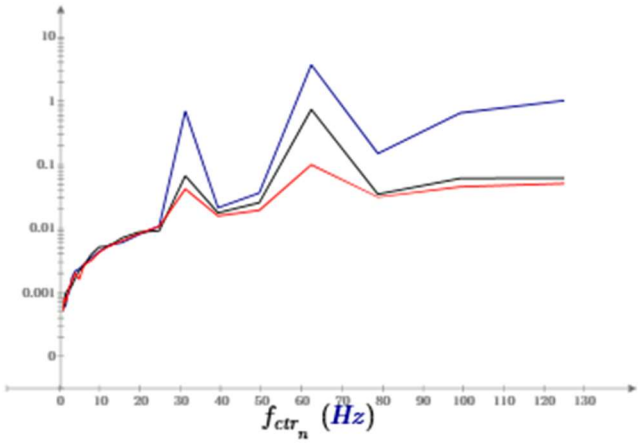

$acc.third.oct.RMS_{1_n}\left(\frac{in}{s^2}\right)$

$acc.third.oct.RMS_{2_n}\left(\frac{in}{s^2}\right)$

$acc.third.oct.RMS_{3_n}\left(\frac{in}{s^2}\right)$

Calculated the velocity third octave bands

$$Vel.third.oct_1 := \left\| \begin{array}{l} \text{for } n \in 1,2..n.max \\ \quad Amp_n \leftarrow 0\,\frac{m}{s} \\ \quad \text{for } i \in 1,2..\frac{Samples}{2}-1 \\ \quad\quad freq_i \leftarrow \delta f \cdot (i-1) \\ \quad\quad \text{if } freq_i > f_{low_n} \wedge freq_i \le f_{high_n} \\ \quad\quad\quad Amp_n \leftarrow Amp_n + Vel.fft.mag_{1_i} \\ Amp \end{array} \right.$$

$$Vel.third.oct_2 := \left\| \begin{array}{l} \text{for } n \in 1,2..n.max \\ \quad Amp_n \leftarrow 0\,\frac{m}{s} \\ \quad \text{for } i \in 1,2..\frac{Samples}{2}-1 \\ \quad\quad freq_i \leftarrow \delta f \cdot (i-1) \\ \quad\quad \text{if } freq_i > f_{low_n} \wedge freq_i \le f_{high_n} \\ \quad\quad\quad Amp_n \leftarrow Amp_n + Vel.fft.mag_{2_i} \\ Amp \end{array} \right.$$

$$Vel.third.oct_3 := \left\| \begin{array}{l} \text{for } n \in 1,2..n.max \\ \quad Amp_n \leftarrow 0\,\frac{m}{s} \\ \quad \text{for } i \in 1,2..\frac{Samples}{2}-1 \\ \quad\quad freq_i \leftarrow \delta f \cdot (i-1) \\ \quad\quad \text{if } freq_i > f_{low_n} \wedge freq_i \le f_{high_n} \\ \quad\quad\quad Amp_n \leftarrow Amp_n + Vel.fft.mag_{3_i} \\ Amp \end{array} \right.$$

$$Vel.third.oct.RMS_1 := \frac{1}{\sqrt{2}} \cdot Vel.third.oct_1$$

$$Vel.third.oct.RMS_2 := \frac{1}{\sqrt{2}} \cdot Vel.third.oct_2$$

$$Vel.third.oct.RMS_3 := \frac{1}{\sqrt{2}} \cdot Vel.third.oct_3$$

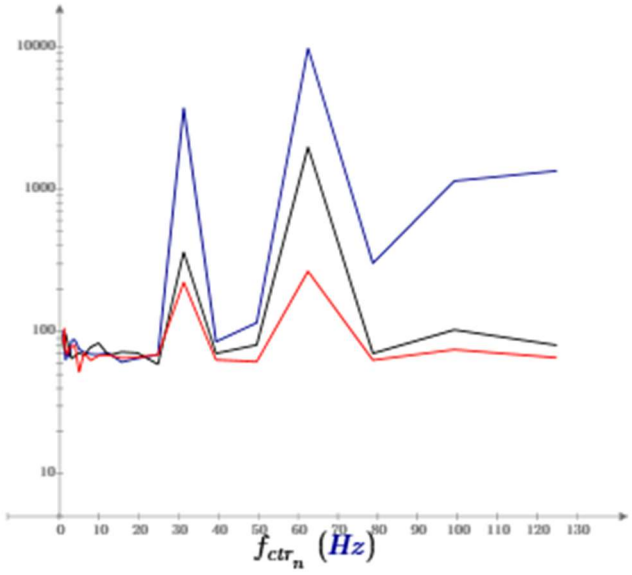

$Vel.third.oct.RMS_{1_n}\left(\frac{in}{s}\cdot 10^{-6}\right)$

$Vel.third.oct.RMS_{2_n}\left(\frac{in}{s}\cdot 10^{-6}\right)$

$Vel.third.oct.RMS_{3_n}\left(\frac{in}{s}\cdot 10^{-6}\right)$

$Disp.third.oct_1 :=$ for $n \in 1,2..n.max$

$Amp_n \leftarrow 0\ m$

for $i \in 1,2..\frac{Samples}{2}-1$

$freq_i \leftarrow \delta f\cdot(i-1)$

if $freq_i > f_{low_n} \wedge freq_i \le f_{high_n}$

$Amp_n \leftarrow Amp_n + Disp.fft.mag_{1_i}$

Amp

$Disp.third.oct_2 :=$ for $n \in 1,2..n.max$

$Amp_n \leftarrow 0\ m$

for $i \in 1,2..\frac{Samples}{2}-1$

$freq_i \leftarrow \delta f\cdot(i-1)$

if $freq_i > f_{low_n} \wedge freq_i \le f_{high_n}$

$Amp_n \leftarrow Amp_n + Disp.fft.mag_{2_i}$

Amp

Calcuate the displacement third octave bands

$$Disp.third.oct_3 := \left\| \begin{array}{l} \text{for } n \in 1,2..n.max \\ \quad \left\| \begin{array}{l} Amp_n \leftarrow 0\ m \\ \text{for } i \in 1,2..\dfrac{Samples}{2}-1 \\ \quad \left\| \begin{array}{l} freq_i \leftarrow \delta f \cdot (i-1) \\ \text{if } freq_i > f_{low_n} \wedge freq_i \le f_{high_n} \\ \quad \left\| Amp_n \leftarrow Amp_n + Disp.fft.mag_{3_i} \right. \end{array} \right. \end{array} \right. \\ Amp \end{array} \right.$$

$$Disp.third.oct.RMS_1 := \frac{1}{\sqrt{2}} \cdot Disp.third.oct_1$$

$$Disp.third.oct.RMS_2 := \frac{1}{\sqrt{2}} \cdot Disp.third.oct_2$$

$$Disp.third.oct.RMS_3 := \frac{1}{\sqrt{2}} \cdot Disp.third.oct_3$$

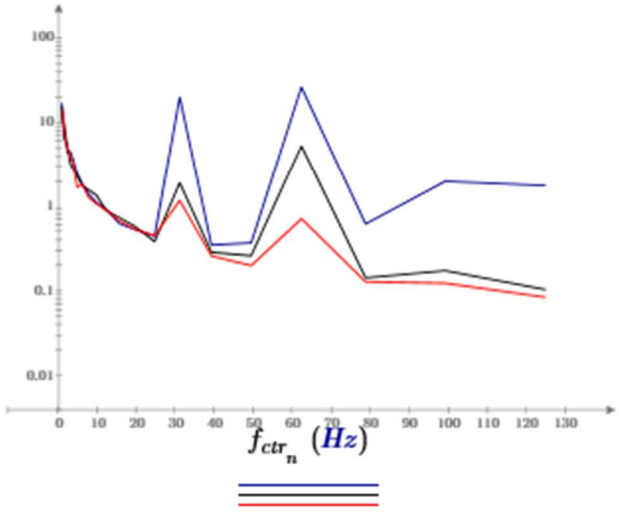

$Disp.third.oct.RMS_{1_n}$ $(in \cdot 10^{-6})$

$Disp.third.oct.RMS_{2_n}$ $(in \cdot 10^{-6})$

$Disp.third.oct.RMS_{3_n}$ $(in \cdot 10^{-6})$

Appendix B: Sample Calculation of Waveform Velocity

This appendix contains the Mathcad Prime code used throughout this thesis to determine possible waveform velocities.

$ORIGIN \equiv 1$ Set matrix origin to match Excel

$\# := 7$ File number to analyze

$file.name := \text{num2str}(\#) = \text{“7”}$

$rr := \text{READCSV}(\text{concat}(\text{“signal\_”}, file.name, \text{“.sig.r.txt”}))$ Read in sensor spacing

$r := rr \cdot in = \begin{bmatrix} 1.6667 \\ 6.6667 \\ 13.6667 \end{bmatrix} ft$ Apply Units

$signal.start := 100$ Data point to start analysis

$signal.length := 250$ Length of data to analyze, needs to be small to apply DC offset

$f_s := 2000 \cdot \frac{1}{s}$ Sampling frequency of data

$\delta t := \frac{1}{f_s} = 0.0005\ s$ Time between samples

$i := 1, 2 .. signal.length$ Index for time vector

$t_i := (i-1) \cdot \delta t$ Time vector

Read in acceleration data and apply units

$$
\begin{aligned}
data := \Big\| & \text{for } j \in \# \\
& \quad k \leftarrow \text{num2str}(j) \\
& \quad file.name \leftarrow \text{concat}(\text{“.\textbackslash Signal\_”}, k, \text{“.xlsx”}) \\
& \quad start \leftarrow \text{num2str}(signal.start) \\
& \quad end.length \leftarrow \text{num2str}(signal.start + signal.length) \\
& \quad CELLS \leftarrow \text{concat}(\text{“[2]C”}, start, \text{“:E”}, end.length) \\
& \quad acc1 \leftarrow \text{READEXCEL}(file.name, CELLS) \\
& \quad acc2 \leftarrow acc1 \\
& \quad acc3 \leftarrow acc2 \cdot \frac{g}{100000} \\
& \quad acc_j \leftarrow acc3 \\
& acc
\end{aligned}
$$

$acc_{1.1} := data^{(1)}_{\#}$ Place sensor 1 values in vector

$acc_{1.1} := acc_{1.1} - \frac{\sum_{i=1}^{signal.length} acc_{1.1_i}}{signal.length}$ Perform DC offset signal 1

$acc_{1.2} := data^{(2)}_{\#}$ Place sensor 2 values in vector

$acc_{1.2} := acc_{1.2} - \frac{\sum_{i=1}^{signal.length} acc_{1.2_i}}{signal.length}$ Perform DC offset signal 2

Plot time domain values of accelerations for both sensors, $acc_{1.1}$ is closer to the source

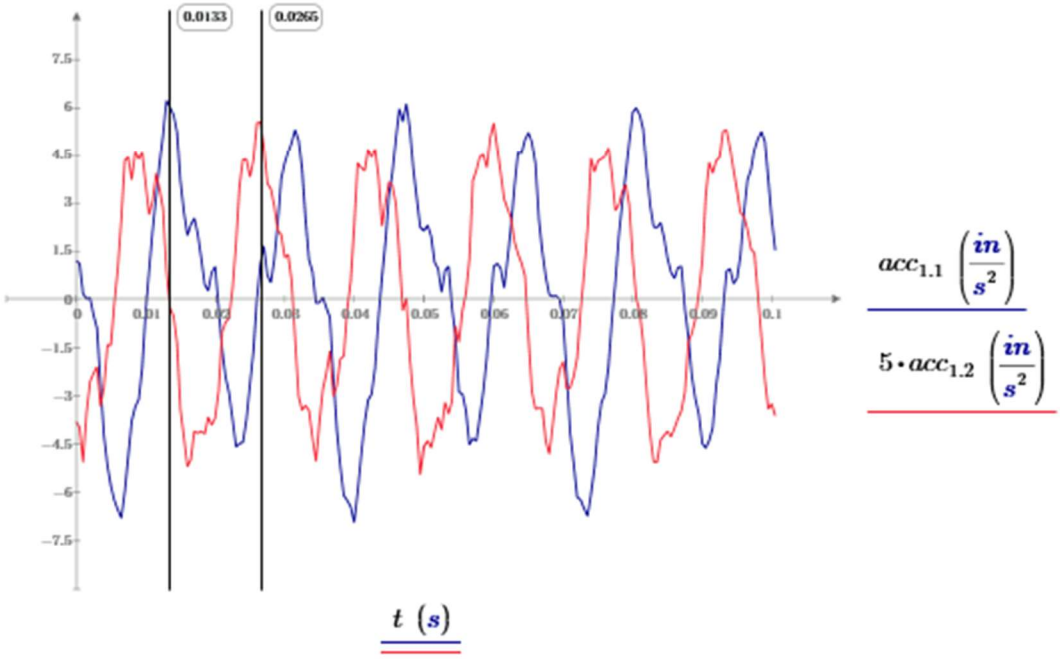

$$lag12 := \mathrm{lcorr}\left(\frac{acc_{1.1}}{\left(\frac{in}{s^2}\right)}, \frac{acc_{1.2}}{\left(\frac{in}{s^2}\right)}\right)$$

Perform Correlation at lags between signals 1 and 2

Plot the correlation at lag times between the two signals

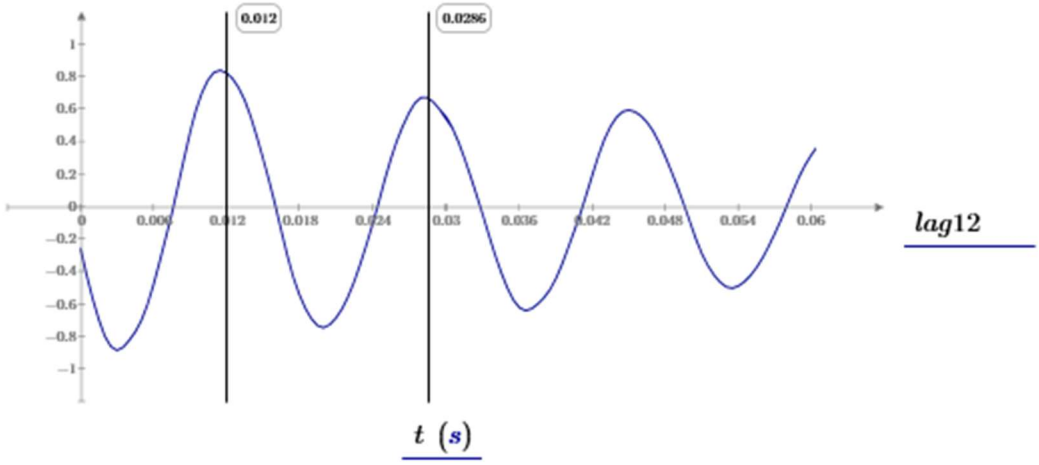

$$Delay := \mathrm{match}\left(\max\left(lag12\right), lag12\right) \cdot \delta t = [0.012]\ s$$

Find the time at maximum correlation

$$freq_{maj} := 59.8\ Hz \qquad \frac{1}{freq_{maj}} = 0.0167\ s$$

Approximate signal repeating frequency

$$dr := \left(r_2 - r_1\right) = 5\ ft$$

Distance between sensor 1 and 2

$$V_{10} := \det\left(\frac{dr}{Delay}\right) = 416.6667\ \frac{ft}{s}$$

Maximum phase velocity of waveform

$$Delay_1 := Delay + \frac{1}{freq_{maj}} = [0.0287]\ s$$

Time until second peak

$$V_{11} := \det\left(\frac{dr}{Delay_1}\right) = 174.0801\ \frac{ft}{s}$$

Second possible velocity

$$Delay_2 := Delay + \frac{2}{freq_{maj}} = [0.0454]\ s$$

Time to third peak

$$V_{12} := \det\left(\frac{dr}{Delay_2}\right) = 110.0236\ \frac{ft}{s}$$

Third possible velocity

Appendix C: Sample Calculation of Floor Space Vibrations

This appendix contains the Mathcad Prime code used to produce the vibration contours for the floor space example described in Chapter 5.

General Information

$data.oct := \text{READCSV}(\text{"\_octave.txt"})$ Read in Third Octave Frequencies

$Data.VC.C := \text{READCSV}(\text{"\_VC.C\_ACC.txt"})$ Read in VC-C Acceleration Spec.

$Data.Laser.Spec := \text{READCSV}(\text{"\_Laser\_Spec\_Acc\_Oct.txt"})$ Read in LaserDyne Spec

$Data.Noise := \text{READCSV}(\text{"\_Noise\_Corrected.txt"})$ Read in Ambient Vibration Noise

$f_{ctr} := data.oct \cdot Hz$ Apply units to variables

$\omega_{ctr} := f_{ctr} \cdot 2\ \pi$

$Acc_{VC.C} := Data.VC.C \cdot \frac{in}{s^2}$

$Acc_{VC.Laser} := Data.Laser.Spec \cdot \frac{in}{s^2}$

$Acc.Noise := Data.Noise \cdot \frac{in}{s^2}$

$n.max := \text{length}(data.oct) = 30$ Number of third octave bands

$n.run := 1,2..n.max$ Index for third octave bands

$n := n.run$

$V_s := 1000\ \frac{ft}{s}$ Calculated Shear Wave Velocity

$\xi := 2.5\%$ Assumed Damping Ratio

$\beta := \frac{\omega_{ctr} \cdot \xi}{V_s}$ Calculate absorption coefficients

$C := 1\ in$ Unit distance

$A_{zero} := 0\ \frac{in}{s^2}$ Apply units to zero acceleration

$X_{max} := 100\ ft$ $Y_{max} := 150\ ft$ Boundary of Floor Space

$\delta x := 12\ in$ $\delta y := \delta x = 1\ ft$ Resolution of Floor Space

$Slab.Scale := 0.8$ Factor for adjusting acceleration values from Vibratory equipment relocated in example

Vibratory Equipment

$data.sig_{1.vib} := \text{READCSV}(\text{"\_d\_signal\_3.sig.txt"})$

Read in third octave accelerations as calculated in Appendix A

$data.r_{1.vib} := \text{READCSV}(\text{"\_d\_signal\_3.sig.r.txt"})$

Read in locations of Acceleration measurements

$Acc_{r.1.vib} := Slab.Scale \cdot data.sig_{1.vib} \cdot \frac{in}{s^2}$

Factor Accelerations for increase slab stiffnes and apply units

$r_{1.vib} := data.r_{1.vib} \cdot in$

$A_{1.vib.min_n} := \left(Acc_{r.1.vib}^{\langle 1 \rangle}\right)_n \cdot \left(\left(\frac{C}{r_{1.vib}^{\widehat{1}}}\right)^{0.5} \cdot e^{-\beta_n \cdot r_{1.vib}^{\widehat{2}}}\right)^{-1}$

Calculate minumim A_1

$A_{1.vib.max_n} := \left(Acc_{r.1.vib}^{\langle 3 \rangle}\right)_n \cdot \left(\left(\frac{C}{r_{1.vib_3}}\right)^{0.5} \cdot e^{-\beta_n \cdot r_{1.vib_3}}\right)^{-1}$

Calculate maximum A_1

Plot minimum and maximum acceleration values in third octave spectrum

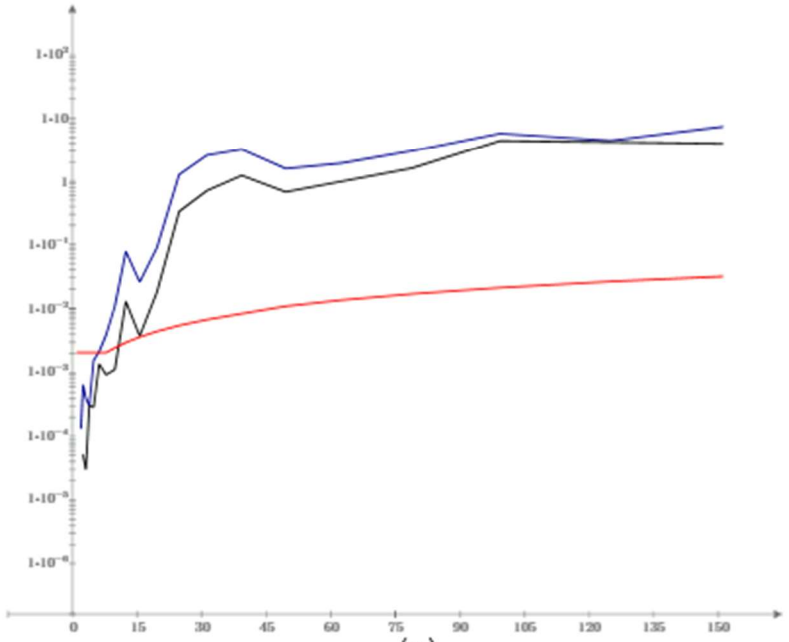

$f_{ctr}\left(\frac{1}{s}\right)$

$A_{1.vib.max}\left(\frac{ft}{s^2}\right)$

$A_{1.vib.min}\left(\frac{ft}{s^2}\right)$

$Acc_{VC.C}\left(\frac{ft}{s^2}\right)$

$$Location := \begin{bmatrix} 25 & 6 & 0\,\frac{deg}{ft} \\ 25 & 16 & 0\,\frac{deg}{ft} \\ 40 & 6 & 0\,\frac{deg}{ft} \\ 40 & 16 & 0\,\frac{deg}{ft} \\ 55 & 6 & 0\,\frac{deg}{ft} \\ 55 & 16 & 0\,\frac{deg}{ft} \end{bmatrix} \cdot ft$$

Itentify locations of vibratory feet on floor space and relative rotation (0 degrees is location of max acceleration)

$$\begin{aligned} &Accel.N := \text{for } n \in n.run \\ &\quad \text{for } x \in 1,2..\frac{X_{max}}{\delta x} \\ &\quad\quad \text{for } y \in 1,2..\frac{Y_{max}}{\delta y} \\ &\quad\quad\quad A_{x,y} \leftarrow Acc.Noise_n \\ &\quad A.fin_n \leftarrow A \\ &A.fin \end{aligned}$$

Apply ambient vibration noise to entire floor space evenly

$$\# := 1$$

$$\begin{aligned} &Accel.1 := \text{for } n \in n.run \\ &\quad \text{for } x \in 1,2..\frac{X_{max}}{\delta x} \\ &\quad\quad \text{for } y \in 1,2..\frac{Y_{max}}{\delta y} \\ &\quad\quad\quad x1 \leftarrow \left(Location^{\langle 1 \rangle}\right)_{\#} - \left(x - \frac{1}{2}\right) \cdot \delta x \\ &\quad\quad\quad y1 \leftarrow \left(Location^{\langle 2 \rangle}\right)_{\#} - \left(y - \frac{1}{2}\right) \cdot \delta y \\ &\quad\quad\quad r \leftarrow \sqrt{x1^2 + y1^2} \\ &\quad\quad\quad \theta \leftarrow \operatorname{atan}\left(\frac{y1}{x1}\right) - \left(Location^{\langle 3 \rangle}\right)_{\#} \\ &\quad\quad\quad \text{if } r < 1\ ft \\ &\quad\quad\quad\quad r \leftarrow 1\ ft \\ &\quad\quad\quad \text{else} \end{aligned}$$

Calculate vibration levels accross floor space caused by each support foot

$r \leftarrow r$

$A_{min} \leftarrow A_{1.vib.min_n}$

$A_{max} \leftarrow A_{1.vib.max_n}$

if $A_{min} \le A_{zero} \vee A_{max} \le A_{zero}$

$A_{calc} \leftarrow A_{zero}$

else

$$A_{calc} \leftarrow \frac{A_{min} \cdot A_{max}}{\sqrt{\left(A_{max} \cdot \sin(\theta)\right)^2 + \left(A_{min} \cdot \cos(\theta)\right)^2}}$$

$$A_{x,y} \leftarrow A_{calc} \cdot \left(\frac{C}{r}\right)^{0.5} \cdot e^{-\beta_n \cdot r}$$

$A.fin_n \leftarrow A$

$A.fin$

$nn := 12$ $f_{ctr_{nn}} = 62.5\ Hz$

Acceleration Contour for one support foot of one vibratory machine at one band

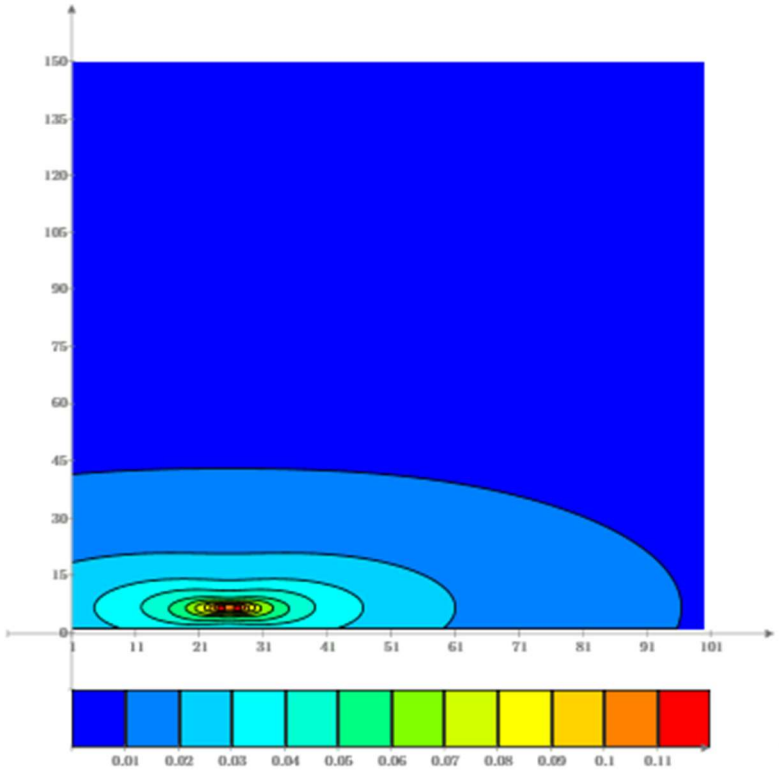

$Accel.1_{nn}$

Combine acceleration values from all sources

$$\overrightarrow{Accel.Ca} := \overrightarrow{Accel.1 + Accel.2 + Accel.3 + Accel.4 + Accel.5 + Accel.6 + Accel.7 + Accel.8}$$
$$\overrightarrow{Accel.C} := \overrightarrow{Accel.Ca + Accel.9 + Accel.10 + Accel.N}$$

$f_{ctr_{nn}} = 62.5\ Hz$ Third Octave Band Shown

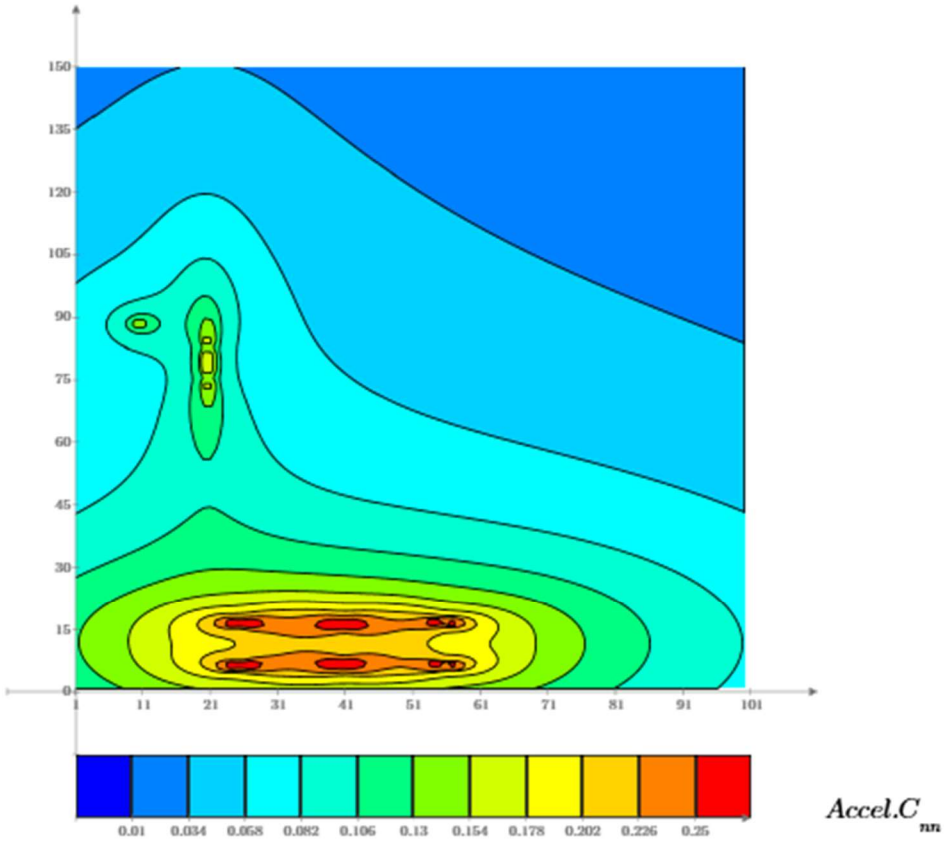

$$Rat_n := \overrightarrow{Accel.C_n \cdot Acc_{VC.Laser_n}^{-1}}$$

Ratio all measured acceleration values to the specification

$f_{ctr_{nn}} = 62.5\ Hz$ Third Octave Band Shown

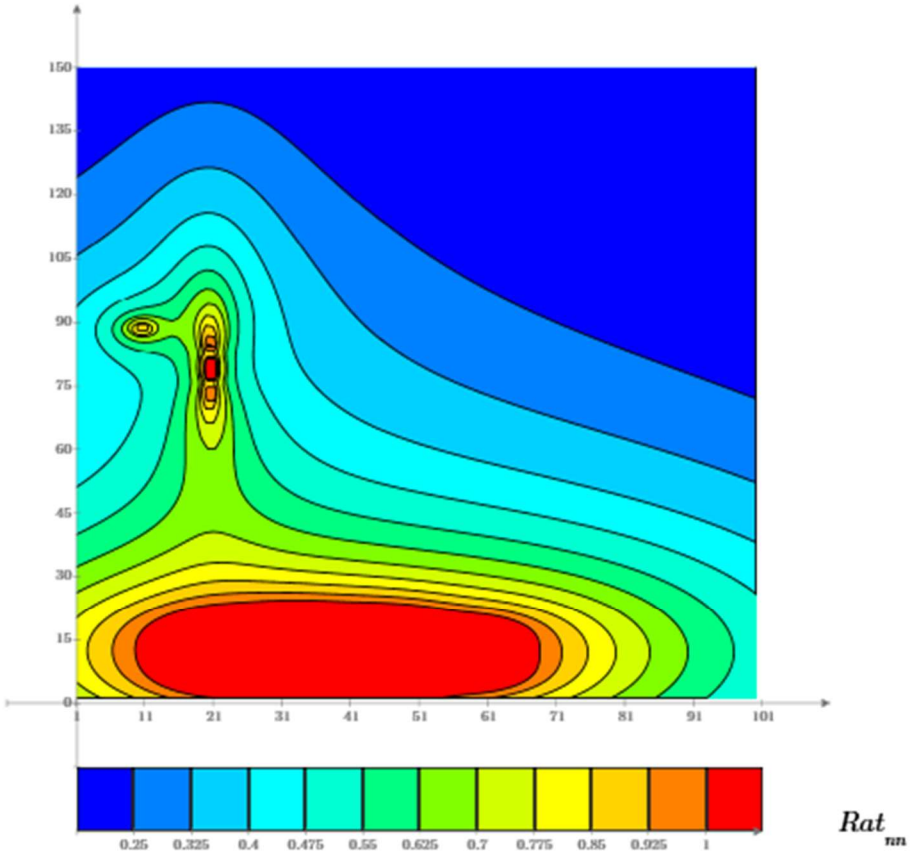

$$
\begin{aligned}
&Rat.Max := \\
&\quad \text{for } x \in 1,2..\frac{X_{max}}{\delta x} \\
&\quad\quad \text{for } y \in 1,2..\frac{Y_{max}}{\delta y} \\
&\quad\quad\quad R_{x,y} \leftarrow 0 \\
&\quad \text{for } x \in 1,2..\frac{X_{max}}{\delta x} \\
&\quad\quad \text{for } y \in 1,2..\frac{Y_{max}}{\delta y} \\
&\quad\quad\quad \text{for } n \in n.run \\
&\quad\quad\quad\quad Ra \leftarrow \det\left(\left(Rat_{n}^{\langle y \rangle}\right)^{\langle z \rangle}\right) \\
&\quad\quad\quad\quad Rb \leftarrow \det\left(\left(R^{\langle z \rangle}\right)^{\langle y \rangle}\right) \\
&\quad\quad\quad\quad \text{if } Ra > Rb \\
&\quad\quad\quad\quad\quad R_{x,y} \leftarrow Ra \\
&\quad R
\end{aligned}
$$

Calculate the max ratio between acceleration values and specification between all third octave bands

Plot of maxium Ratios